Cosmic Inflation at the Crossroads

Jerome Martin, Christophe Ringeval, Vincent Vennin

Cosmic Inflation at the Crossroads

Jérôme Martin,[a] **Christophe Ringeval**[b,a] **and Vincent Vennin**[c,a]

[a]Institut d'Astrophysique de Paris, 98bis boulevard Arago, 75014 Paris, France
[b]Cosmology, Universe and Relativity at Louvain (CURL), Institute of Mathematics and Physics, University of Louvain, 2 Chemin du Cyclotron, 1348 Louvain-la-Neuve, Belgium
[c]Laboratoire de Physique de l'École Normale Supérieure, ENS, CNRS, Université PSL, Sorbonne Université, Université Paris Cité, 75005 Paris, France

E-mail: jmartin@iap.fr, christophe.ringeval@uclouvain.be, vincent.vennin@ens.fr

Abstract. The capability of Cosmic Inflation to explain the latest Cosmic Microwave Background and Baryonic Acoustic Oscillation data is assessed by performing Bayesian model comparison within the landscape of nearly three-hundred models of single-field slow-roll inflation. We present the first Bayesian data analysis based on the third-order slow-roll primordial power spectra. In particular, the fourth Hubble-flow function ε_4 remains unbounded while the third function verifies, at two-sigma, $\varepsilon_3 \in [-0.4, 0.5]$, which is perfectly compatible with the slow-roll predictions for the running of the spectral index. We also observe some residual excess of B-modes within the BICEP/Keck data favoring, at a non-statistically significant level, non-vanishing primordial tensor modes: $\log(\varepsilon_1) > -3.9$, at 68% confidence level. Then, for 287 models of single-field inflation, we compute the Bayesian evidence, the Bayesian dimensionality and the marginalized posteriors of all the models' parameters, including the ones associated with the reheating era. The average information gain on the reheating parameter $R_{\rm reh}$ reaches 1.3 ± 0.18 bits, which is more than a factor two improvement compared to the first Planck data release. As such, inflationary model predictions cannot meet data accuracy without specifying, or marginalizing over, the reheating kinematics. We also find that more than 40% of the scenarios are now strongly disfavored, which shows that the constraining power of cosmological data is winning against the increase of the number of proposed models. In addition, about 20% of all models have evidences within the most probable region and are all favored according to the Jeffreys' scale of Bayesian evidences.

Contents

1 Introduction **2**

2 Post-Planck landscape of single-field inflation **3**

3 Analysis methods **5**
3.1 Data compression using the slow-roll power spectra 5
3.2 Model predictions 7
3.3 One reheating parameter to rule them all 8
3.4 Posteriors and evidences 10
3.5 Fast nested sampling with machine learning 11
3.6 Workflow 13

4 Third-order slow-roll data analysis **13**
4.1 Data sets 13
4.2 Priors 14
4.3 Marginalized posteriors 15
4.4 Other consistency checks 18
4.5 Effective likelihood 20

5 Bayesian model comparison **22**
5.1 Priors and model space 23
5.2 Posteriors and evidences 24
5.3 Bayesian dimensionality 29
5.4 Information gain on the reheating 29

6 Conclusion **31**

A Posteriors for the non-primordial parameters **33**

B Prior choices for the new models **33**
B.1 Axion Hilltop Inflation (AHI) 35
B.2 Cublicly Corrected Starobinsky Inflation (CCSI) 35
B.3 Double Exponential Inflation (DEI) 36
B.4 Dual Inflation (DI) 36
B.5 Double Well Inflation (DWI) 37
B.6 Exponential SUSY Inflation (ESI) 37
B.7 Fiber Inflation (FI) 37
B.8 Generalized Double Well Inflation (GDWI) 38
B.9 Hyperbolic Inflation (HBI) 38
B.10 Higgs Inflation (HI) 39
B.11 Hybrid Natural Inflation (HNI) 39
B.12 Mutated Hilltop Inflation (MHI) 39
B.13 Non-renormalizable Corrected Loop Inflation (NCLI) 40
B.14 N-Formalism Inflation (NFI) 40
B.15 Non-Minimal Large Field Inflation (NMLFI) 41

B.16 Pure Arctan Inflation (PAI) 42
B.17 Radiatively Corrected Inflection Point Inflation (RCIPI) 42
B.18 Radiatively Corrected Large Field Inflation (RCLFI) 43
B.19 String Axion Inflation I (SAII) 43
B.20 String Axion Inflation II (SAIII) 44
B.21 Superconformal α-Attractor B Inflation (SABI) 44
B.22 Superconformal α-Attractor T Inflation (SATI) 45
B.23 Symmetry Breaking Kähler Inflation (SBKI) 45
B.24 S-Dual Inflation (SDI) 46
B.25 Smeared Higgs Inflation (SHI) 46
B.26 Starobinsky Inflation (SI) 46
B.27 Mukhanov Inflation (VFMI) 47

C Posterior distributions for the best models 47

1 Introduction

In the last decades, the quest for understanding the physical conditions that prevailed in the very early universe, prior to the radiation dominated epoch of the standard hot Big Bang model, has been revolutionized twice.

The first breakthrough was the advent of a scenario, cosmic inflation, that, for the first time, was able to offer a consistent and convincing description of the universe in its early stages of evolution. Based on the principles of General Relativity and Quantum Mechanics, cosmic inflation can explain the puzzles of the hot Big Bang model and, in addition, provides a mechanism for the origin of the structures observed in the universe [1–12]. Moreover, it has led to a prediction, namely that the spectral index of the scalar power spectrum should be close to one but, crucially, not exactly one, that has now been confirmed at a high statistical confidence level [13–15].

Obviously, the theory has not escaped critical evaluation, eliciting a range of criticisms. A detailed discussion of these criticisms, with a possible answer for each of them, can (for instance) be found in Ref. [16]. One of the most popular fault-finding made against inflation, which, if true, would be especially relevant in the context of the present paper, is that it would not be a falsifiable theory. It is based on the idea that inflation, if viewed as a paradigm, can always be modified to account for new data. Indeed, there exist different incarnations of inflation and, if a particular version turns out to be incompatible with some data set, then there is always the possibility to invoke another, possibly more complicated, realization. For instance, if some new data show that the scalar primordial power spectrum contains superimposed oscillations, then single-field slow-roll inflation starting in the Bunch-Davis vacuum would be ruled out. But a non slow-roll model, with a potential having a feature at the required scale [17], or some trans-Planckian initial [18–21] conditions, could explain the new data. If, in addition to the presence of oscillations, one also discovers that, say, non-Gaussianities are non-negligible, then one could further modify the scenario, for example by introducing additional fields, or non-minimal kinetic terms. A priori, this process has no end, hence the naive claim that inflation would be non falsifiable. This argument, however, is not specific to inflation. It could be made, for instance, against quantum field theory (QFT). Indeed, QFT also comes in different realizations and one could imagine changing the gauge group or adding new fields each time new particles are discovered. Clearly, it is meaningless to try ruling out the paradigm of QFT *per se* but, nevertheless, each of its incarnations is of course falsifiable, as beautifully exemplified by the establishment of the standard model of particle physics. And so it is for inflation.

Another example of a popular criticism against inflation that has turned out to be inadequate concerns the initial conditions. For a long time, it was believed that inflation can start only if, initially, the universe is already quite homogeneous, thus questioning the relevance of a scenario which is precisely supposed to dynamically achieve this property. However, a series of recent works have demonstrated that, on the contrary, even initially strongly inhomogeneous situations can lead to a phase of inflation [22–27]. The jury might be still out in the sense that the most general case has yet to be treated; there are indeed always some assumptions about the type of inhomogeneities initially present [28]. This is because, technically, the subject is not easy, requiring to carry out full General Relativity simulations. It is, however, fair to say that the trend seems to be in favor of inflation since configurations that were previously believed to prevent inflation have in fact been shown to be perfectly compatible with this theory.

The fact that, despite many attempts, the numerous criticisms against inflation have not really threatened its conceptual attraction and explanatory power, together, of course, with its adequation with the data, are probably the reasons why inflation remains considered by a vast majority of practitioner cosmologists as the leading theory for understanding the very early universe.

The second game changer, which occurred at the same time our understanding of inflation was gradually improved and deepened (namely, roughly speaking, in the last 30 or 40 years), is the fact that high-accuracy cosmological data became progressively available. As briefly mentioned before, this has allowed us to confirm that vanilla inflation is a good description of the early universe and that its emblematic prediction $0 < |n_{\rm S} - 1| \ll 1$ is verified. Recall that this prediction was made before the data were accurate enough to confirm it; it is, therefore, not a postdiction but a genuine prediction. The high-accuracy data now concern different observables but the role played by the Cosmic Microwave Background (CMB) anisotropy measurements has been crucial. It started with the first detection by the NASA COBE satellite [29], followed by the first measurement of multiple Doppler peaks by the WMAP satellite [30] and, more recently, culminated with the publication of the final results obtained by the ESA cosmic-variance limited mission Planck [14]. Other results obtained either by balloon-born [31–36] and/or ground based [37–44] telescopes should not be forgotten and the fact that the CMB is polarized [45] is, and will be, of major importance.

The concomitant nature of the two major aforementioned developments suggests that one has reached a particular stage in the history of the subject. In other words, cosmic inflation is at the crossroads and, before new observations become available, it is the right time to assess where do we stand and to study what we have finally learned about inflation. This will also allow us to understand what is to be expected when new data become available, both from CMB (CMB-S4, LiteBIRD, etc.) [46, 47] and large-scale structure (EUCLID, SKA, etc.) surveys [48, 49]. In this paper, we are interested in the simplest incarnation of inflation (namely, single-field slow-roll inflation with minimal kinetic terms, see Section 2) and aim at assessing its compatibility with recent astrophysical and cosmological data.

In order to carry out this task, we have developed new and efficient analysis methods that are presented in Section 3 whereas new results concerning the slow-roll power spectra are presented in Section 4. In Section 5, pipelining these tools with basic machine-learning methods, we perform Bayesian model comparison in the space of 287 models of inflation. We complement Bayesian evidences with the computation of various other Bayesian quantities, such as the Bayesian dimensionality and the information gain on the reheating, to determine which inflationary scenarios are the most probable given the data. We also present the posterior probability distributions for the parameters associated with the best models in the appendix (all data will be made available online [50]). Our conclusion are presented in Section 6.

2 Post-Planck landscape of single-field inflation

As described in the introduction, cosmic inflation comes in various incarnations. However, a major piece of information inferred from the Planck data is that one of these incarnations, as a matter of fact the simplest one, based on a slowly rolling scalar field, with minimal kinetic term, turns out to be favored. This conclusion is supported, for instance, by the absence of Non-Gaussianities, of non-adiabatic modes or of non-trivial features in the power spectra of primordial fluctuations. From an effective field theory (EFT) perspective, one may wonder

why the phenomenology of inflation appears single field while most of its embedding feature various high-energy degrees of freedom (this may be explained by volume selection effects, as recently shown in Ref. [51]). But according to the principle of parsimony, our task is to focus on the simplest "vanilla" models, since more complicated versions of inflation are, for the moment, not required to understand the data

Another important piece of information recently obtained is that, for the vanilla scenarios, the reheating stage that follows inflation itself is, to some extent, already constrained. These constraints are, however, not very tight and, moreover, depend on the shape of inflaton potential considered. Overall, Planck 2015 and BICEP2/KECK yield to an information gain of 0.82 ± 0.13 bits on the reheating history of slow-roll models [52]. The Planck 2013 data were giving a gain of, typically, half a bit.

Finally, there also exist constraints on the shape of the inflaton potential itself. Models can be organized according to the Schwarz–Terrero-Escalante (STE) classification [53]. There are three main categories depending on the behavior of the Hubble-flow functions (defined in Section 3): the first category corresponds to models with $\epsilon_2 > 2\epsilon_1 > 0$, namely models for which the kinetic energy increases during inflation as well as the ratio of the kinetic energy to the total energy; the second category represents potentials where $0 < \epsilon_2 < 2\epsilon_1$, that is to say where the kinetic energy decreases while the ratio of the kinetic energy to the total energy still increases. Finally, the third category is such that both quantities decrease during inflation. As shown in Ref. [54], Planck data have clearly favored models in the first category. A Bayesian analysis (model selection) further reveals that plateau models, exemplified by the Starobinsky model (but it is important to keep in mind that the performances of many other models are comparable), are the most effective explanation of the data. It is truly remarkable that cosmological data can lead to constraints on physical phenomena that could possible occur at energies as high as $10^{16}\,\mathrm{GeV}$.

This brief status of the art rests on models and methods presented in the first edition of *Encyclopædia Inflationaris* [55], published in 2013. In this article, we aim at presenting an updated status report given the peculiar situation of the cosmic inflation theory which, as already pointed out in the introduction, is today at something of a crossroads, midway between the old and new generations of cosmological measurements.

In order to carry out this task, new methods must be designed in order to take maximum advantage of the recent theoretical and observational developments. On the theoretical front, since the first edition of *Encyclopædia Inflationaris* [55], several new models of inflation have been put forward. As a consequence, in order to have an up-to-date description of the landscape of models, a second edition of *Encyclopædia Inflationaris*, including these new scenarios, has recently been published [56]. The new potential functions in the new edition (here ordered alphabetically) are: Axion Hilltop Inflation (AHI), Cubicly Corrected Starobinsky Inflation (CCSI), Double Exponential Inflation (DEI), Dual Inflation (DI), Fibre Inflation (FI), Generalized Double Well Inflation (GDWI), Hyperbolic Inflation (HBI), Hybrid Natural Inflation (HNI), Non-Renormalizable Corrected Loop Inflation (NCLI), N-Formalism Inflation (NFI), Non-Minimal Large Field Inflation (NMLFI), Pure Arctan Inflation (PAI), Radiatively Corrected Inflection Point Inflation (RCIPI), Radiatively Corrected Large Field Inflation (RCLFI), String Axion Inflation I (SAII), String Axion Inflation II (SAIII), Superconformal Alpha Attractor A Inflation (SAAI), Super-conformal Alpha Attractor B Inflation (SABI), Super-conformal Alpha Attractor T Inflation (SATI), Symmetry Breaking Kähler Inflation (SBKI), S-Dual Inflation (SDI), Smeared Higgs Inflation (SHI), T-Model Inflation (TMI), Mukhanov Inflation (VFMI). With these new scenarios, the total number of models

included has increased by 113 to reach 287. It is important to remark that a model of inflation is not only characterized by a potential function but also by the prior distributions of the parameters appearing in each potential. In other words, two different inflationary models can share a same potential with different priors for its parameters, for instance if these models come from different high-energy embedding. As such, there can be more models than potential functions.

3 Analysis methods

In this section, we describe the theoretical grounds and analysis workflow used to perform Bayesian model comparison and parameter estimation in the space of the single-field slow-roll models of inflation. The basic idea is to compress all the available information associated with the cosmological data into an small set of parameters for which inflationary predictions can be quickly, and accurately, made. For slow-roll inflation, these parameters are the Hubble-flow functions, encoding the drift of the Hubble parameter H,

$$\epsilon_{i+1}(N) \equiv \frac{\mathrm{d}\ln|\epsilon_i|}{\mathrm{d}N}\,, \quad \epsilon_0(N) = \frac{M_{\rm Pl}}{H}\,, \tag{3.1}$$

evaluated at a peculiar e-fold number N_* during inflation. This number is defined as the e-fold at which an observable pivot wavenumber k_* crosses the Hubble radius during inflation. More precisely, it is the e-fold such that $k_*\eta(N_*) = -1$ where η is conformal time (this coincides with Hubble crossing, $k = aH$, at leading order in slow roll only, but it is taken as a generic definition). The actual value of k_* is an observer choice, and, in the following, we choose $k_* = 0.05\,\mathrm{Mpc}^{-1}$, which lies in the middle of the observed range of modes. Once k_* is set, N_* is no longer a free parameter: it is completely fixed by both the inflationary model parameters and the kinematics of the reheating era. In the following, we give some details explaining why the Hubble-flow functions are best-suited to parameterize the inflationary dynamics, how to properly deal with the reheating era and how one can extract the posterior probability distributions for the inflationary theoretical parameters associated with a given model.

3.1 Data compression using the slow-roll power spectra

During inflation, it is possible to analytically solve the evolution of linear perturbations in General Relativity by performing a functional expansion in terms of the Hubble flow functions $\epsilon_i(N)$ [53, 57–65]. The sole assumption in deriving such an analytical solution is that all the ϵ_i are small and of the same order (at least above the truncation order), which is the mere definition of slow-roll inflation. The analytical expressions for the primordial power spectra have been the subject of various works in the last two decades [64–72], and are currently known at third order in the Hubble flow functions [73]. Using the shorthand notation $\epsilon_{i*} = \epsilon_i(N_*)$ as well as $H_* = H(N_*)$, the primordial scalar power spectrum reads

$$\begin{aligned}\mathcal{P}_\zeta(k) = \frac{H_*^2}{8\pi^2 M_{\rm Pl}^2\epsilon_{1*}}\Bigg\{&1 - 2(C+1)\epsilon_{1*} - C\epsilon_{2*} + \left(\frac{\pi^2}{2} + 2C^2 + 2C - 3\right)\epsilon_{1*}^2 \\ &+ \left(\frac{7\pi^2}{12} + C^2 - C - 6\right)\epsilon_{1*}\epsilon_{2*} + \frac{1}{8}\big(\pi^2 + 4C^2 - 8\big)\epsilon_{2*}^2 + \frac{1}{24}(\pi^2 - 12C^2)\epsilon_{2*}\epsilon_{3*} \\ &- \frac{1}{24}\big[4C^3 + 3\big(\pi^2 - 8\big)C + 14\zeta(3) - 16\big]\big(8\epsilon_{1*}^3 + \epsilon_{2*}^3\big)\end{aligned}$$

$$
\begin{aligned}
&+\frac{1}{12}\big[13\pi^2-8(\pi^2-9)C+36C^2-84\zeta(3)\big]\epsilon_{1*}^2\epsilon_{2*}\\
&-\frac{1}{24}\big[8C^3-15\pi^2+6(\pi^2-4)C-12C^2+100\zeta(3)+16\big]\epsilon_{1*}\epsilon_{2*}^2\\
&+\frac{1}{24}\big[\pi^2C-4C^3-8\zeta(3)+16\big]\big(\epsilon_{2*}\epsilon_{3*}^2+\epsilon_{2*}\epsilon_{3*}\epsilon_{4*}\big)+\frac{1}{24}\big[12C^3+\big(5\pi^2-48\big)C\big]\epsilon_{2*}^2\epsilon_{3*}\\
&+\frac{1}{12}\big[8C^3+\pi^2+6\big(\pi^2-12\big)C-12C^2-8\zeta(3)-8\big]\epsilon_{1*}\epsilon_{2*}\epsilon_{3*}\\
&+\ln\left(\frac{k}{k_*}\right)\bigg[-2\epsilon_{1*}-\epsilon_{2*}+2(2C+1)\epsilon_{1*}^2+(2C-1)\epsilon_{1*}\epsilon_{2*}+C\epsilon_{2*}^2-C\epsilon_{2*}\epsilon_{3*}\\
&-\frac{1}{8}\big(\pi^2+4C^2-8\big)\big(8\epsilon_{1*}^3+\epsilon_{2*}^3\big)-\frac{2}{3}\big(\pi^2-9C-9\big)\epsilon_{1*}^2\epsilon_{2*}-\frac{1}{4}\big(\pi^2+4C^2-4C-4\big)\epsilon_{1*}\epsilon_{2*}^2\\
&+\frac{1}{2}\big(\pi^2+4C^2-4C-12\big)\epsilon_{1*}\epsilon_{2*}\epsilon_{3*}\\
&+\frac{1}{24}\big(\pi^2-12C^2\big)\left(\epsilon_{2*}\epsilon_{3*}^2+\epsilon_{2*}\epsilon_{3*}\epsilon_{4*}\right)+\frac{1}{24}\big(5\pi^2+36C^2-48\big)\epsilon_{2*}^2\epsilon_{3*}\bigg]\\
&+\frac{1}{2}\ln^2\left(\frac{k}{k_*}\right)\bigg[4\epsilon_{1*}^2+2\epsilon_{1*}\epsilon_{2*}+\epsilon_{2*}^2-\epsilon_{2*}\epsilon_{3*}+6\epsilon_{1*}^2\epsilon_{2*}-(2C-1)\big(\epsilon_{1*}\epsilon_{2*}^2-2\epsilon_{1*}\epsilon_{2*}\epsilon_{3*}\big)\\
&-C\left(8\epsilon_{1*}^3+\epsilon_{2*}^3-3\epsilon_{2*}^2\epsilon_{3*}+\epsilon_{2*}\epsilon_{3*}^2+\epsilon_{2*}\epsilon_{3*}\epsilon_{4*}\right)\bigg]\\
&+\frac{1}{6}\ln^3\left(\frac{k}{k_*}\right)\big(-8\epsilon_{1*}^3-2\epsilon_{1*}\epsilon_{2*}^2+4\epsilon_{1*}\epsilon_{2*}\epsilon_{3*}-\epsilon_{2*}^3+3\epsilon_{2*}^2\epsilon_{3*}-\epsilon_{2*}\epsilon_{3*}^2-\epsilon_{2*}\epsilon_{3*}\epsilon_{4*}\big)\bigg\},
\end{aligned}
\tag{3.2}
$$

while the primordial power spectrum for gravitational waves is given by

$$
\begin{aligned}
\mathcal{P}_h(k)=\frac{2H_*^2}{\pi^2M_{\rm Pl}^2}\bigg\{&1-2(C+1)\epsilon_{1*}+\frac{1}{2}\big(\pi^2+4C^2+4C-6\big)\epsilon_{1*}^2\\
&+\frac{1}{12}(\pi^2-12C^2-24C-24)\epsilon_{1*}\epsilon_{2*}-\frac{1}{3}\big[4C^3+3(\pi^2-8)C+14\zeta(3)-16\big]\epsilon_{1*}^3\\
&+\frac{1}{12}\big[24C^3+13\pi^2+2(5\pi^2-36)C+36C^2-96\big]\epsilon_{1*}^2\epsilon_{2*}\\
&-\frac{1}{12}\big[4C^3-\pi^2-(\pi^2-24)C+12C^2+8\zeta(3)+8\big]\big(\epsilon_{1*}\epsilon_{2*}^2+\epsilon_{1*}\epsilon_{2*}\epsilon_{3*}\big)\\
&+\ln\left(\frac{k}{k_*}\right)\bigg[-2\epsilon_{1*}+2(2C+1)\epsilon_{1*}^2-2(C+1)\epsilon_{1*}\epsilon_{2*}-\big(\pi^2+4C^2-8\big)\epsilon_{1*}^3\\
&+\frac{1}{6}\big(5\pi^2+36C^2+36C-36\big)\epsilon_{1*}^2\epsilon_{2*}+\frac{1}{12}\big(\pi^2-12C^2-24C-24\big)\big(\epsilon_{1*}\epsilon_{2*}^2+\epsilon_{1*}\epsilon_{2*}\epsilon_{3*}\big)\bigg]\\
&+\ln^2\left(\frac{k}{k_*}\right)\bigg[2\epsilon_{1*}^2-\epsilon_{1*}\epsilon_{2*}-4C\epsilon_{1*}^3+3(2C+1)\epsilon_{1*}^2\epsilon_{2*}-(C+1)\big(\epsilon_{1*}\epsilon_{2*}^2+\epsilon_{1*}\epsilon_{2*}\epsilon_{3*}\big)\bigg]\\
&+\frac{1}{3}\ln^3\left(\frac{k}{k_*}\right)\big(-4\epsilon_{1*}^3+6\epsilon_{1*}^2\epsilon_{2*}-\epsilon_{1*}\epsilon_{2*}^2-\epsilon_{1*}\epsilon_{2*}\epsilon_{3*}\big)\bigg\}.
\end{aligned}
\tag{3.3}
$$

Some irrational numbers appear in Eqs. (3.2) and (3.3), there is π, a constant C related to the Euler constant $\gamma_{\rm E}$ by

$$
C\equiv\gamma_{\rm E}+\ln 2-2\simeq-0.729637,
\tag{3.4}
$$

and the Riemann Zeta function $\zeta(3) \simeq 1.20206$. As explicit in these expressions, once k_* is chosen, the k-dependence of the tensor and scalar primordial power spectra is completely fixed by the parameters $(\epsilon_{0*}, \epsilon_{1*}, \epsilon_{2*}, \epsilon_{3*}, \epsilon_{4*})$. As discussed in Refs. [63, 74], performing data analysis using Eqs. (3.2) and (3.3) is not the same as postulating a power-law shape for the primordial power spectra. Indeed, the latter option can be viewed as adding an infinite number of extra-terms that are not consistent with the actual slow-roll dynamics. Still, Eqs. (3.2) and (3.3) are approximate, but that approximation is under control and missing terms are of order $\mathcal{O}\left(\epsilon_*^4\right)$. As we will see later on, this is more than enough to match the present data accuracy. Defining

$$P_* \equiv \mathcal{P}_\zeta(k_*), \tag{3.5}$$

one can also trade the parameter ϵ_{0*} for P_*, which is better suited for data analysis. Indeed, the amplitude of the CMB anisotropies is a well-measured quantity, which is in direct correspondence with P_*. Notice from Eq. (3.2) that recovering ϵ_{0*} from P_* requires the knowledge of all the other ϵ_{i*}.

The observable predictions for the whole class of single-field slow-roll models can thus be encoded within the small parameter set (P_*, ϵ_{i*}) by using Eqs. (3.2) and (3.3) as functional forms for the primordial power spectra. As a consequence, for any data set, one could add the slow-roll parameters into the inference problem and extract their posterior probability distribution. This is done in Section 4 for the latest cosmological data.

Given a specific inflationary model $\mathcal{M}$, within the slow-roll class, what remains to be done is to compute the actual values of the (P_*, ϵ_{i*}) parameters. We now turn to this question.

3.2 Model predictions

For the minimally coupled single-field inflationary models, with a canonical kinetic term, the potential $V(\phi)$, complemented with the Friedmann-Lemaître equations, completely fixes the dynamics. In particular, one can define an infinite hierarchy of potential-related functions, denoted $\epsilon_{v_i}(\phi)$, defined as [75, 76]

$$\epsilon_{v_{n+1}}(\phi) \equiv \sqrt{2\epsilon_{v_1}} M_{\rm Pl} \frac{\mathrm{d}\ln|\epsilon_{v_n}|}{\mathrm{d}\phi}, \quad \epsilon_{v_0}(\phi) = \sqrt{\frac{3M_{\rm Pl}^4}{V}}. \tag{3.6}$$

The functions $\epsilon_{v_i}(\phi)$ can be straightforwardly derived from the functional shape of the potential and are, sometimes, also referred to as the "slow-roll parameters". The reason underlying such a confusing naming being that the Hubble-flow and ϵ_{v_i} hierarchies match at leading order in an expansion in Hubble flow functions. More simply stated, one has $\epsilon_{v_i} = \epsilon_i + \mathcal{O}\left(\epsilon^2\right)$ for all i [58]. However, if one wants to consistently make predictions at a given order in the Hubble-flow functions, say order three as to match the accuracy at which Eqs. (3.2) and (3.3) have been derived, one has to use the following mapping

$$\begin{aligned}
\epsilon_1 &= \epsilon_{v_1} - \frac{1}{3}\epsilon_{v_1}\epsilon_{v_2} - \frac{1}{9}\epsilon_{v_1}^2\epsilon_{v_2} + \frac{5}{36}\epsilon_{v_1}\epsilon_{v_2}^2 + \frac{1}{9}\epsilon_{v_1}\epsilon_{v_2}\epsilon_{v_3},\\
\epsilon_2 &= \epsilon_{v_2} - \frac{1}{6}\epsilon_{v_2}^2 - \frac{1}{3}\epsilon_{v_2}\epsilon_{v_3} - \frac{1}{6}\epsilon_{v_1}\epsilon_{v_2}^2 + \frac{1}{18}\epsilon_{v_2}^3 - \frac{1}{9}\epsilon_{v_1}\epsilon_{v_2}\epsilon_{v_3} + \frac{5}{18}\epsilon_{v_2}^2\epsilon_{v_3} + \frac{1}{9}\epsilon_{v_2}\epsilon_{v_3}^2 + \frac{1}{9}\epsilon_{v_2}\epsilon_{v_2}\epsilon_{v_4},\\
\epsilon_3 &= \epsilon_{v_3} - \frac{1}{3}\epsilon_{v_2}\epsilon_{v_3} - \frac{1}{3}\epsilon_{v_3}\epsilon_{v_4} - \frac{1}{6}\epsilon_{v_1}\epsilon_{v_2}^2 - \frac{1}{3}\epsilon_{v_1}\epsilon_{v_2}\epsilon_{v_3} + \frac{1}{6}\epsilon_{v_2}^2\epsilon_{v_3} + \frac{5}{18}\epsilon_{v_2}\epsilon_{v_3}^2 - \frac{1}{9}\epsilon_{v_1}\epsilon_{v_3}\epsilon_{v_4}\\
&\quad + \frac{5}{18}\epsilon_{v_2}\epsilon_{v_3}\epsilon_{v_4} + \frac{1}{9}\epsilon_{v_3}^2\epsilon_{v_4} + \frac{1}{9}\epsilon_{v_3}\epsilon_{v_4}^2 + \frac{1}{9}\epsilon_{v_3}\epsilon_{v_4}\epsilon_{v_5},\\
\epsilon_4 &= \epsilon_{v_4} - \frac{1}{3}\epsilon_{v_2}\epsilon_{v_3} - \frac{1}{6}\epsilon_{v_2}\epsilon_{v_4} - \frac{1}{3}\epsilon_{v_4}\epsilon_{v_5} + \cdots.
\end{aligned} \tag{3.7}$$

These expressions have been derived from the Friedmann-Lemaître equations, using Eqs. (3.1) and (3.6) and assuming a field trajectory $\phi(N)$ on shell, i.e., solving the Klein-Gordon equation, which reads [16]

$$\frac{2}{6-\Gamma^2}\frac{\mathrm{d}\Gamma}{\mathrm{d}N}+\Gamma=-M_{\mathrm{Pl}}\frac{\mathrm{d}\ln\bigl(V/M_{\mathrm{Pl}}^4\bigr)}{\mathrm{d}\phi}\,, \tag{3.8}$$

where we have defined $\Gamma = M_{\mathrm{Pl}}^{-1}\mathrm{d}\phi/\mathrm{d}N$. From Eq. (3.7), one sees that one would need up to ϵ_{v_5} to determine ϵ_4 at second order in the Hubble-flow functions. However, because ϵ_{4*} is always multiplied by $\epsilon_{2*}\epsilon_{3*}$ in Eq. (3.2), maintaining third-order accuracy for $\mathcal{P}(k)$ actually requires ϵ_{4*} to be known at leading order only. Hence, we have omitted here the highest-order terms.

In practice, all the $\epsilon_{v_i}(\phi)$ functions can be straightforwardly obtained by taking the successive derivatives of $V(\phi)$ according to Eq. (3.6). The field trajectory $\phi(N)$, or, equivalently, the relation giving the number of e-folds N given a field value can also be obtained within the slow-roll framework. Indeed, Eq. (3.8) is similar to the equation of motion of a relativistic particle with a constant friction term and accelerated by an external force deriving from the potential $\ln\bigl(V/M_{\mathrm{Pl}}^4\bigr)$. After a transient regime, the field reaches its "terminal velocity" and settles into the solution

$$\Gamma\simeq-M_{\mathrm{Pl}}\frac{\mathrm{d}\ln\bigl(V/M_{\mathrm{Pl}}^4\bigr)}{\mathrm{d}\phi}\,, \tag{3.9}$$

which is the "slow-roll" regime, an attractor. On the attactor, and up to a constant term, one gets from Eq. (3.9),

$$N=-\frac{1}{M_{\mathrm{Pl}}^2}\int^{\phi}\frac{V(\psi)}{V'(\psi)}\mathrm{d}\psi. \tag{3.10}$$

In some regimes, as for instance in ultra slow-roll, or, at the end of inflation, Eq. (3.9) may become inaccurate thereby requiring a numerical integration of Eq. (3.8).

Given a specific inflationary model, Eqs. (3.6) to (3.10) allow us to determine, at the wanted precision, all the Hubble flow functions $\epsilon_i(N)$ given a potential $V(\phi)$. This potential is uniquely specified by some intrinsic model parameters that will be referred to as $\boldsymbol{\theta}_{\mathrm{inf}}$. In practice, the determination of the $\epsilon_i(N)$ functions given $\boldsymbol{\theta}_{\mathrm{inf}}$ is automated by a modern Fortran library `ASPIC` [77], supporting all the inflationary models discussed in the "Opiparous Edition" of the *Encyclopædia Inflationaris* paper [56]. Let us stress that various motivated models are non-minimally coupled to gravity. For these, various extensions of the method discussed in this section have been implemented, they are discussed at length in Ref. [56] and they have been numerically implemented in the `ASPIC` code. In summary, the slow-roll approximation, and its extensions, allow us to determine all the necessary $\epsilon_i(N)$ functions given the theoretical parameters $\boldsymbol{\theta}_{\mathrm{inf}}$.

3.3 One reheating parameter to rule them all

During inflation and the subsequent cosmological era, the wavelengths of cosmological perturbations are stretched by the expansion of the universe. As such, the correspondence between a mode k/a_0 observed today and its blue-shifted value k/a during inflation requires to know the complete history of the universe in between. As mentioned above, the value of N_*, to be used as an argument of the $\epsilon_i(N_*)$ in Eqs. (3.2) and (3.3), is defined by $k_*\eta(N_*) = -1$. As shown in Refs. [52, 78–81], this condition is equivalent, at leading order in the Hubble-flow

functions, to the following algebraic equation determining the value of N_*

$$\Delta N_* \equiv N_* - N_{\rm end} = -\ln R_{\rm rad} + N_0 + \frac{1}{4}\ln\left[\frac{9}{\epsilon_{1*}\left(3-\epsilon_{1\rm end}\right)}\frac{V_{\rm end}}{V_*}\right] - \frac{1}{4}\ln\left(\frac{H_*^2}{M_{\rm Pl}^2\epsilon_{1*}}\right), \quad (3.11)$$

where $V_* = V[\phi(N_*)]$ and $V_{\rm end} = V[\phi(N_{\rm end})]$, the index "end" denoting the end of inflation. Using Eq. (3.10), this equation can also be viewed as an algebraic equation on the field value ϕ_*. The quantity N_0 is the typical number of e-folds of decelerated expansion and reads

$$N_0 \equiv \ln\left[\frac{k_*/a_0}{\left(3\mathcal{Q}_{\rm reh}\Omega_{\rm rad}H_0^2\right)^{1/4}}\right], \quad (3.12)$$

where $\mathcal{Q}_{\rm reh}$ is a measure of the change of number of entropic and energetic relativistic degrees of freedom between the beginning of the radiation era and today [79]. The parameter $R_{\rm rad}$ in Eq. (3.11) is the so-called *reheating parameter* defined as

$$R_{\rm rad} \equiv \frac{a_{\rm end}}{a_{\rm reh}}\left(\frac{\rho_{\rm end}}{\rho_{\rm reh}}\right)^{1/4}. \quad (3.13)$$

It encodes all the relevant kinematic effects the reheating may induce on the conserved super-Hubble cosmological perturbations [82, 83]. In Eq. (3.13), $\rho_{\rm end}$ is the energy density of the universe at the end of inflation and $\rho_{\rm reh}$ stands for the energy density at the beginning of the radiation era (i.e., the end of the reheating era). Clearly, one must have $\rho_{\rm reh} \leq \rho_{\rm end}$, and, in order not to spoil Big-Bang Nucleosynthesis (BBN), we should have $\rho_{\rm reh} > \rho_{\rm nuc}$. Using energy conservation during the reheating era, one can also show that [56]

$$\ln R_{\rm rad} = \frac{\Delta N_{\rm reh}}{4}\left(-1+3\overline{w}_{\rm reh}\right) = \frac{1-3\overline{w}_{\rm reh}}{12\left(1+\overline{w}_{\rm reh}\right)}\ln\left(\frac{\rho_{\rm reh}}{\rho_{\rm end}}\right), \quad (3.14)$$

where $\Delta N_{\rm reh}$ is the duration of reheating in e-folds and $\overline{w}_{\rm reh}$ is the average equation of state parameter of the universe during that period. These other forms of $R_{\rm rad}$ show that a radiation-like reheating era, having $\overline{w}_{\rm reh} = 1/3$, and not necessarily thermalized, is indistinguishable from an instantaneous reheating from the point of view of the cosmological perturbations. Such a statement should make clear that specifying only $\Delta N_{\rm reh}$ is not enough to make inflationary predictions. As explicit in Eq. (3.11), whichever representation of the reheating era is chosen $\boldsymbol{\theta}_{\rm reh} = (\Delta N_{\rm reh}, \overline{w}_{\rm reh})$, $\boldsymbol{\theta}_{\rm reh} = (\overline{w}_{\rm reh}, \rho_{\rm reh})$, or others, the overall stretching induced on the cosmological perturbations will always be given by one number: $R_{\rm rad}$. As such, the simplest motivated way to parameterize the reheating era is, a priori, to use the parameter $\boldsymbol{\theta}_{\rm reh} = R_{\rm rad}$.

Recapping that N_* is the parameter fixing the actual values of the $\epsilon_{i*} \equiv \epsilon_i(N_*)$, one should expect any cosmological data to be sensitive to ΔN_*. However, the last term of Eq. (3.11) is, at leading order in the Hubble flow functions, equal to $8\pi^2 P_*$, the amplitude of the scalar spectrum which is a very well measured quantity. As such, Eq. (3.11) shows that there is a strong degeneracy between $R_{\rm rad}$, P_* and ΔN_* in inferring their posterior probability distribution from any cosmological data sets. This issue was discussed, and solved, in Refs. [82, 83] by introducing the *rescaled reheating parameter* $R_{\rm reh}$ defined by

$$\ln R_{\rm reh} \equiv \ln R_{\rm rad} + \frac{1}{4}\ln\left(\frac{\rho_{\rm end}}{M_{\rm Pl}^4}\right). \quad (3.15)$$

Indeed, from the Friedmann-Lemaître equation, one has

$$\rho_{\rm end} = \frac{3V_{\rm end}}{3-\epsilon_{1\rm end}} = \frac{V_{\rm end}}{V_*}\frac{3V_*}{3-\epsilon_{1\rm end}} = 3M_{\rm Pl}^2H_*^2\frac{V_{\rm end}}{V_*}\frac{3-\epsilon_{1*}}{3-\epsilon_{1\rm end}}\,, \tag{3.16}$$

One always has $\epsilon_{1*} \ll 1$ and Eq. (3.15) can be inverted as

$$\ln R_{\rm rad} = \ln R_{\rm reh} - \frac{1}{4}\ln\left(\frac{H_*^2}{M_{\rm Pl}^2\epsilon_{1*}}\right) - \frac{1}{4}\ln\left(\frac{9V_{\rm end}}{V_*}\frac{\epsilon_{1*}}{3-\epsilon_{1\rm end}}\right). \tag{3.17}$$

Plugging Eq. (3.17) into Eq. (3.11), the terms in $H_*^2/(M_{\rm Pl}^2\epsilon_{1*})$ cancel out and one finally gets

$$\Delta N_* = -\ln R_{\rm reh} + N_0 + \frac{1}{2}\ln\left(\frac{9}{3-\epsilon_{1\rm end}}\frac{V_{\rm end}}{V_*}\right). \tag{3.18}$$

As a result, performing cosmological data analysis with the rescaled reheating parameter $R_{\rm reh}$ completely suppresses the degeneracies between the kinematics of the reheating and the amplitude of the scalar perturbations P_*. Even though the previous calculation has been made at leading order in the Hubble flow functions, it is possible to show that $R_{\rm reh}$, as defined in Eq. (3.15), allows one to decouple ΔN_* and $\mathcal{P}(k_*)$ out of the slow-roll assumptions, i.e., assuming only linear perturbations within General Relativity [83]. For this reason, the simplest and optimal choice for parameterizing the reheating is to use $\boldsymbol{\theta}_{\rm reh} = R_{\rm reh}$. Let us notice that, given an inflationary model, the quantity $\rho_{\rm end}$ is determined by the parameters $\boldsymbol{\theta}_{\rm inf}$. As such, Eq. (3.15) shows that, at fixed $\boldsymbol{\theta}_{\rm inf}$, $R_{\rm rad}$ and $R_{\rm reh}$ are deterministically related. Their posterior probability distributions will however differ and will be correlated to the ones associated with $\boldsymbol{\theta}_{\rm inf}$.

3.4 Posteriors and evidences

All inflationary scenarios considered in this work are assumed to be followed by a reheating era, possibly instantaneous, and which ends when the standard Friedmann-Lemaître radiation era starts. In this picture, we are comparing to data a consistent embedding of each inflationary model within the standard cosmological framework. This implies that the theoretical parameters of a model $\mathcal{M}$ are made of the pure inflationary model parameters $\boldsymbol{\theta}_{\rm inf}$, the reheating parameters $\boldsymbol{\theta}_{\rm reh}$, all the standard cosmological and astrophysical parameters $\boldsymbol{\theta}_{\rm s}$, possibly complemented by some instrumental nuisance parameters.

Given some cosmological data set $\boldsymbol{D}$, let us denote the posterior probability distribution of the parameters $\{\boldsymbol{\theta}_{\rm inf}, \boldsymbol{\theta}_{\rm reh}, \boldsymbol{\theta}_{\rm s}\}$, within the hypothesis that inflation has occurred according to model $\mathcal{M}$, by $P(\boldsymbol{\theta}_{\rm inf}, \boldsymbol{\theta}_{\rm reh}, \boldsymbol{\theta}_{\rm s}|\boldsymbol{D}, \mathcal{M})$. This multidimensional probability distribution can be determined by sampling methods, given a likelihood functional $P(\boldsymbol{D}|\boldsymbol{\theta}_{\rm inf}, \boldsymbol{\theta}_{\rm reh}, \boldsymbol{\theta}_{\rm s}, \mathcal{M})$, the prior probability distributions for all parameters $\pi(\boldsymbol{\theta}_{\rm inf}, \boldsymbol{\theta}_{\rm reh}, \boldsymbol{\theta}_{\rm s}) = P(\boldsymbol{\theta}_{\rm inf}, \boldsymbol{\theta}_{\rm reh}, \boldsymbol{\theta}_{\rm s}|\mathcal{M})$, and by using the Bayes' theorem

$$P(\boldsymbol{\theta}_{\rm inf}, \boldsymbol{\theta}_{\rm reh}, \boldsymbol{\theta}_{\rm s}|\boldsymbol{D}, \mathcal{M}) = \frac{P(\boldsymbol{D}|\boldsymbol{\theta}_{\rm inf}, \boldsymbol{\theta}_{\rm reh}, \boldsymbol{\theta}_{\rm s}, \mathcal{M})\,\pi(\boldsymbol{\theta}_{\rm inf}, \boldsymbol{\theta}_{\rm reh}, \boldsymbol{\theta}_{\rm s})}{\mathcal{E}(\boldsymbol{D}|\mathcal{M})}\,. \tag{3.19}$$

The normalization constant $\mathcal{E}(\boldsymbol{D}|\mathcal{M})$ is the Bayesian evidence, or, strictly speaking, the model likelihood: the probability of having observed the data $\boldsymbol{D}$ given the hypothesis that inflation occurred according to model $\mathcal{M}$. From Eq. (3.19), it reads

$$\mathcal{E}(\boldsymbol{D}|\mathcal{M}) = \int P(\boldsymbol{D}|\boldsymbol{\theta}_{\rm inf}, \boldsymbol{\theta}_{\rm reh}, \boldsymbol{\theta}_{\rm s}, \mathcal{M})\,\pi(\boldsymbol{\theta}_{\rm inf}, \boldsymbol{\theta}_{\rm reh}, \boldsymbol{\theta}_{\rm s})\,{\rm d}\boldsymbol{\theta}_{\rm inf}{\rm d}\boldsymbol{\theta}_{\rm reh}{\rm d}\boldsymbol{\theta}_{\rm s}. \tag{3.20}$$

The Bayesian evidence allows us to determine the probability of a given model to explain the data. Indeed, using again the Bayes' theorem one has

$$P(\mathcal{M}|\boldsymbol{D}) = \frac{\mathcal{E}(\boldsymbol{D}|\mathcal{M})\, P(\mathcal{M})}{P(\boldsymbol{D})}\,, \tag{3.21}$$

where $P(\boldsymbol{D})$ is a model-free normalization factor and $P(\mathcal{M})$ is the prior probability of model $\mathcal{M}$. In order to compare models $\mathcal{M}_1$ and $\mathcal{M}_2$, one can evaluate their probability ratio to explain the data, namely

$$\frac{P(\mathcal{M}_1|\boldsymbol{D})}{P(\mathcal{M}_2|\boldsymbol{D})} = B_2^1\, \frac{P(\mathcal{M}_1)}{P(\mathcal{M}_2)}\,, \tag{3.22}$$

where we have introduced the ratio of their evidences, namely, the Bayes factor

$$B_2^1 = \frac{\mathcal{E}(\boldsymbol{D}|\mathcal{M}_1)}{\mathcal{E}(\boldsymbol{D}|\mathcal{M}_2)}\,. \tag{3.23}$$

Without any prejudice on which models, $\mathcal{M}_1$ or $\mathcal{M}_2$, is better suited to explain the data, one has $P(\mathcal{M}_1) = P(\mathcal{M}_2)$ and Eq. (3.23) shows that the Bayesian evidences are the quantities of interest to determine what are the best models [84].

In practice, Eq. (3.20) shows that determining $\mathcal{E}(\boldsymbol{D}|\mathcal{M})$ requires to compute a multi-dimensional integral of the likelihood multiplied by the prior over all the parameters. This can be performed by using nested-sampling methods [85–89]. However, this is computationally time consuming, especially if the likelihood evaluation is slow, and the task becomes extremely challenging when the number of models $\mathcal{M}$ is large, as in the present case.

3.5 Fast nested sampling with machine learning

In order to speed-up the computation of evidences and of the posterior probability distribution for all the primordial parameters $\boldsymbol{\theta}_{\rm inf}$ and $\boldsymbol{\theta}_{\rm reh}$ associated with each model $\mathcal{M}$, we have applied the method discussed in Ref. [90] to the third-order power spectra of Eqs. (3.2) and (3.3).

It consists in determining, and machine-learning, an effective likelihood $\mathcal{L}_{\rm eff}$ for the primordial parameters constructed over some model-free Hubble-flow functions, say ε_i, and such that

$$\mathcal{L}_{\rm eff}(\boldsymbol{D}|\varepsilon_0,\varepsilon_1,\varepsilon_2,\varepsilon_3) \propto \int P(\boldsymbol{D}|\boldsymbol{\theta}_{\rm s},\varepsilon_0,\varepsilon_1,\varepsilon_2,\varepsilon_3,\varepsilon_4)\,\pi(\varepsilon_4)\,\pi(\boldsymbol{\theta}_{\rm s})\,{\rm d}\varepsilon_4{\rm d}\boldsymbol{\theta}_{\rm s}. \tag{3.24}$$

The full likelihood $P(\boldsymbol{D}|\boldsymbol{\theta}_{\rm s},\varepsilon_0,\varepsilon_1,\varepsilon_2,\varepsilon_3,\varepsilon_4)$ is associated with the primordial power spectra of Eqs. (3.2) and (3.3) where all the ϵ_{i*} are systematically replaced with the model-free ε_i.

Determining $\mathcal{L}_{\rm eff}$ requires to marginalize a full likelihood over many parameters, the $\boldsymbol{\theta}_{\rm s}$ and ε_4 here. This is done in Section 4 by performing an exploration of the full parameter space using Markov-Chains-Monte-Carlo (MCMC) methods [91, 92].

Let us prove here that Eq. (3.24) is indeed sufficient to make Bayesian inference in the space of primordial parameters $\{\boldsymbol{\theta}_{\rm inf},\boldsymbol{\theta}_{\rm reh}\}$. Within a given inflationary model, say $\mathcal{M}$, there is a deterministic relationship $\epsilon_{i*}(\boldsymbol{\theta}_{\rm inf},\boldsymbol{\theta}_{\rm reh})$ between the values of the Hubble-flow functions and the model parameters. Notice the presence of the reheating parameters for the reasons explained in Section 3.3. One can therefore add to the inference problem a new set of hyperparameters, the $\boldsymbol{\varepsilon} = \{\varepsilon_0,\varepsilon_1,\dots\}$, whose values are precisely defined to be the functional forms $\epsilon_{i*}(\boldsymbol{\theta}_{\rm inf},\boldsymbol{\theta}_{\rm reh})$ for $i \geq 1$ and $\varepsilon_0 = P_*$ when one is concerned with a particular

model $\mathcal{M}$, but are unspecified otherwise. Explicitly, the hyperparameters are deterministic and satisfy

$$P(\boldsymbol{\varepsilon}|\boldsymbol{\theta}_{\rm inf},\boldsymbol{\theta}_{\rm reh},\mathcal{M}) \equiv \delta(\varepsilon_0 - P_*)\prod_i \delta(\varepsilon_i - \epsilon_{i*})\,. \tag{3.25}$$

If we don't specify the model, it is still possible to perform data analysis based on the slow-roll power spectra of Eqs. (3.2) and (3.3), now parameterized by the $\boldsymbol{\varepsilon}$ instead of the ϵ_{i*}, still with $\varepsilon_0 = P_*$, and we will refer to this model-free situation as hypothesis I. From MCMC exploration, one can determine the full posterior distribution $P(\boldsymbol{\theta}_{\rm s},\boldsymbol{\varepsilon}|\boldsymbol{D},I)$, under the model-free hypothesis I.

The posterior for the primordial parameters associated with $\mathcal{M}$ is obtained by marginalizing over all the other parameters and reads

$$P(\boldsymbol{\theta}_{\rm inf},\boldsymbol{\theta}_{\rm reh}|\boldsymbol{D},\mathcal{M}) = \int P(\boldsymbol{\theta}_{\rm inf},\boldsymbol{\theta}_{\rm reh},\boldsymbol{\theta}_{\rm s},\boldsymbol{\varepsilon}|\boldsymbol{D},\mathcal{M},I)\,{\rm d}\boldsymbol{\varepsilon}{\rm d}\boldsymbol{\theta}_{\rm s}. \tag{3.26}$$

Using the Bayes' theorem, the right-hand side can be rewritten as

$$P(\boldsymbol{\theta}_{\rm inf},\boldsymbol{\theta}_{\rm reh},\boldsymbol{\theta}_{\rm s},\boldsymbol{\varepsilon}|\boldsymbol{D},\mathcal{M},I) = \frac{P(\boldsymbol{\theta}_{\rm inf},\boldsymbol{\theta}_{\rm reh},\boldsymbol{\theta}_{\rm s},\boldsymbol{\varepsilon}|\mathcal{M},I)\,P(\boldsymbol{D}|\boldsymbol{\theta}_{\rm inf},\boldsymbol{\theta}_{\rm reh},\boldsymbol{\theta}_{\rm s},\boldsymbol{\varepsilon},\mathcal{M},I)}{P(\boldsymbol{D}|\mathcal{M},I)}\,, \tag{3.27}$$

which can be further simplified using the product rule:

$$P(\boldsymbol{\theta}_{\rm inf},\boldsymbol{\theta}_{\rm reh},\boldsymbol{\theta}_{\rm s},\boldsymbol{\varepsilon}|\mathcal{M},I) = P(\boldsymbol{\theta}_{\rm inf},\boldsymbol{\theta}_{\rm reh},\boldsymbol{\theta}_{\rm s}|\mathcal{M},I)\,P(\boldsymbol{\varepsilon}|\boldsymbol{\theta}_{\rm inf},\boldsymbol{\theta}_{\rm reh},\boldsymbol{\theta}_{\rm s},\mathcal{M},I)\,. \tag{3.28}$$

Assuming that I is generic enough to contain all models, for inflation occurring according to model $\mathcal{M}\subset I$, the last term is conditioned by $\mathcal{M}$ only and one can use Eq. (3.25). Moreover, assuming that $\{\boldsymbol{\theta}_{\rm inf},\boldsymbol{\theta}_{\rm reh}\}$ and $\{\boldsymbol{\theta}_{\rm s}\}$ are independent, one gets

$$P(\boldsymbol{\theta}_{\rm inf},\boldsymbol{\theta}_{\rm reh},\boldsymbol{\theta}_{\rm s},\boldsymbol{\varepsilon}|\mathcal{M},I) = P(\boldsymbol{\theta}_{\rm inf},\boldsymbol{\theta}_{\rm reh}|\mathcal{M})\,P(\boldsymbol{\theta}_{\rm s}|I)\,\delta(\varepsilon_0 - P_*)\prod_i \delta(\varepsilon_i - \epsilon_{i*})\,. \tag{3.29}$$

Plugging this expression into Eq. (3.27), and provided that the full likelihood has no explicit dependence on $\{\boldsymbol{\theta}_{\rm inf},\boldsymbol{\theta}_{\rm reh}\}$, Eq. (3.26) becomes

$$P(\boldsymbol{\theta}_{\rm inf},\boldsymbol{\theta}_{\rm reh}|\boldsymbol{D},\mathcal{M}) = \frac{\mathcal{L}_{\rm eff}[\boldsymbol{D}|P_*(\boldsymbol{\theta}_{\rm inf},\boldsymbol{\theta}_{\rm reh}),\epsilon_{i*}(\boldsymbol{\theta}_{\rm inf},\boldsymbol{\theta}_{\rm reh})]\,\pi(\boldsymbol{\theta}_{\rm inf},\boldsymbol{\theta}_{\rm reh})}{\mathcal{E}(\boldsymbol{D}|\mathcal{M})}\,, \tag{3.30}$$

where

$$\mathcal{L}_{\rm eff}(\boldsymbol{D}|\boldsymbol{\varepsilon}) \equiv \frac{P(D)}{\mathcal{E}(\boldsymbol{D}|I)}\int P(\boldsymbol{D}|\boldsymbol{\theta}_{\rm s},\boldsymbol{\varepsilon})\,P(\boldsymbol{\theta}_{\rm s}|I)\,{\rm d}\boldsymbol{\theta}_{\rm s}. \tag{3.31}$$

Once I is set, the overall factor will be a constant for all $\mathcal{M}$ and will disappear in the Bayes' factors of Eq. (3.23). As announced, we have dramatically reduced the dimensionality of the likelihood. The determination of $\mathcal{L}_{\rm eff}$ is complex, but, once done and fitted, Bayesian data analysis for any model $\mathcal{M}$ can be performed with Eq. (3.30) only. Provided the machine learned $\mathcal{L}_{\rm eff}$ is fast and accurate, considerable speed-up can be achieved in the determination of the posteriors $P(\boldsymbol{\theta}_{\rm inf},\boldsymbol{\theta}_{\rm reh}|\boldsymbol{D},\mathcal{M})$ and evidences $\mathcal{E}(\boldsymbol{D}|\mathcal{M})$.

An important remark is that hyperparameters to which the data are not sensitive can be marginalized over instead of being kept in the effective likelihood. Conversely, if one of the primordial parameters, say θ_1, would enter explicitly in the full likelihood (i.e., not only via the ϵ_{i*} functions), it could be kept as a new parameter in $\mathcal{L}_{\rm eff}$ thereby ensuring no information

loss. As shown in the next section, the current data are not sensitive to the values of ε_4, and even though our full data analysis is based on third-order power spectra, and includes ε_4, the effective likelihood in Eq. (3.24) does not include ε_4 anymore. Let us stress that defining $\mathcal{L}_{\rm eff}$ by marginalizing over ε_4, as opposed to drop ε_4 from the very beginning, ensures the robustness of our results with respect to all possible third-order slow-roll corrections.

3.6 Workflow

As detailed in the previous sections, the analysis workflow is bootstrapped by a complete data analysis of the cosmological data using the third-order slow-roll primordial power spectra of Eqs. (3.2) and (3.3). This step, described in Section 4, allows us to determine $\mathcal{L}_{\rm eff}$, which is then fitted over the four-dimensional space $\{P_*, \varepsilon_1, \varepsilon_2, \varepsilon_3\}$ using machine-learning methods.

Next, as presented in Section 5, for all models $\mathcal{M}$ under scrutiny, we determine the evidence $\mathcal{E}(\boldsymbol{D}|\mathcal{M})$, the information gain and other relevant statistical measures, by nested sampling methods running over the machine-learned $\mathcal{L}_{\rm eff}$.

4 Third-order slow-roll data analysis

In this section, we present novel results coming from a full data analysis based on the third-order slow-roll primordial power spectra and using the latest CMB and BAO data. Some technical details are given as this analysis constitutes the first attempt to constrain ε_4 while providing more robust bounds on ε_1, ε_2 and ε_3 as they are marginalized over ε_4.

The computation of the full posterior probability distribution $P(\boldsymbol{\theta}_{\rm s}, P_*, \varepsilon_1, \varepsilon_2, \varepsilon_3, \varepsilon_4|\boldsymbol{D}, I)$ has been achieved using a modified version of the public Fortran code `COSMOMC` [91]. It has been interfaced with a modified version of the `CAMB` code [93], in which we have replaced the initial power spectrum module by a new slow-roll module encoding the third-order slow-roll power spectra of Eqs. (3.2) and (3.3).

The last public version of the `COSMOMC` code dates back from 2022 and we had to update various parts of the code to include newest data. Our choice of using `COSMOMC` instead of more recent and, possibly, more user-friendly Monte-Carlo-Markov-Chains samplers, such as the `Cobaya` Python code [92], has been motivated by the needs to robustly run massively parallel MCMC to get tens of million of samples over more than fifty dimensions. These unusually large numbers are indeed needed to properly sample the four-dimensional likelihood $\mathcal{L}_{\rm eff}(\boldsymbol{D}|P_*, \varepsilon_1, \varepsilon_2, \varepsilon_3)$, which is fed to a machine-learning algorithm afterwards. The four-dimensional samples to determine $\mathcal{L}_{\rm eff}$ have been computed by marginalizing the full posterior on all but the four dimensions $\{P_*, \varepsilon_1, \varepsilon_2, \varepsilon_3\}$. For this purpose, we have coded and used N-dimensional marginalization function within the `GetDist` Python code [54, 94, 95].

4.1 Data sets

The cosmological data sets $\boldsymbol{D}$ used are the latest Planck satellite data [96], the BICEP/Keck array B-mode polarization 2021 measurements [97], the South Pole Telescope third generation TE and EE angular power spectra [98], and a compilation of Baryonic Acoustic Oscillations data from the Sloan Digital Sky Survey IV [99, 100].

In more details, for the Planck data, we have used the 2020 post-legacy release with the small angular scales TT, TE and EE power spectra extracted from the `PR4/NPIPE` maps [101, 102]. The likelihood is the `CamSpec` code [103], in its Fortran version 12.6, and discussed in Ref. [104]. For the low multipoles, we have used the official `SimAll` likelihood

built on the large scales EE polarization measurements, also refereed to as the `lowE` data [96]. Finally, we have also included the lensing potential measurements as described in Ref. [105].

The BICEP/Keck B-mode data are from the latest release presented in Ref. [97], using both the WMAP and Planck dust tracers for map cleaning [13, 101]. The likelihoods are public, provided by the BICEP/Keck team, and they are ready-to-use for `COSMOMC`.

The South Pole Telescope data are from the SPT-3G survey described in Ref. [106] and consist in high multipoles measurements for the TE and EE angular power spectra. The likelihood codes for `COSMOMC` are provided by the SPT collaboration and have been incorporated within the multiplatform library `clik`[1].

The Baryon Acoustic Oscillation data are the DR16 compilation, built using multiple tracers: the Main Galaxy Sample, the Luminous Red Galaxies, the Emission Line Galaxies, the Quasars and Lymann-α forests from eBOSS [107–113]. The likelihood data files are public and provided by the SDSS collaboration. They have been used to upgrade the BAO likelihood module provided with `COSMOMC`.

In order to maximize the constraining power of the combined data sets, we have chosen not to include the Atacama Cosmology Telescope data [114, 115], due to a possible small tension with Planck [116], in addition to some optimization issues in calling a Python likelihood from `COSMOMC`. Also, within the Planck data sets, we have excluded the first thirty low multipoles from the TT channel (the so-called `lowl` likelihood) due to their known under power compared to the higher multipoles [117]. Notice that the low multipole data in the TE and EE channels are included and they have been shown to be, at least, as powerful as the TT channel in constraining the shape of the primordial power spectra, while not being in tension with the small scales [118].

4.2 Priors

In addition to assume third-order slow-roll power spectra generating both scalar and tensor perturbations, we consider a spatially flat Friedmann-Lemaître model described by the usual four cosmological parameters. They are the density parameter for baryons $\Omega_{\rm b}h^2$, for cold dark matter $\Omega_{\rm dm}h^2$ (both multiplied by h^2), $100\theta_{\rm MC}$, the angular size of the sound radius at last scattering (multiplied by 100), and the reionization optical depth τ. As already mentioned, these are complemented by the four Hubble-flow parameters $\{P_*, \varepsilon_1, \varepsilon_2, \varepsilon_3\}$. In addition to these eight fundamental cosmological parameters, the data sets come with a relatively large number of nuisance and foreground parameters. There is little interest to enumerate them here, their priors are already set in their associated likelihoods and are discussed at length in the references cited in Section 4.1. In total, the nuisance and foreground parameters amount to 49 dimensions.

Concerning the priors for the four cosmological parameters, they have been taken as flat distributions, wide enough to encompass their currently preferred values $\Omega_{\rm b}h^2 \in [0.05, 0.1]$, $\Omega_{\rm dm}h^2 \in [0.01, 0.99]$, $100\theta_{\rm MC} \in [0.5, 10]$, $\tau \in [0.01, 0.8]$. An additional hard prior is set on the Hubble parameter today $H_0 \in [40, 100]$. Although we do not expect the primordial parameters to be sensitive to the following settings, non-linear lensing corrections have been switched on in `CAMB` while we have let to the default various other parameters: the number of effective neutrinos is 3.046 (as for the Planck analysis), the sum of their masses is set to 0.06 eV, and the Helium mass fraction is enforced from BBN constraints. For the primordial parameters, the pivot scale is set at $k_* = 0.05\,{\rm Mpc}^{-1}$. The scalar amplitude, P_*, is sampled

[1] https://github.com/benabed/clik

from a flat prior on $\ln\left(10^{10}P_*\right) \in [2.4, 3.6]$, largely encompassing the required amplitude to match the one of the CMB fluctuations. The order of magnitude of the first Hubble-flow parameter is unknown, it is positive definite and it mostly determines the tensor-to-scalar ratio. As such, it has been sampled from a Jeffreys' prior, set as a flat prior on $\log(\varepsilon_1) \in [-5, -0.7]$ (decimal logarithm). For the three other Hubble-flow functions, we have chosen a flat prior $\varepsilon_{2,3,4} \in [-0, 2, 0.2]$ in order to enforce the slow-roll condition that these parameters should be smaller than unity. However, as we discuss in Section 4.4, this choice could be questioned for the parameter ε_3. Indeed, as shown in the next section, our data sets are putting some constraints on ε_3: its posterior distribution is not flat in the range $[-0, 2, 0.2]$ but it is not vanishing at the boundaries. This necessarily triggers some sensitivity with respect to the prior range. For this reason, we have performed two complete MCMC analysis, one with the aforementioned prior choices, referred to as "strictly slow roll" (labeled as "Strict SR" in the figures), and another one with the extended prior $\varepsilon_3 \in [-1, 1]$, which saturates the slow-roll conditions and referred to as "extended slow roll" (labeled as "Extended SR").

4.3 Marginalized posteriors

The MCMC chains has been generated using `COSMOMC`, running in parallel over 96 `MPI`-processes, each processor running the Boltzmann solver `CAMB`, `OpenMP`-parallelized over 8 threads (processors AMD `EPYC-7742`). The chains have been stopped once the number of recorded samples reached 25 million, for which the R-statistics criterion of convergence (Gelman-Rubin) is as low as 10^{-3} [91].

In Fig. 1, we have plotted the marginalized posterior probability distribution for all eight cosmological parameters, including the Hubble-flow ones. These are obtained by marginalizing over the other nuisance parameters, the one-dimensional posteriors of which can be found in Appendix A. Fig. 2 shows the most interesting two-dimensional posteriors in the Hubble-flow parameter space. These posteriors show that the fourth Hubble flow function is unconstrained by the data, its posterior is flat. On the contrary, the posterior for ε_3 is peaked around vanishing values and this shows that the current CMB and BAO data are sensitive to a running of a spectral index typical of slow roll. As can be checked in Fig. 2, ε_3 is correlated with ε_2, and the one- and two-dimensional posteriors are not vanishing at the boundary of the strict slow-roll prior range $[-0.2, 0.2]$.

Let us notice the interesting posterior for $\log(\varepsilon_1)$ which is clearly peaked at a value well inside our prior range. We measure, indeed, a weak statistical preference, at one-sigma, for the one-dimensional posterior

$$\log(\varepsilon_1) > -3.9, \qquad (68\%\ \texttt{CL}), \tag{4.1}$$

moving down to $\log(\varepsilon_1) > -4.9$ at 95% CL. We have checked that this excess is coming from the BICEP/Keck data and it means that, in spite of the marginalization over dust contamination, there is still some B-mode excess remaining. This effect was visible on the posteriors presented by the Planck collaboration [15], but with the latest data, and using slow-roll power spectra, its significance has increased. Let us also stress that we have chosen a Jeffreys' prior for ε_1, which naturally favor small values. This excess is more pronounced when one assumes a flat prior instead. This is illustrated in Fig. 5 where we have used importance sampling to re-weight the samples according to a flat prior on ε_1 and computed the power law parameter posteriors. These are the spectral index $n_{\rm S}$, the running of the spectral index $\alpha_{\rm S}$ and the tensor-to-scalar ratio r_ϵ. The one-sigma contour is closed in all

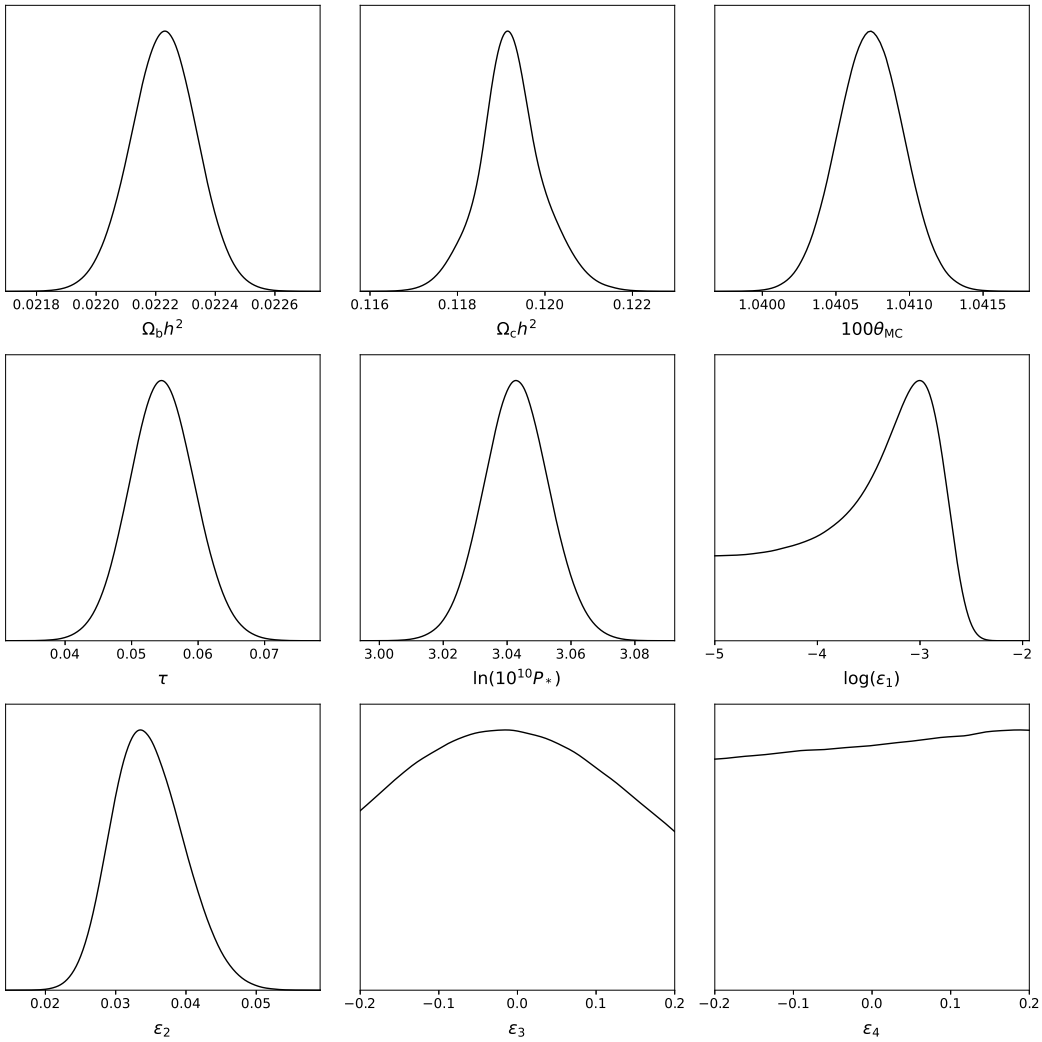

Figure 1. One-dimensional marginalized posterior distributions for the bare cosmological parameters and the third-order Hubble flow parameters P_*, ε_1, ε_2, ε_3 and ε_4. The data sets $\boldsymbol{D}$ used are described in Section 4.1 and the prior is strictly slow-roll $\varepsilon_3 \in [-0.2, 0.2]$. Notice the sensitivity of the data to ε_3 whereas ε_4 is unconstrained (see also Fig. 2). The peak in the posterior for $\log(\varepsilon_1)$ shows that, despite marginalization of the BICEP/Keck data over dust contamination, there remains in the current data a B-mode excess which is slightly favoring, at one-sigma, tensor modes of slow-roll inflationary origin (see text).

two-dimensional posteriors involving the tensor-to-scalar ratio r_ϵ. Also, let us stress that this small residual excess is robust to third-order slow-roll corrections, which are automatically marginalized over when looking at the $\log(\varepsilon_1)$ posterior. Still, one-sigma is non-statistically significant, and, at three-sigma, only an upper bound remains

$$\log(\varepsilon_1) < -2.6, \qquad (98\% \text{ CL}). \tag{4.2}$$

Still, it will be worth paying attention to this trend in the future, since the favored values found here will be well inside the sensitivity of the LiteBIRD satellite [119].

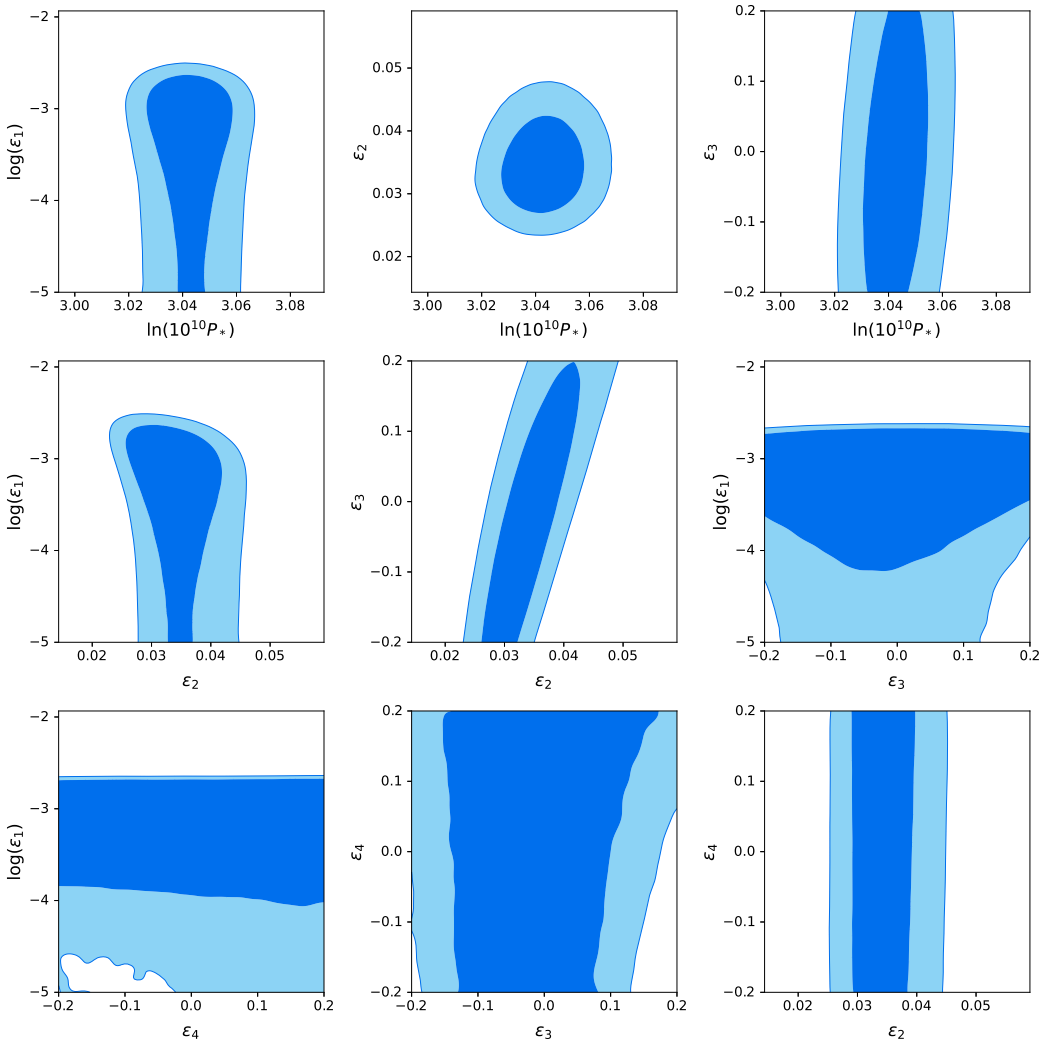

Figure 2. Two-dimensional marginalized posterior distributions within the Hubble-flow parameter space for the strict slow-roll prior $\varepsilon_3 \in [-0.2, 0.2]$ (see also Fig. 1).

In order to quantify the effects associated with the choice of the ε_3 prior, we have duplicated the analysis starting from the extended prior choice $\varepsilon_3 \in [-1, 1]$. The marginalized posteriors are represented in Figs. 3 and 4 and compared to the ones of Figs. 1 and 2. The bare cosmological parameters are unaffected, as expected, but the posterior for ε_2 is slightly enlarged due to the degeneracies existing between ε_2 and ε_3, these ones being enhanced when the latter take values close to unity. Similar degeneracies between ε_3 and ε_4 are also responsible for the tiny positive bias visible in the one-dimensional posterior of ε_4 in Fig. 3. Let us stress that the posterior for ε_1 is unchanged, confirming the robustness of the peak amplitude with respect to ε_3. The one-sigma bound of Eq. (4.1) ends up being unaffected by the extended prior choice[2]. Finally, the posterior for ε_3 is now well bounded within the

[2]By the very nature of an improper Jeffreys' prior, Eq. (4.1) has, however, some sensitivity to the choice of the lower bound of the $\log(\varepsilon_1)$ prior. Assuming much smaller minimal values of $\log(\varepsilon_1)$ would decrease its significance.

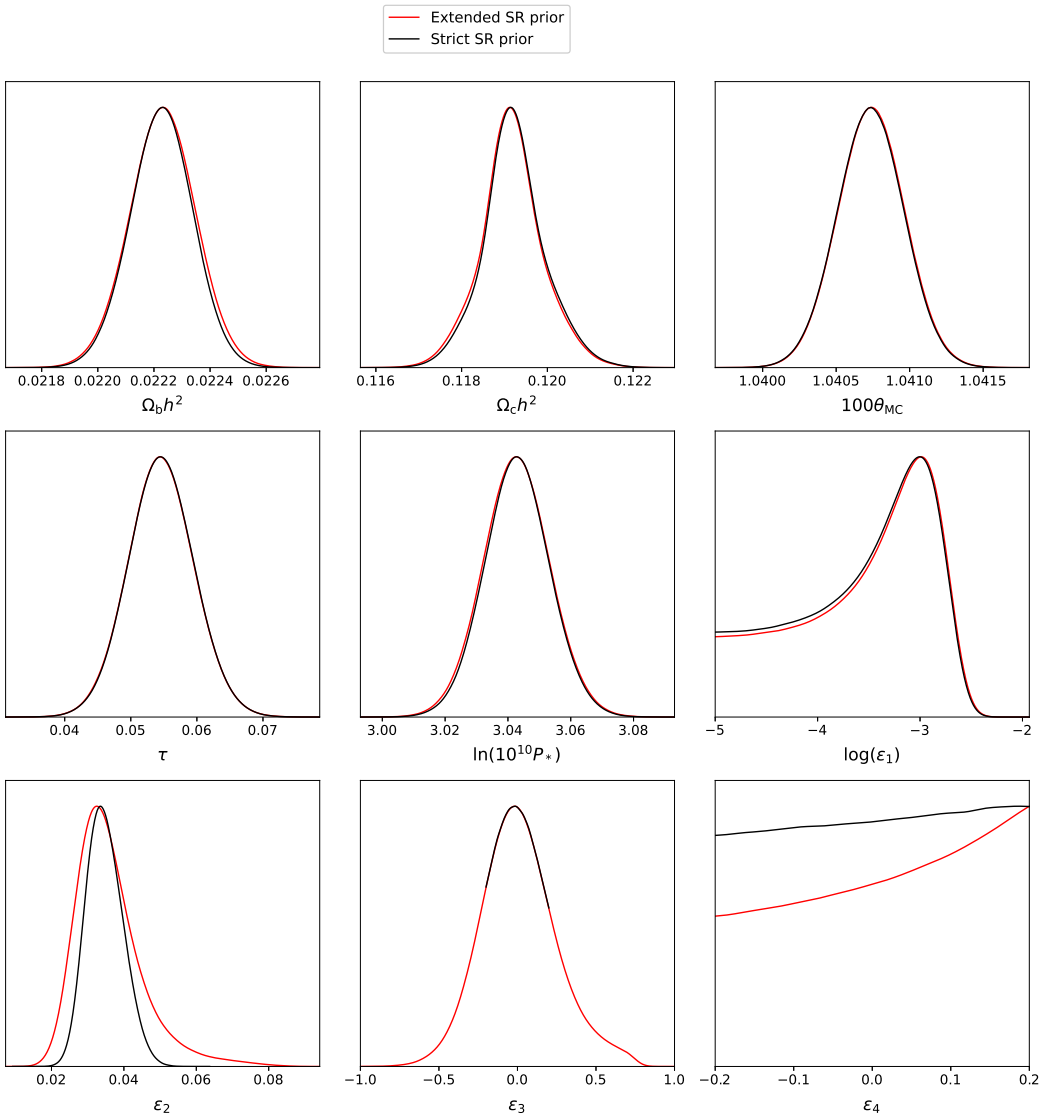

Figure 3. One-dimensional marginalized posterior distributions, normalized to their maximum, for the bare cosmological parameters and the third-order Hubble-flow parameters for the extended slow-roll prior on $\varepsilon_3 \in [-1, 1]$ (red). The black curves are the one- and two-sigma contours of Fig. 1 obtained under the strict prior $\varepsilon_3 \in [-0.2, 0.2]$. The posterior of ε_3 is well bounded within the prior. Notice the appearance of a tail in the ε_2 posterior due to its correlations with ε_3.

extended prior range $[-1, 1]$, which confirms that the current data are strongly disfavoring any running which is not of slow-roll magnitude [15]. We find the mean value $\langle\varepsilon_3\rangle = 0.015$ in the credible interval

$$-0.44 < \varepsilon_3 < 0.55, \qquad (95\%\ \texttt{CL}). \tag{4.3}$$

4.4 Other consistency checks

Our results have been cross-checked using the Planck official likelihood `Plik` running on the Planck 2018 legacy data [96, 120]. The posteriors are all compatible and we do not observe

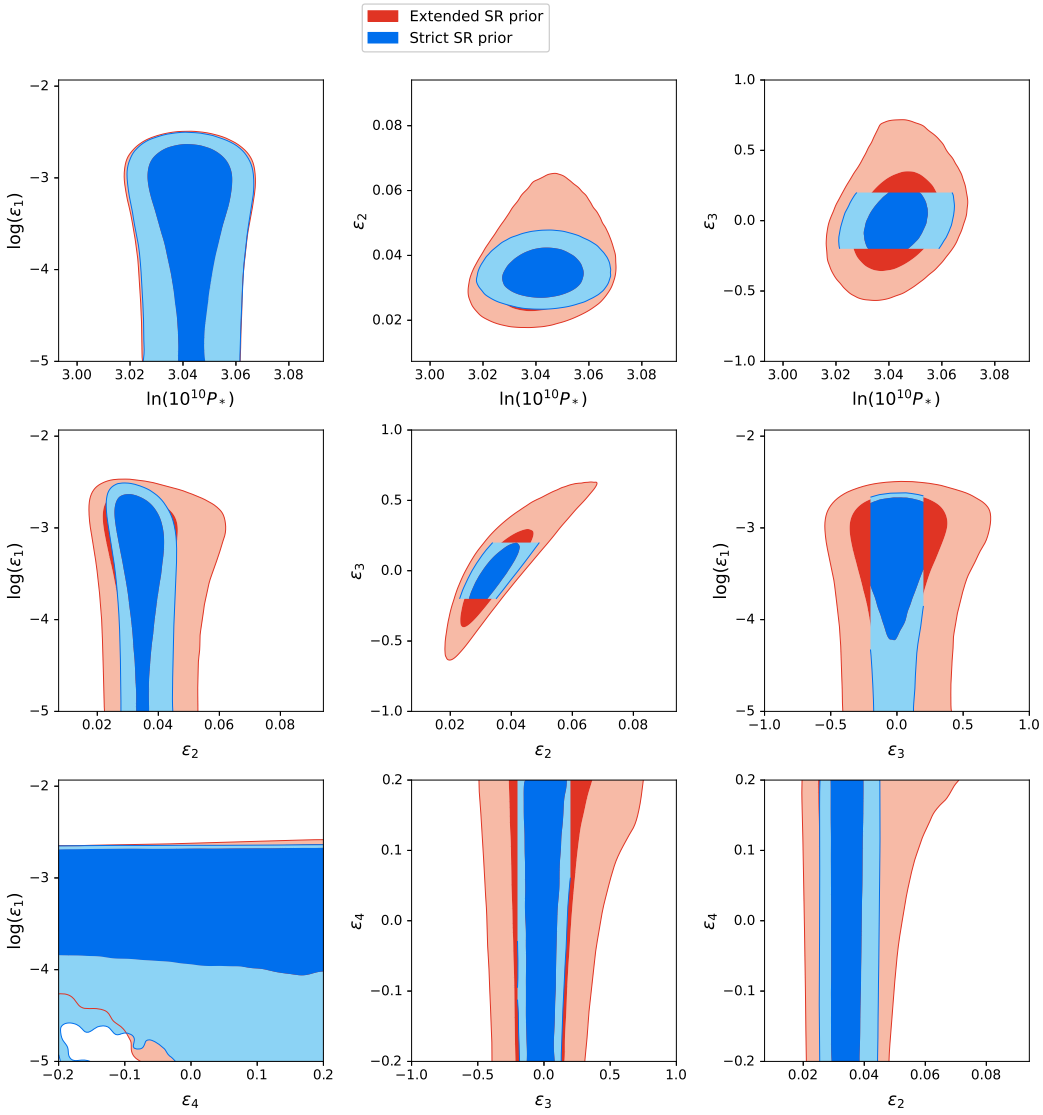

Figure 4. Two-dimensional marginalized posterior distributions within the Hubble-flow parameter space for the extended slow-roll prior range $\varepsilon_3 \in [-1, 1]$ and compared to the strict slow-roll posteriors (in red), see also Fig. 1. Notice the wider posterior for ε_2 and the slight bias induced on the posterior for ε_4.

more than half a sigma degradation in any parameter constraints by doing so. We have also cross-checked our implementation of the BAO likelihoods for `COSMOMC` by comparing the posteriors to small MCMC explorations made using the Python package `Cobaya` [92].

In the following, we marginalize the 25 million samples over 54 dimensions to determine the four-dimensional posterior probability distribution $P(P_*, \varepsilon_1, \varepsilon_2, \varepsilon_3|\boldsymbol{D})$ that will be used as the effective likelihood to perform Bayesian model comparison in Section 5. Although not explicit in the following, all computations have been duplicated in order to quantify the possible effects associated with the strict and extended prior choices on ε_3. As mentioned above, because ε_4 is unconstrained, it is part of the parameter set over which we marginalize

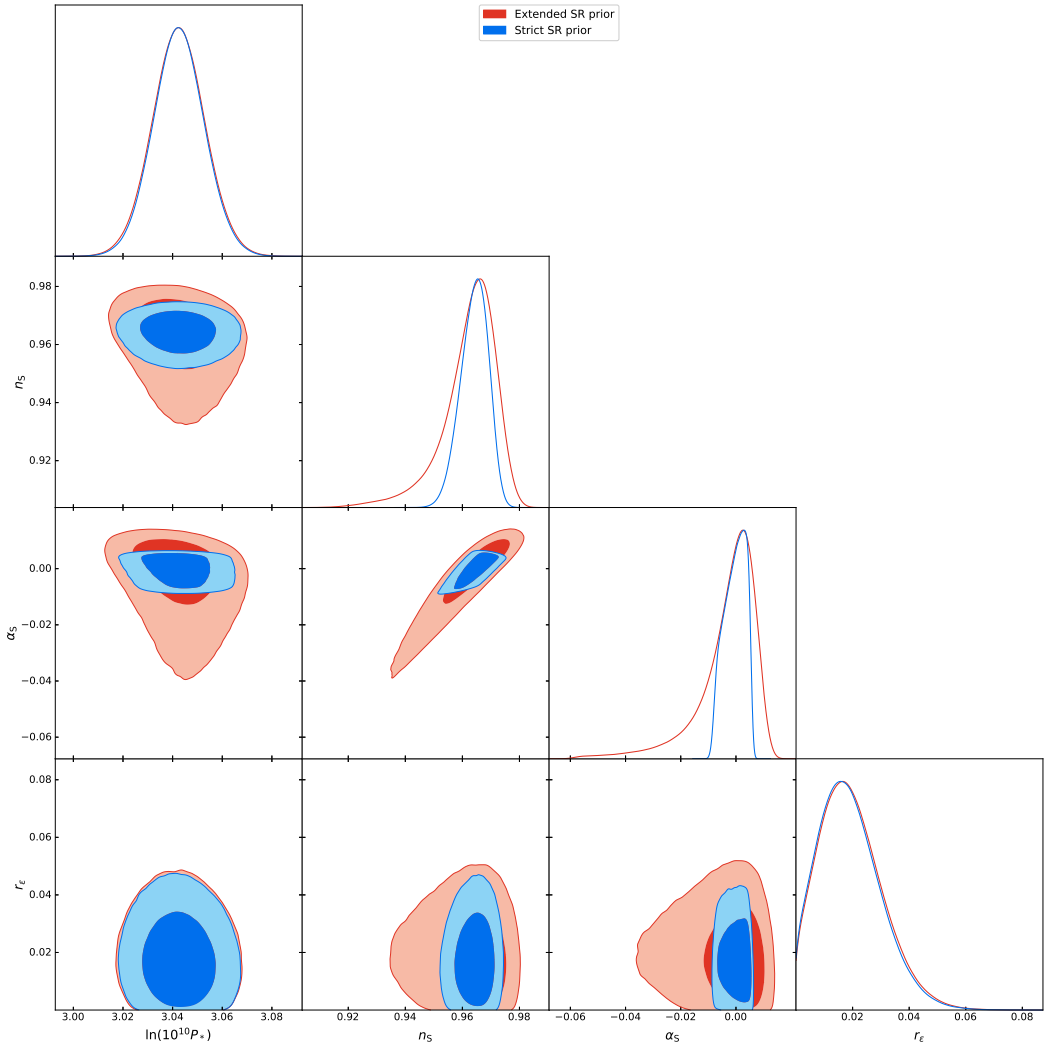

Figure 5. One- and two-dimensional marginalized posterior distributions within the power-law parameter space $\{P_*, n_S, r_\epsilon, \alpha_S\}$ where n_S is the spectral index, r_ϵ the tensor-to-scalar ratio and α_S the running of the spectral index. These have been obtained by importance sampling from the Hubble-flow posteriors, the samples have been re-weighted to correspond to a flat prior on ε_1. As such the prior *is not* associated with a power-law shaped spectrum but with Eqs. (3.2) and (3.3). The colors are the same as in Fig. 4 and correspond to the strict and extended prior choices on ε_3.

the posteriors.

4.5 Effective likelihood

Up to a multiplicative constant, $\mathcal{L}_{\rm eff} \propto P(P_*, \varepsilon_1, \varepsilon_2, \varepsilon_3|\boldsymbol{D})$ and its two-dimensional slices are already represented in Figs. 2 and 4. In order to "fit" this four-dimensional function, we have first determined $P(P_*, \varepsilon_1, \varepsilon_2, \varepsilon_3|\boldsymbol{D})$, binned over 20^4 bins, as computed by the N-dimensional `GetDist` marginalization functions [94]. Given 25 millions MCMC samples, had the bins been equally sampled (which is not the case for MCMC), each of them would have contained typically 10^2 samples and this yields a typical 10% error per bin. This binned posterior is

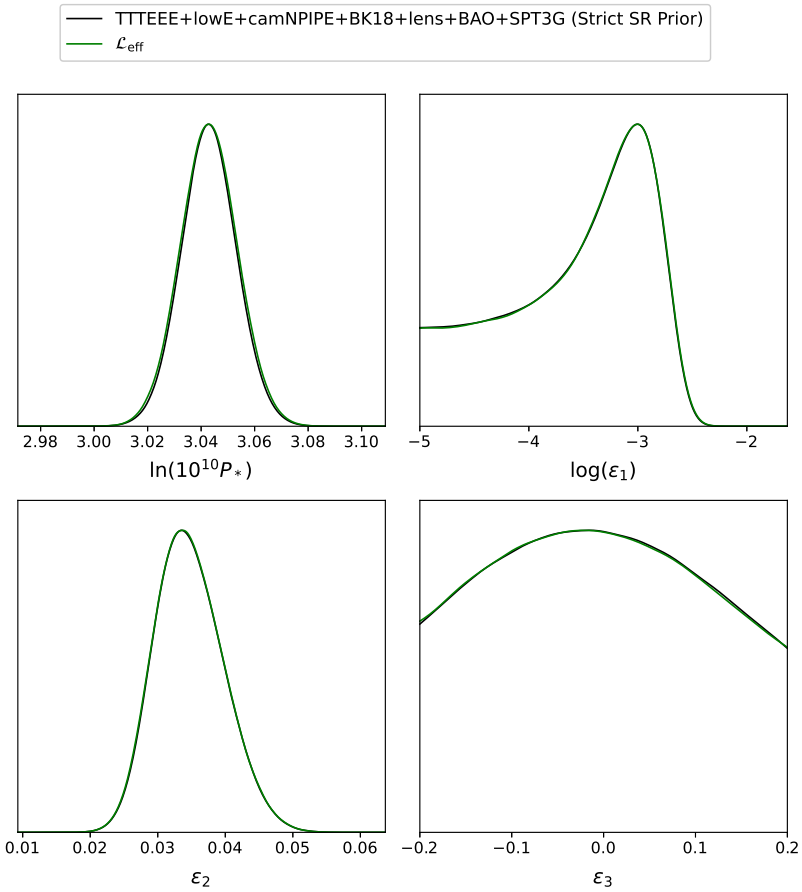

Figure 6. Comparison between the one-dimensional posteriors in the Hubble-flow parameter space $\{P_*, \varepsilon_1, \varepsilon_2, \varepsilon_3\}$ obtained by nested sampling over our machine-learned $\mathcal{L}_{\rm eff}$ (green), and the exact ones (black) of Fig. 1, the latter being obtained from marginalization of the full likelihood over the 54-dimensions. The differences are barely visible, see also Fig. 7.

thus not very practical per se but can be efficiently used to train a basic-machine learning algorithm to smoothly fit its four-dimensional shape. We have used a modified quadratic Shepard's method [121, 122], which can be viewed as a neural network having one input layer of four nodes (P_*, ε_1, ε_2, ε_3), one internal layer of 300 nodes, and, a single node output layer providing the value of $\mathcal{L}_{\rm eff}$. Determining the optimal weights has been done using a least square fitting method running on the binned posterior.

As with any neural networks, there is no definite way to ensure the accuracy of the fitted multivariate function, a priori. Therefore, in order to validate that the machine-learned $\mathcal{L}_{\rm eff}(P_*, \varepsilon_1, \varepsilon_2, \varepsilon_3)$ is accurate enough for posteriors and evidences, we have probed its multidimensional shape using the nested sampling algorithm `PolyChord` [88, 89] (running with 40000 live points). It has been cross-checked with another nested sampler, `MultiNest` [87], ran with 100000 live points. Using nested sampling, as opposed to MCMC, allows us to probe the tails of $\mathcal{L}_{\rm eff}$ thereby testing if the neural network provides a proper fit in regions not having many samples to start with. In addition, the nested sampling gives accurate information on the minimal values reached by $\mathcal{L}_{\rm eff}$ and these values are also the lower bound

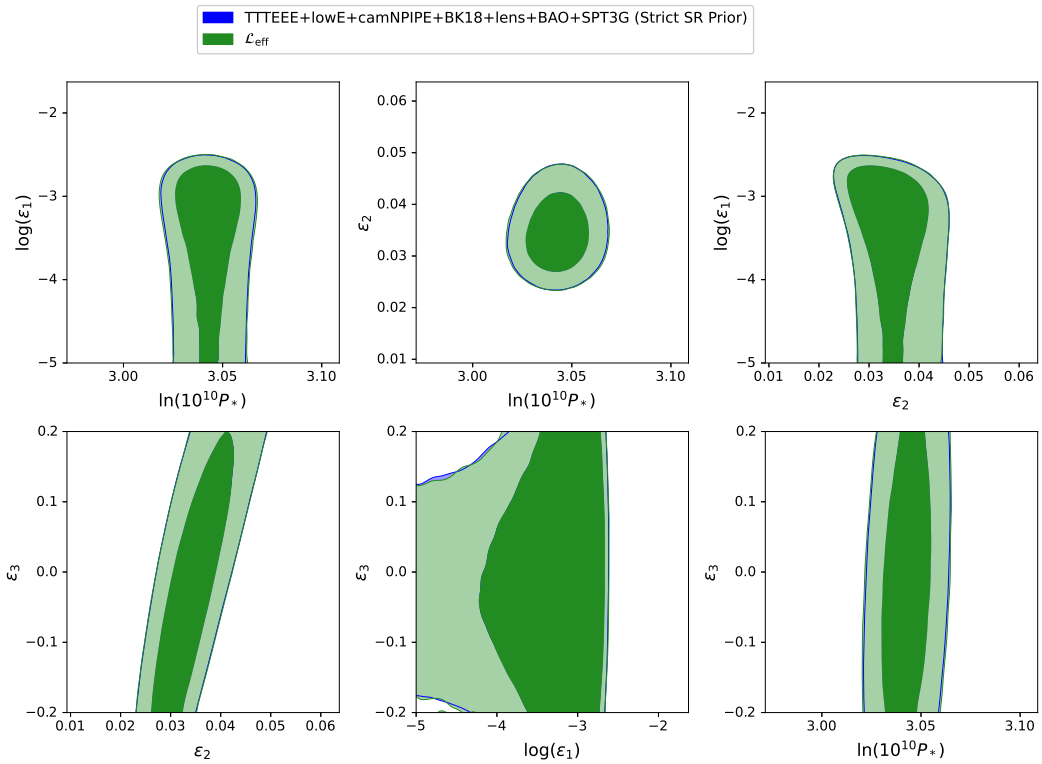

Figure 7. Comparison between the two-dimensional posteriors in the Hubble-flow parameter space $\{P_*, \varepsilon_1, \varepsilon_2, \varepsilon_3\}$ obtained by nested sampling over our machine-learned $\mathcal{L}_{\rm eff}$ (green) to the exact ones (blue) of Fig. 2.

of the minimal evidence ratios reachable with our effective likelihood. We find $\mathcal{L}_{\rm eff}^{\rm min} \simeq e^{-11}$ (for a maximum likelihood $\mathcal{L}_{\rm eff}^{\rm max} = 1$). Let us mention that we extrapolate $\mathcal{L}_{\rm eff}$ outside its prior definition by a constant value along the $\log(\varepsilon_1) < -5$ direction, realistic inflationary models could indeed generate very low tensor-to-scalar ratios. Moreover, within the strict slow-roll prior, we have to deal with a non-vanishing $\mathcal{L}_{\rm eff}$ along the ε_3 direction. We have made the most conservative choice of extrapolating $\mathcal{L}_{\rm eff}$ by a constant value for $|\varepsilon_3| > 0.2$. For the extended prior choice, there is no need to do any extrapolation as the likelihood vanishes outside the prior of ε_3.

In Figs. 6 and 7 we compare the one- and two-dimensional posteriors obtained by nested-sampling the machine-learned $\mathcal{L}_{\rm eff}$ (green curves) to the ones of Figs. 1 and 2, the latter having being obtained by full MCMC marginalization of the exact posteriors. There is no visible difference. In Section 5, we use this machine-learned $\mathcal{L}_{\rm eff}$ in Eq. (3.30) to carry out fast parameter estimation of $\{\boldsymbol{\theta}_{\rm inf}, \boldsymbol{\theta}_{\rm reh}\}$ for all slow-roll models $\mathcal{M}$ and to compute their evidences $\mathcal{E}(\boldsymbol{D}|\mathcal{M})$.

5 Bayesian model comparison

In this section, we perform parameter estimation and model comparison for 287 models of single-field slow-inflation along the lines discussed in Section 3. The theoretical motivations, derivation of the $\epsilon_{v_i}(\phi)$ functions, and various other technical considerations for each of

these models can be found in the "Opiparous Edition" of the *Encyclopædia Inflationaris* in Ref. [56]. Let us stress that for a given potential in Ref. [56], there are usually more than one inflationary model, as various different theoretical setups can yield the same field potential, with different values, and hence priors, for the primordial parameters $\boldsymbol{\theta}_{\rm inf}$ and $\boldsymbol{\theta}_{\rm reh}$. These priors are listed in Appendix B.

Let us summarize how the calculations are performed. Having at our disposal the reheating Eqs. (3.11) to (3.18), and the `ASPIC` library, we can quickly compute $P_*(\boldsymbol{\theta}_{\rm inf}, \boldsymbol{\theta}_{\rm reh})$ and $\epsilon_{1,2,3*}(\boldsymbol{\theta}_{\rm inf}, \boldsymbol{\theta}_{\rm reh})$ for each of the 287 models. Plugging these numbers into the machine-learned effective likelihood $\mathcal{L}_{\rm eff}(\boldsymbol{D}|P_*, \varepsilon_1, \varepsilon_2, \varepsilon_3)$, it is, in principle, straightforward to derive the posteriors of the primordial parameters $P(\boldsymbol{\theta}_{\rm inf}, \boldsymbol{\theta}_{\rm reh}|\mathcal{M})$ as well as the evidence $\mathcal{E}(\boldsymbol{D}|\mathcal{M})$ using Eqs. (3.20) and (3.30).

For this purpose, we have developed a modern Fortran code, named `Bayaspic`, which is interfacing the machine-learned likelihood to the `ASPIC` library. This code is also a nested sampler which is using `PolyChord` or, as a user choice, `MultiNest`. The `Bayaspic` code also deals with the prior choices and is in charge of scheduling computations over the 287 models. For this purpose, it is parallelized using the Message Passing Interface (`MPI`) and this allows us to perform nested sampling on many models at the same time. The Hubble-flow parameters can take quite different amounts of computing time to be evaluated, thereby triggering some differences in the running times for each of the inflationary models. The fastest-to-compute models, sampled with `PolyChord` and 20000 live points, are processed in about ten minutes of CPU-time. The requested precision on their evidence is set at $Z_{\rm tol} = 10^{-3}$, and this generates chains containing a few hundred thousand samples. The slowest to compute is named Dual Inflation (see Appendix B.4), a model for which none of the slow-roll calculations can be done analytically, and it takes two days for the nested sampling to reach the same precision. At the end of the day, even if straightforward, the task is numerically challenging and the amount of data produced under the form of nested-sampled chains is about 300 GB.

These chains are then analyzed using a code we have developed, named `infdistbayes`, coded as various Python modules and using some functions built over the `GetDist` and `anesthetic` codes [94, 123]. Analyzing multiple chains at once is basically parallelized with a Bash script and the output of `infdistbayes` are 287 one- and two-dimensional posteriors, figures, and various statistical outputs, including the Bayesian evidences and the Bayesian dimensionality [124].

As detailed in Section 5.4, the code `infdistbayes` is also used to compute the information gain on the reheating parameter (or any other parameters) directly, i.e., by integrating the marginalized posteriors. In order to do so, one needs to know the prior distributions $\pi(\boldsymbol{\theta}_{\rm inf}, \boldsymbol{\theta}_{\rm reh})$, which are not all analytically encoded. As such, to avoid any bias due to badly determined priors, we have actually performed two nested-sampling explorations of the 287 models: one with the actual $\mathcal{L}_{\rm eff}$ discussed above, and another one with a constant $\mathcal{L}_{\rm eff} = 1$ which ensures that we are sampling the priors. In order to cross-check our results, we have also duplicated these two runs by using `MultiNest` instead of `PolyChord`, and, we have again duplicated everything by starting from another $\mathcal{L}_{\rm eff}$ machine-learned over the Hubble-flow posteriors associated with the extended prior on ε_3 (see Section 4). All in all, 2 TB of data are to be dealt with.

5.1 Priors and model space

For each model $\mathcal{M}$, we have to choose the prior probability distribution for the primordial parameters $\boldsymbol{\theta}_{\rm inf}$ and the reheating parameter $\boldsymbol{\theta}_{\rm reh}$. For the former, they are chosen according

to the underlying theoretical model presented in *Encyclopædia Inflationaris* [56]. These ones are detailed, model by model, in Appendix B for the 113 new models added in the "Opiparous Edition" while the remaining 174 models have been set with the exact same priors presented in Ref. [54] (see Appendix A). Let us notice that, compared to Ref. [54], we have dropped 19 models that were either extremely fine-tuned and strongly disfavored, or, extrapolated in disfavored slow-roll violating regions (see Appendix B).

As discussed in Section 3.3, the reheating occurring after inflation enforces that $\rho_{\rm reh} \leq \rho_{\rm end}$ while we do certainly want the mean equation of state of the universe during that period to satisfy $-1/3 < \overline{w}_{\rm reh} < 1$, the lower bound ensuring that the universe has really stopped inflating. Even though the energy scale at which the reheating ended is unknown, not spoiling Big-Bang Nucleosynthesis demands $\rho_{\rm reh} > \rho_{\rm nuc}$ and we have set a safe lower limit at $\rho_{\rm nuc}^{1/4} = 10\,{\rm MeV}$. From Eq. (3.14), having $\rho_{\rm end} < M_{\rm Pl}^4$, these numbers yield a maximally extended prior for the reheating parameter $R_{\rm rad}$, which is a flat distribution for $\ln R_{\rm rad} \in [-46, 15]$. This is indeed consistent with our complete ignorance about the order of magnitude of the values of $R_{\rm rad}$. However, as motivated in Section 3.3, it is far more accurate to sample the reheating kinematics using the rescaled parameter $\boldsymbol{\theta}_{\rm reh} = \ln R_{\rm reh}$ defined by Eq. (3.15). The prior range for $\ln R_{\rm reh}$ is also confined within $[-46, 15]$ but, because $\rho_{\rm end}$ depends on $\boldsymbol{\theta}_{\rm inf}$, some values within this range are actually excluded on a model-by-model basis and the actual prior of $\ln R_{\rm reh}$ is correlated with $\pi(\boldsymbol{\theta}_{\rm inf})$. In practice, we start by sampling from the flat prior distribution $\ln R_{\rm reh} \in [-46, 15]$ and, then, add a hard prior during the computation which ignores all values $\ln R_{\rm reh} > 15 + (1/3)\ln[\rho_{\rm end}(\boldsymbol{\theta}_{\rm inf})/M_{\rm Pl}^4]$.

5.2 Posteriors and evidences

The posterior probability distributions $P(\boldsymbol{\theta}_{\rm inf}, \boldsymbol{\theta}_{\rm reh}|\boldsymbol{D})$ for a subset of the 287 tested models have been plotted in Appendix C. We have limited ourselves to the most interesting best models according to the criteria discussed in this appendix. All the other posteriors will be made available online [50].

In Figs. 8 and 9, we have reported the natural logarithm of the Bayes factors of all these inflationary models as horizontal bars. The Bayes factors are in reference to the Bayesian evidence of slow roll itself, i.e.,

$$B_{\rm SR3}^{\mathcal{M}} \equiv \frac{\mathcal{E}(\boldsymbol{D}|\mathcal{M})}{\mathcal{E}(\boldsymbol{D}|\mathcal{M}_{\rm SR3})}\,, \tag{5.1}$$

where $\mathcal{M}_{\rm SR3} = I$ denotes the so-called "slow-roll model". This one is defined as the model for which the primordial power spectra are given by Eqs. (3.2) and (3.3) with the strict (or, possibly, extended) slow-roll prior $\varepsilon_i \in [-0.2, 0.2]$ and $\ln\left(10^{10}P_*\right) \in [2.4, 3.6]$. Its evidence is given by the complete marginalization of the full posterior discussed in Section 4

$$\mathcal{E}(\boldsymbol{D}|\mathcal{M}_{\rm SR3}) = \int P(\boldsymbol{D}|\boldsymbol{\theta}_{\rm s}, P_*, \varepsilon_1, \varepsilon_2, \varepsilon_3, \varepsilon_4)\, \pi(\boldsymbol{\theta}_{\rm s}, P_*, \varepsilon_1, \varepsilon_2, \varepsilon_3, \varepsilon_4)\, {\rm d}\boldsymbol{\theta}_{\rm s}{\rm d}P_*{\rm d}\varepsilon_1{\rm d}\varepsilon_2{\rm d}\varepsilon_3{\rm d}\varepsilon_4, \tag{5.2}$$

and we find (strict slow-roll prior)

$$\ln\left[\mathcal{E}(\boldsymbol{D}|\mathcal{M}_{\rm SR3})\right] = -4.525 \pm 0.008. \tag{5.3}$$

Assuming non-committal model priors $\pi(\mathcal{M}_i) = 1/287$, the Bayes factors immediately give us the probability of all models to explain the data

$$P(\mathcal{M}|\boldsymbol{D}) = \frac{B_{\rm SR3}^{\mathcal{M}}}{\sum_i B_{\rm SR3}^{\mathcal{M}_i}}\,. \tag{5.4}$$

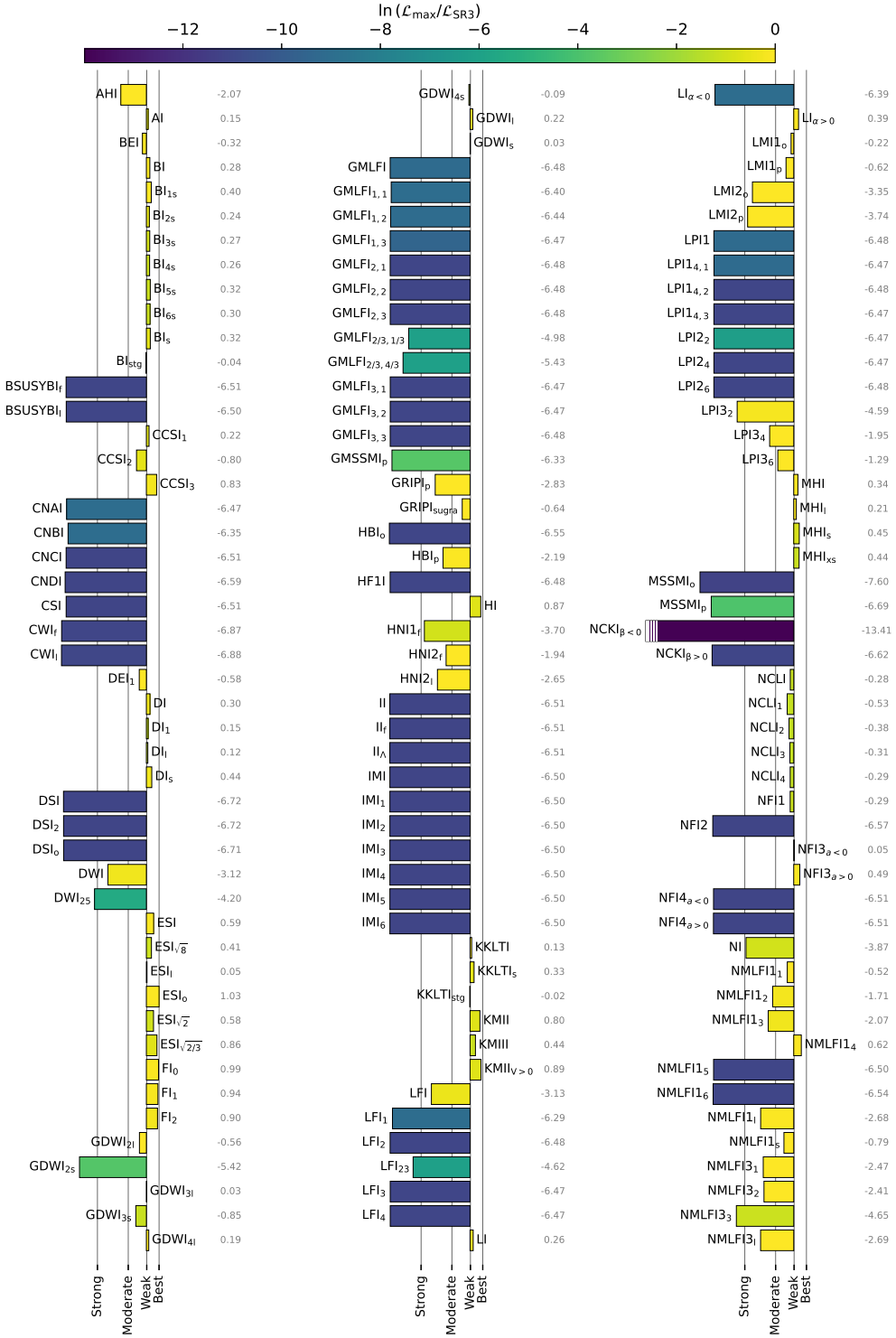

Figure 8. Logarithm of the Bayes factors $B^{\mathcal{M}}_{\mathrm{SR3}}$, in reference to the Bayesian evidence of the slow-roll third-order power spectra. The length of each bar corresponds to the logarithm of the Bayesian evidence, whose value is also displayed in light gray. The color scale shows the best likelihood, again in reference to best fit of the slow-roll spectra. The color scale is also the best possible Bayes factor the model could get, would the prior be associated with a Dirac-distribution at the best fit. Continued in Fig. 9.

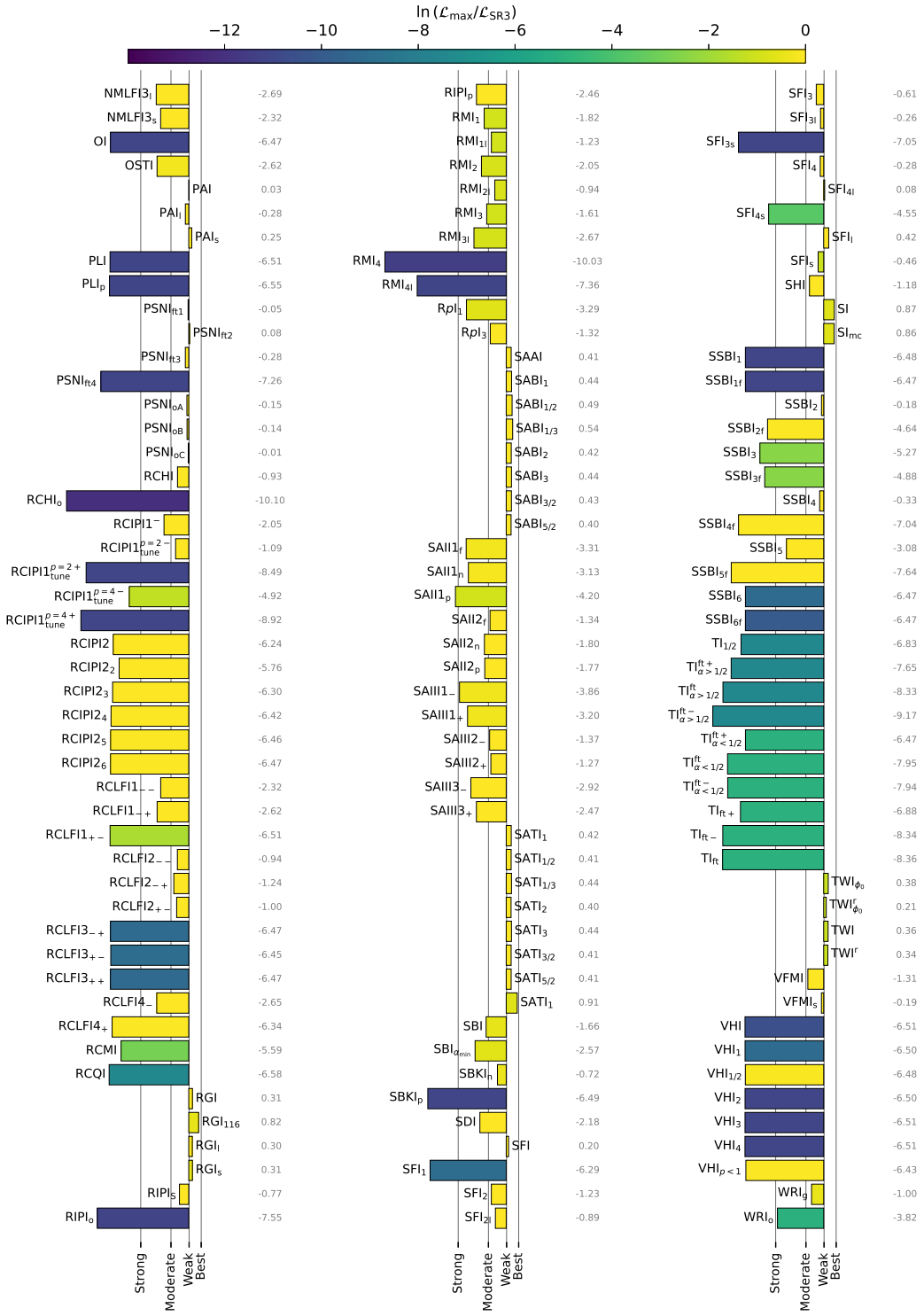

Figure 9. Logarithm of the Bayes factors $B^{\mathcal{M}}_{\mathrm{SR3}}$, in reference to the Bayesian evidence of the slow-roll third-order power spectra. Fig. 8 continued.

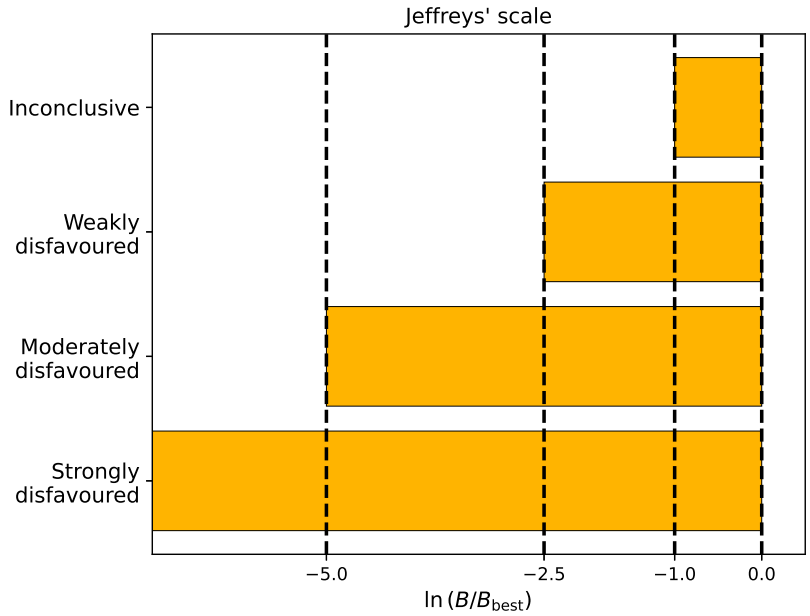

Figure 10. Jeffreys' scale for measuring the strength of evidence when comparing a model having a Bayes factor B to the best $B_{\rm best}$. This scale appears as vertical gray lines in Figs. 8 and 9.

As such, left-extended bars in Figs. 8 and 9 are associated with models $\mathcal{M}$ that are less probable than $\mathcal{M}_{\rm SR3}$ to explain the data sets $\boldsymbol{D}$ whereas models having a bar extended to the right are more probable. We have also reported in these figures the Jeffreys' scale, as gray vertical lines, evaluating the strength of evidences between the model under scrutiny $\mathcal{M}$ and the best of all $\mathcal{M}_{\rm best}$. It belongs to the Exponential SUSY Inflation scenarios and appears as $\mathrm{ESI_o}$ in the figures with

$$\ln\left[\mathcal{E}(\mathcal{M}_{\rm best}|\boldsymbol{D})\right] = -3.49 \pm 0.01. \tag{5.5}$$

The gray vertical lines are the boundaries of the four categories associated with the Jeffreys' scale discussed in Refs. [125, 126] and summarized in Fig. 10. All models having $\ln\left(B^{\mathcal{M}}_{\rm best}\right) > -1.0$, having an horizontal bar with an edge right of the gray line labeled "Best", are as good as $\mathrm{ESI_o}$ in explaining the data sets $\boldsymbol{D}$. On the contrary, all models having $\ln\left(B^{\mathcal{M}}_{\rm best}\right) < -5.0$ are "strongly disfavoured" compared to the bests. Let us remark that the lowest Bayes factors saturate at a relatively large negative value. This saturation is artificial and related to our numerical limitation of having $\ln\left(\mathcal{L}^{\rm min}_{\rm eff}\right) = -11$ for the effective likelihood. As such, it is very well possible that these models would actually have even worse Bayes factors.

As the figures show, quite a large number of models are landing in the "strongly disfavoured" category and it is safe to say that these are ruled-out. However, there are also quite a significant number of models being in the "best" (or inconclusive) region and, for those, it is interesting to determine what it takes for them to fit the data so well. In Ref. [54], we had used the so-called Bayesian Complexity [127] to assess how many effective parameters were needed for each model to fit the data. In the next section, in the same spirit, we derive their Bayesian dimensionality as introduced in Ref. [124].

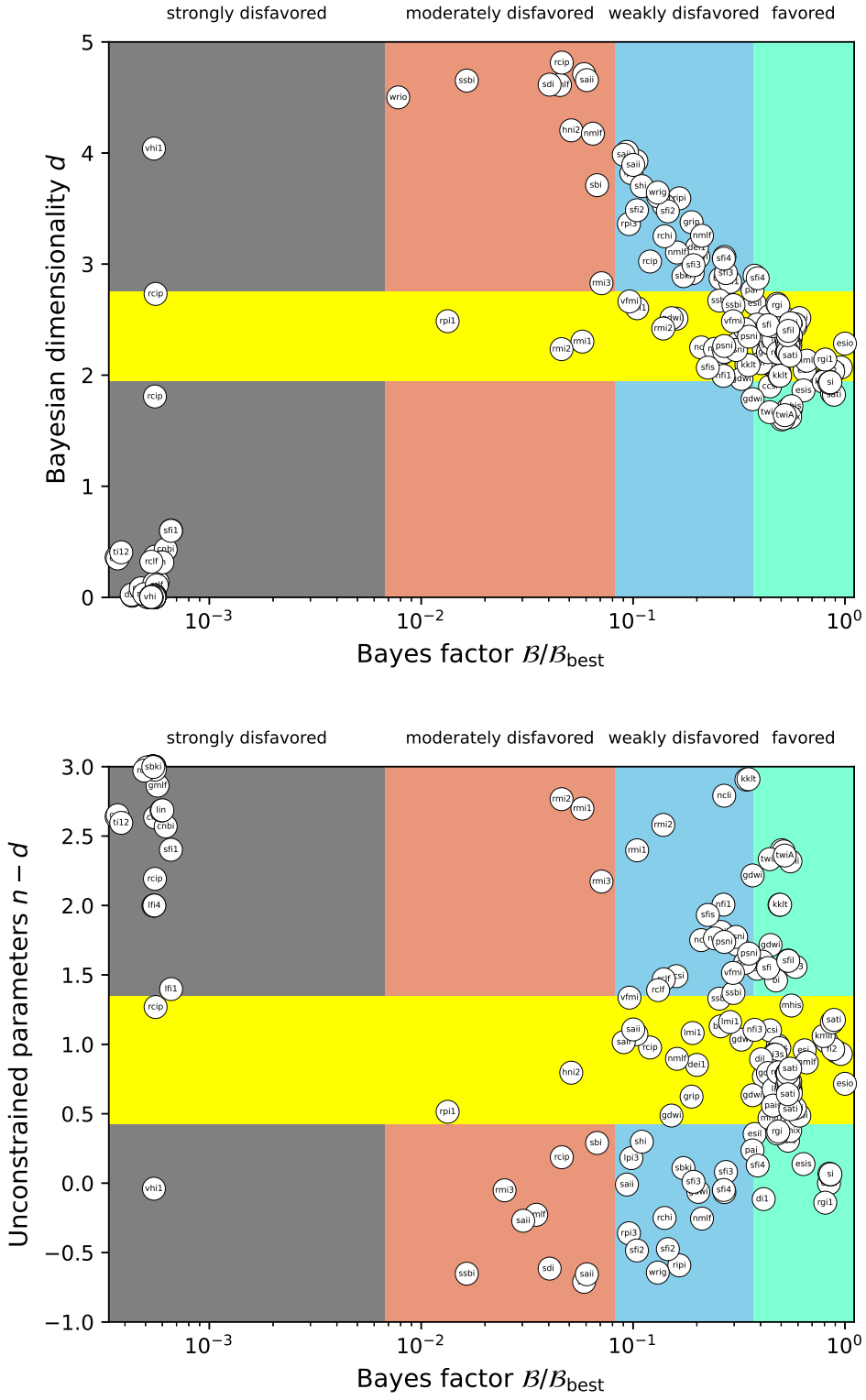

Figure 11. Bayesian dimensionality d (top panel) and number of unconstrained parameters $n - d$ (bottom panel), plotted against Bayes factors $B_{\rm best}$ for the 287 models analyzed (n is the number of model parameter). The yellow region is centered over the mean value of d (top) and $n - d$ (bottom), with a width given by its standard deviation (weighted according to the model probability).

5.3 Bayesian dimensionality

The Bayesian dimensionality is a measure of the number of parameters that are constrained by the posterior probability distribution. Introducing the total information gain $D_{\rm KL}$, namely the Kullback-Leibler divergence between the prior and the posterior integrated over all parameters [128], we have

$$D_{\rm KL} = \int P(\boldsymbol{\theta}|\boldsymbol{D}) \ln \left[\frac{P(\boldsymbol{\theta}|\boldsymbol{D})}{\pi(\boldsymbol{\theta})}\right] {\rm d}\boldsymbol{\theta}, \tag{5.6}$$

where we have used the shorthand notation $\boldsymbol{\theta} = \{\boldsymbol{\theta}_{\rm s}, \boldsymbol{\theta}_{\rm inf}, \boldsymbol{\theta}_{\rm reh}\}$. The Bayesian dimensionality is defined by [124]

$$d = 2 \int P(\boldsymbol{\theta}|\boldsymbol{D}) \left\{\ln \left[\frac{P(\boldsymbol{\theta}|\boldsymbol{D})}{\pi(\boldsymbol{\theta})}\right] - D_{\rm KL}\right\}^2 {\rm d}\boldsymbol{\theta}. \tag{5.7}$$

In terms of the Shannon's information

$$\mathcal{I} = \ln \left[\frac{P(\boldsymbol{\theta}|\boldsymbol{D})}{\pi(\boldsymbol{\theta})}\right], \tag{5.8}$$

one sees that $D_{\rm KL} = \langle \mathcal{I} \rangle$ is the first moment of $\mathcal{I}$ over the posterior while $d/2 = \langle \mathcal{I}^2 \rangle - \langle \mathcal{I} \rangle^2$ is related to its variance. As discussed at length in Ref. [124], d has many features wanted for being used as a measure of the effective number of parameters. For instance, it has almost no dependence on the prior distribution, it is equal to unity for a one-dimensional Gaussian posterior and vanishes for a flat posterior. It is also accurately computable by nested-sampling and we have used the Python package `anesthetic` (incorporated within `infdistbayes`) [123] to determine the value of d for the 287 models analyzed here.

In Fig. 11, all models have been represented by a circle in the plane $(B_{\rm best}, d)$. There is a clear correlation between Bayes factor and Bayesian dimensionality, the latter increasing for the most disfavored models. This is expected as, for models that poorly fit the data, the posterior is forced to peak in the small prior corners that are closest to (but still far from) the favored regions. In this sense, but in this sense only, they are well constrained. As such, Bayesian dimensionality alone should be interpreted with care: data sets can indeed be very constraining for models providing a very bad fit. Let us also notice the few strongly disfavored models with Bayes' factors slightly less than 10^{-3}. Their Bayes' factors are not accurate and their apparent vertical alignment comes from our flat extrapolation of the effective likelihood along the ε_3 direction for values outside the strict prior range $[-0.2, 0.2]$. In particular, we have checked that, using the $\mathcal{L}_{\rm eff}$ associated with the extended prior range $\varepsilon_3 \in [-1, 1]$, these models end up being displaced to much lower evidences, as expected.

For all models, we also keep a record of their number of free parameters n, namely the total number of $\boldsymbol{\theta}_{\rm inf}$ and $\boldsymbol{\theta}_{\rm reh}$. As such, $n - d$ is, for a given model, a measure of the number of unconstrained parameters. Let is notice that, for sharply peaked posteriors, d can be greater than n [124]. In these cases, the number of "free parameters" can become negative and this simply signals that the posteriors of the n model parameters are sharper than Gaussian distributions. In the bottom panel of Fig. 11, we have positioned all models in the plane $(B_{\rm best}, n - d)$. Looking at the most probable models, we find scenarios having typically one unconstrained parameter, and scenarios having none; the latter being the most economical models explaining well the data.

5.4 Information gain on the reheating

Many favored models have less than one unconstrained parameter and this implies that the data are constraining the kinematics of the reheating era [78, 80, 129, 130]. This can be

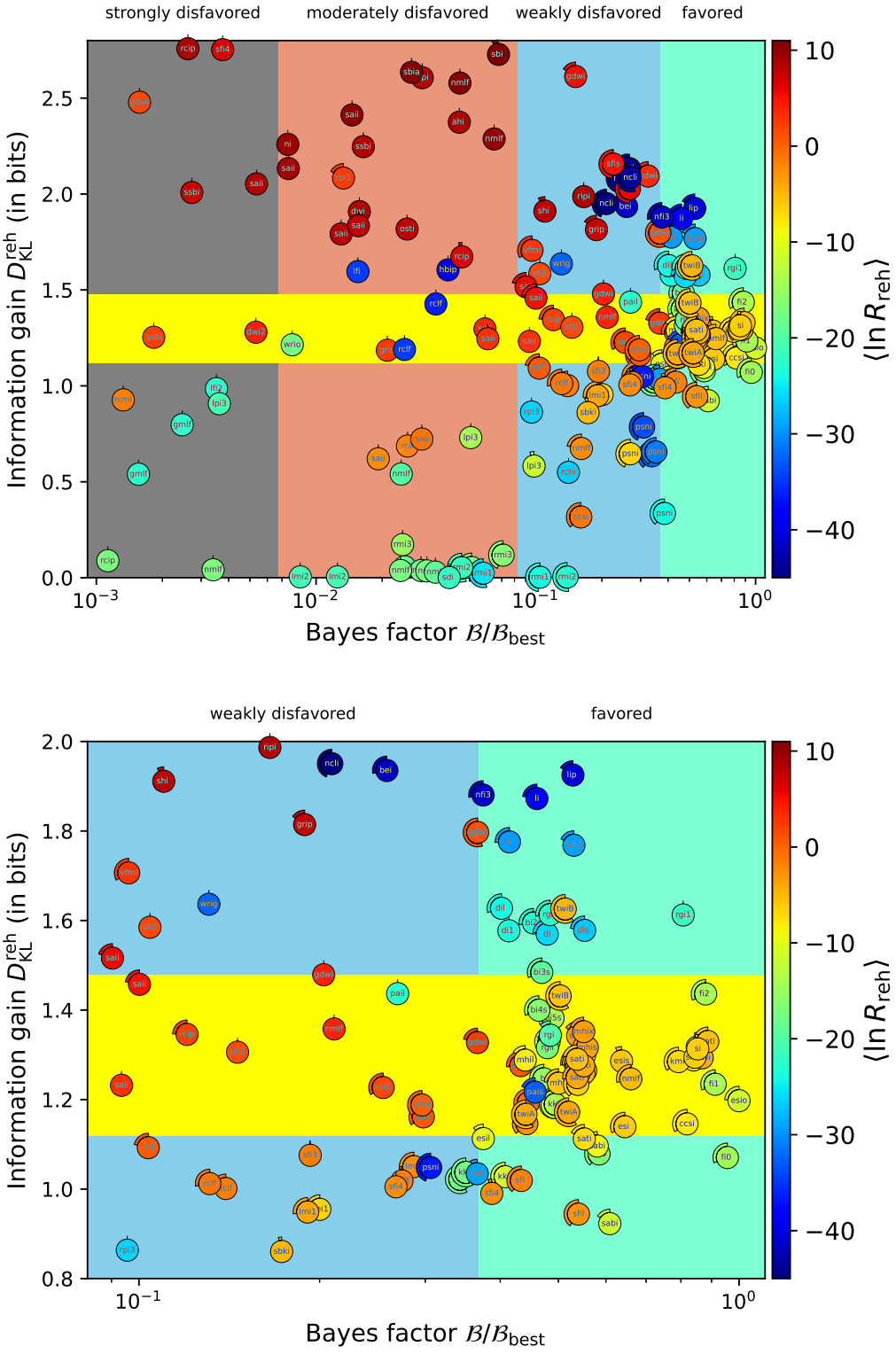

Figure 12. Information gain on the rescaled reheating parameter $\ln R_{\rm reh}$ as a function of the Bayes' factors. The color scale displays the mean value of $\ln R_{\rm reh}$ over its posterior while the anti-clockwise gauge circling all models measures the fraction of unconstrained model parameters $\max\left[(n-d)/n, 0\right]$.

quantified by computing the information gain, i.e., the Kullback-Leibler divergence, between the prior and the posterior, of the reheating parameter, $\ln R_{\rm reh}$ here. Defining

$$D_{\rm KL}^{\rm reh} = \int P(\ln R_{\rm reh}|\boldsymbol{D}) \ln \left[\frac{P(\ln R_{\rm reh}|\boldsymbol{D})}{\pi(\ln R_{\rm reh})}\right] {\rm d}\ln R_{\rm reh}, \tag{5.9}$$

we have plotted in Fig. 12 all models in the plane $(B_{\rm best}, D_{\rm KL}^{\rm reh})$. Each scenario is represented by a colored circle, the color of which gives the mean value $\langle \ln R_{\rm reh}\rangle$ over its posterior $P(\ln R_{\rm reh}|\boldsymbol{D})$. Each circle is enlarged by an anti-clockwise gauge displaying $(n-d)/n$, i.e., the percentage of unconstrained model parameters. As such, when this extra-shell collapses to a single tick, it means that all model parameters are constrained (or over-constrained with $n-d<0$). When the shell closes around, it means that all model parameters are unconstrained. As already noticed in Section 5.3, models providing a "bad fit" to the data have essentially all their model parameters constrained and this gauge is most relevant for the best models.

The horizontal yellow band in Fig. 12 is centered around the mean value of $D_{\rm KL}^{\rm reh}$, and has a width given by its standard deviation. These have been calculated according to the posterior probability of all models to explain the data and we get (in bits)

$$\left\langle D_{\rm KL}^{\rm reh}\right\rangle = \sum_i P(\mathcal{M}_i|\boldsymbol{D})\, D_{\rm KL}^{\rm reh}(\mathcal{M}_i) \simeq 1.3, \tag{5.10}$$

with

$$\sqrt{\left\langle \left(D_{\rm KL}^{\rm reh}\right)^2\right\rangle - \left\langle D_{\rm KL}^{\rm reh}\right\rangle^2} \simeq 0.36. \tag{5.11}$$

These figures have increased by more than a factor of two compared to the first Planck data release, which is a significant achievement. Indeed, according to Ref. [52], one had $\left\langle D_{\rm KL}^{\rm reh}\right\rangle \simeq 0.55 \pm 0.14$ for Planck 2013, $\left\langle D_{\rm KL}^{\rm reh}\right\rangle \simeq 0.82 \pm 0.13$ for Planck 2015 with BICEP/KECK data. Because the reheating parameter is constrained for all best models, by at least one bit (see Fig. 12), inflationary model building is no longer about deriving an inflationary potential only: the reheating kinematics also needs to be specified. In other words, at exact same field potential and background evolution during inflation, two different reheating histories will yield two different Bayesian evidences: they can be distinguished by present cosmological data.

6 Conclusion

We have presented a comprehensive Bayesian data analysis, and model comparison, within the landscape of nearly 300 models of single-field slow-roll inflation. Such an analysis produces a large amount of information, the posterior probability distributions of all the model's parameters have indeed been computed, a sub-sample of which being presented in Appendix C. As such, we could very well discuss, model per model, the theoretical consequences of the preferred values of their parameters. Instead, in this paper, we have chosen to discuss global features, determined by averaging over the landscape various properties shared by all models and weighted by the probability of each model to explain the data $P(\mathcal{M}|\boldsymbol{D})$. One of the main result is the significant boost in sensitivity of current cosmological data to the kinematics of the reheating era. Most of the current proposed models of inflation are loosely making predictions on how long, and with which equation of state, the reheating era proceeded. As we

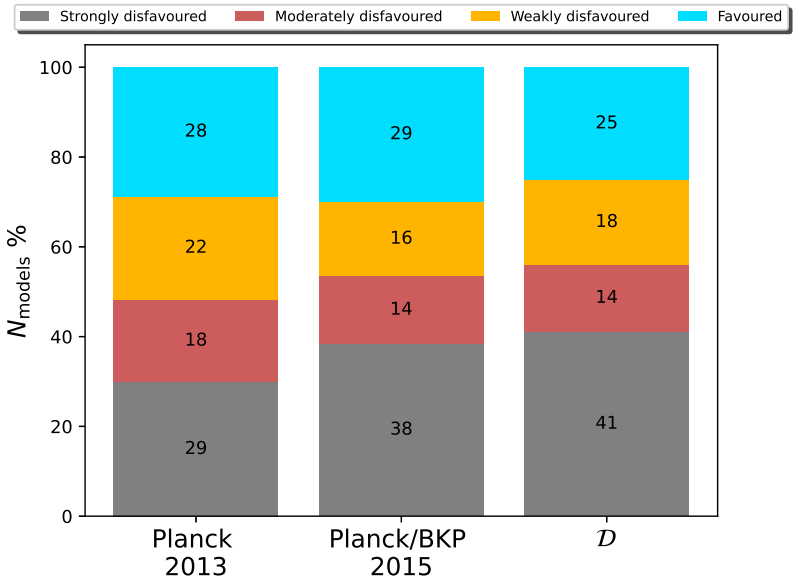

Figure 13. Probability distribution of the models within the four Jeffreys' categories with respect to the three cosmological data sets used within the past decade in Ref. [54], Ref. [52] and the present work ***D***. The constraining power of data is winning against the increase of theoretical inflationary models.

have detailed in Section 3.3, the observable consequences of the reheating kinematics can be fully encoded in the rescaled reheating parameter $R_{\rm reh}$. In the absence of specific information on its value, starting from the most uninformative prior (see Section 5.1), we find that the present data give us a posterior with 1.3 bits of information, more than a two-fold increase within a decade of CMB and LSS measurements.

It is also informative to compare the distribution of models within the four Jeffreys' categories of evidences. As represented in Fig. 13, in spite of the inclusion of 113 new models in the present work, we find that the constraining power of the data is slightly pushing more and more models into the disfavored regions. Let us remark that many of these new 113 models have been proposed *after* the Planck 2013 data release. Still, many of them are actually not able to explain the data better than various simple models proposed well before. For one part, this comes from the inclusion of new model parameters, that can penalize complex models by the Occam's razor effects intrinsically present within Bayesian evidences. For other parts, some of these models still ignore reheating kinematics, and when these are properly taken into account, as we have done here, the model predictions are landing out of the data favored regions.

On another aspect, our results definitely demonstrate that theoretical realizations of cosmic inflation are testable and can be falsified. As Fig. 13 shows, more than 40% of the proposed scenarios are presently ruled-out. Let us stress than even if the current range of wavenumbers probed by CMB and LSS data corresponds to a relatively small window along the inflaton's potential, of about a few e-folds, our marginalization over all reheating histories is making this window moving along the potential by tens of e-folds. The Bayesian evidence for each model is thus sensitive to a large part of the inflationary potential and strongly

disfavoured scenarios are unlikely to be resuscitated by tweaking their potential outside the CMB window with the hope of slightly shifting its location. Nevertheless, one may have a situation in which a strongly disfavoured model is able to fit the data well but only within a fine-tuned region of its potential (see, e.g., the RCIPI2 cases). Such a potential shape might be salvaged but only within a new theoretical embedding making definite predictions for the reheating era. The predicted reheating history should, however, be such that it allows for the fine-tuned region of the potential to land exactly onto the cosmological window, a difficult task indeed.

After the first chapter concluded recently, inflation is therefore ready for the second one where new high-accuracy data will help us to constrain this scientific theory even more. All the data analysis pipeline presented here is indeed readily applicable to other cosmological data sets, and, in particular, we plan to use it for the soon to be released Euclid LSS data. Clearly, probing the small length scales is expected to provide tighter bounds on ε_3, and this will propagate into disfavoring models having too large running of the spectral index. Finally, we hope the future LiteBIRD data will clarify the curious remaining excess in B-modes observed in the present work.

Acknowledgments

We are indebted to Steven Gratton and Erik Rosenberg for having provided us with their latest `CamSpec` likelihood module for `COSMOMC`. This work is supported by the ESA Belgian Federal PRODEX Grant N°4000143201. Computing support has been provided by the CURL cosmo development cluster and the Center for High Performance Computing and Mass Storage (CISM) at UCLouvain.

A Posteriors for the non-primordial parameters

The MCMC exploration of the full parameter space, as performed in Section 4, is necessary to determine the effective likelihood defined in Eq. (3.31). In Section 4, we have presented only the posterior probability distributions for the cosmological and primordial parameters. These have been obtained by marginalizing over the remaining 49 astrophysical and instrumental parameters, whose posteriors have been plotted in Fig. 14. The definitions, priors, and notations for these are identical to the ones of Refs. [101, 103–105].

B Prior choices for the new models

In the following, we summarize the prior probability distributions chosen for the primordial parameters, generically referred to as c_1, c_2, $c_3\ldots$ associated with the 113 new inflationary models $\mathcal{M}$ that were not part of the models discussed in the Appendix A of Ref. [54]. As mentioned in Section 5.1, we have dropped 19 models from the original batch of Ref. [54]. These are strongly disfavored models associated with extreme fine-tuning: $\mathrm{GMSSMI}_{\mathrm{opA}}$, $\mathrm{GMSSMI}_{\mathrm{omA}}$, $\mathrm{GMSSMI}_{\mathrm{opB}}$, $\mathrm{GMSSMI}_{\mathrm{omB}}$, $\mathrm{GMSSMI}_{\mathrm{em}}$, $\mathrm{GMSSMI}_{\mathrm{ep}}$, $\mathrm{GRIPI}_{\mathrm{opA}}$, $\mathrm{GRIPI}_{\mathrm{omA}}$, $\mathrm{GRIPI}_{\mathrm{opB}}$, $\mathrm{GRIPI}_{\mathrm{omB}}$, $\mathrm{GRIPI}_{\mathrm{ep}}$, $\mathrm{GRIPI}_{\mathrm{em}}$, $\mathrm{TI}^{\mathrm{e}}_{\alpha<1/2}$, $\mathrm{TI}^{\mathrm{e}}_{\alpha>1/2}$, TI^{e}, and, RPI2. We have also put aside three favored, but quite peculiar models, that were exploring slow-roll violating regions for some values of their parameters. They are $\mathrm{PSNI}_{\mathrm{epA}}$, $\mathrm{PSNI}_{\mathrm{epB}}$ and $\mathrm{PSNI}_{\mathrm{epC}}$, the evidences of which were analytically extrapolated based on three other slow-roll models (still included): $\mathrm{PSNI}_{\mathrm{oA}}$, $\mathrm{PSNI}_{\mathrm{oB}}$ and $\mathrm{PSNI}_{\mathrm{oC}}$, respectively. As shown in Ref. [54], the evidences

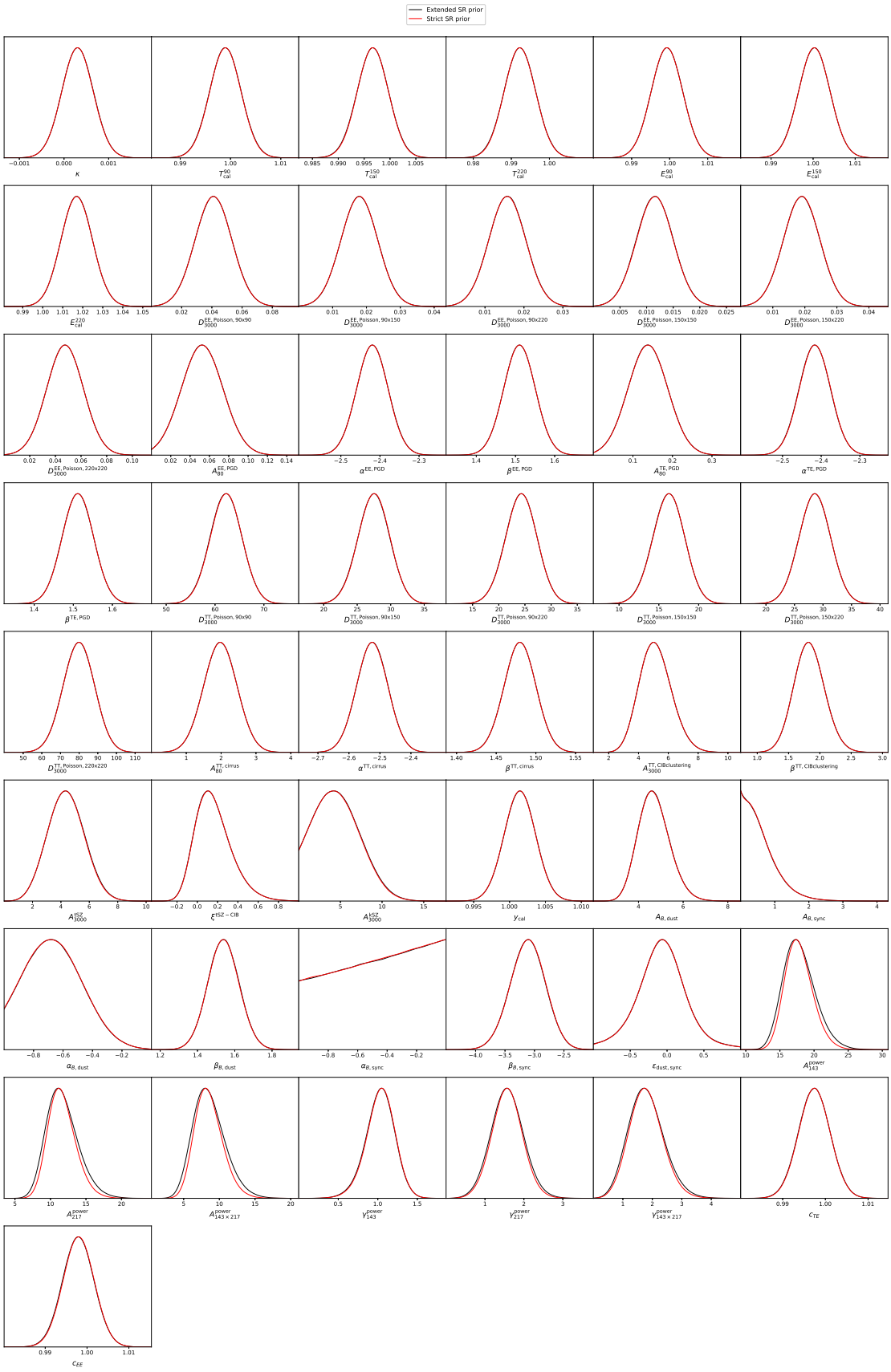

Figure 14. One-dimensional posteriors for the 49 non-cosmological, nor primordial, parameters for both the strict and extended slow-roll priors.

of the former are only slightly reduced with respect to the latter. The interested reader may find the analytical formulas to derive the evidences of $\mathrm{PSNI}_{\mathrm{epA}}$, $\mathrm{PSNI}_{\mathrm{epB}}$, $\mathrm{PSNI}_{\mathrm{epC}}$ in the Appendix A of Ref. [54], see Eq. (A72). Let us stress that the drop of these 19 models has been consistently taken into account in the comparison made in Fig. 13.

The new models presented below are introduced with a minimal amount of information to justify the prior choices: all the physical and technical details, for each of these scenarios, can be found in the "Opiparous Edition" of *Encyclopædia Inflationaris* in Ref. [56].

B.1 Axion Hilltop Inflation (AHI)

Axion Hilltop Inflation has a potential of the form

$$V(\phi) = M^4 \left[\nu_0 - 2\cos\left(\frac{\phi}{f}\right) + \left(\pi - \frac{\phi}{f}\right)\sin\left(\frac{\phi}{f}\right)\right], \tag{B.1}$$

which involves one parameter f, a typical vacuum expectation value, whose order of magnitude is unknown. We have therefore chosen a Jeffreys' prior, namely an uniform prior of the logarithm of f.

Name	c_1-prior
AHI	$\log(f/M_{\mathrm{Pl}}) \in [-3, 3]$

B.2 Cublicly Corrected Starobinsky Inflation (CCSI)

This is a modified gravity model in which a cubic power of the Ricci scalar is added as a correction to the Starobinsky model. In the Einstein frame, the potential reads

$$V(\phi) = \frac{M_{\mathrm{g}}^2\mu^2}{2}\left(1 - e^{-y}\right)^2 \frac{1 + \sqrt{1 + 3\alpha\left(e^y - 1\right)} + 2\alpha\left(e^y - 1\right)}{\left[1 + \sqrt{1 + 3\alpha\left(e^y - 1\right)}\right]^3}, \tag{B.2}$$

where $y = \sqrt{2/3}\,\phi/M_{\mathrm{g}}$ and $M_{\mathrm{g}} \simeq M_{\mathrm{Pl}}$. There is one small parameter α, and setting $\alpha = 0$ gives back the Starobinsky model, see Appendix B.26. Such a potential generates three distinct inflationary regimes, CCSI_1, CCSI_2, CCSI_3. One of them, CCSI_2, is quite fine-tuned as requiring a very small coupling constant, an external mechanism to stop inflation (for instance, a tachyonic instability), and some tuning of the field value at which this mechanism occurs to be viable: $\phi_{\mathrm{end}} > \phi_{\mathrm{end}}^{\mathrm{min}}$ where $\phi_{\mathrm{end}}^{\mathrm{min}}$ is set to ensure that inflation lasts, at least, for 120 e-folds. As such, we have analyzed these three different scenarios separately.

Name	c_1-prior	c_2-prior
CCSI_1	$\log(\alpha) \in [-6, 0]$	-
CCSI_2	$\log(\alpha) \in [-6, -3]$	$\phi_{\mathrm{end}}/\phi_{\mathrm{end}}^{\mathrm{min}} \in [1, 5]$
CCSI_3	$\log(\alpha) \in [-6, 0]$	-

B.3 Double Exponential Inflation (DEI)

The potential of this phenomenological model is given by

$$V(\phi) = M^4 \left(e^{\beta \frac{\phi}{\phi_0}} - \beta^2 e^{\frac{1}{\beta}\frac{\phi}{\phi_0}} \right), \tag{B.3}$$

where the two exponential terms are set to generate a large hilltop region. This is a two-parameter model with $\phi_0 > M_{\rm Pl}$, the order of magnitude being unknown, and $0 < \beta < 1$.

Name	c_1-prior	c_2-prior
DEI_1	$\beta \in [0, 1]$	$\log(\phi_0/M_{\rm Pl}) \in [0, 3]$

B.4 Dual Inflation (DI)

Dual Inflation is a UV-complete and non-perturbative inflation model coming from an $N = 2$ Supersymmetric Yang-Mills theory. The potential has no simple from, but can be parameterized as

$$\begin{aligned} V(m) &= \frac{f_0^2 \Lambda^2}{\pi^2} \left\{ 1 + V_0 - 2\frac{K - E}{mK} - \frac{\pi}{mKK'} \nu^2(m) \Theta[\nu(m)] \right\}, \\ \nu(m) &\equiv 1 - \frac{8\sqrt{2}}{\pi^2} \frac{\Lambda}{f_0} \frac{K(E' - K')^2}{m^{1/2}}, \\ \phi(m) &= \Lambda \frac{2\sqrt{2}}{\pi} \int_m^1 \frac{\sqrt{K(p^{1/2}) K'(p^{1/2})}}{p^{3/2}} \, \mathrm{d}p, \end{aligned} \tag{B.4}$$

where $\Theta(x)$ stands for the Heaviside function, V_0 is an order unity uplifting constant (which has to be numerically determined). The functions $E(x)$, $K(x)$, $E'(x)$ and $K'(x)$ are known as the first- and second-kind complete elliptic integrals. The potential is parameterized by f_0 and the typical vacuum expectation value Λ. The internal consistency of the theory requires $f_0 < \Lambda$ and, as such, we work with the dimensionless parameter $f = f_0/\Lambda < 1$. Dual Inflation is also a model predicting the amplitude of the CMB anisotropies (the mass scale of the potential is $M \propto \sqrt{f_0 \Lambda}$), $\Lambda(f)$ is thus not free. DI is finally a one parameter model parameterized by f only. We have split it into various motivated priors as described in the following table.

Name	c_1-prior
DI	$\log(f) \in [-5, 0]$
$\mathrm{DI_s}$	$\log(f) \in [-5, -2]$
$\mathrm{DI_l}$	$\log(f) \in [-2, 0]$
DI_1	$f = 1$

B.5 Double Well Inflation (DWI)

This models are a phenomenological UV-completion of the Small Field quadratic inflation models (SFI_2) and have already been considered in Ref. [54]. Their potential reads

$$V(\phi) = M^4 \left[\left(\frac{\phi}{\phi_0} \right)^2 - 1 \right]^2 . \tag{B.5}$$

They do significantly differ from SFI_2 in the super-Planckian field regime and we have added a missing realization of this effect as a motivated prior in DWI_{25}.

Name	c_1-prior
DWI_{25}	$\phi_0/M_{\mathrm{Pl}} = 25$

B.6 Exponential SUSY Inflation (ESI)

The potential reads

$$V(\phi) = M^4 \left(1 - e^{-q\phi/M_{\mathrm{Pl}}} \right) , \tag{B.6}$$

with a unique model parameter q. This class of models was already presented in Ref. [54], but a new theoretical realization was proposed since then, in which $q = \sqrt{8}$ [56]. We have therefore introduced the new model $\mathrm{ESI}_{\sqrt{8}}$.

Name	c_1-prior
$\mathrm{ESI}_{\sqrt{8}}$	$q = \sqrt{8}$

B.7 Fiber Inflation (FI)

This is a model built upon String Theory, where the potential reads

$$V(\phi) = M^4 \left[\left(1 + \frac{2}{3}\delta \right) e^{-\frac{4}{\sqrt{3}}\frac{\phi}{M_{\mathrm{Pl}}}} - 4 \left(1 + \frac{\delta}{6} \right) e^{-\frac{1}{\sqrt{3}}\frac{\phi}{M_{\mathrm{Pl}}}} + \frac{\delta}{1+n} e^{\frac{2(1+n)}{\sqrt{3}}\frac{\phi}{M_{\mathrm{Pl}}}} + 3 - \frac{\delta}{1+n} \right] . \tag{B.7}$$

Here, n is an integer number and δ is a small positive number, of unknown order or magnitude, but related to a string coupling q by $\delta \propto q^{4(1+n/3)}$. We have therefore considered the three scenarios listed in the following table.

Name	c_1-prior	c_2-prior
FI_0	$\log(\delta) \in [-8, -4]$	$n = 0$
FI_1	$\log(\delta) \in [-32/3, -16/3]$	$n = 1$
FI_2	$\log(\delta) \in [-40/3, -20/3]$	$n = 2$

Some peculiar values of δ may lead to slow-roll violations and, for the three scenarios, we have added a hard prior ignoring all inflating regions in which $\varepsilon_1 > 0.2$ or having a total number of e-folds less than 120.

B.8 Generalized Double Well Inflation (GDWI)

This is a phenomenological completion of the non-quadratic Small Field Inflationary model SFI introduced in Ref. [16]. The potential reads

$$V(\phi) = M^4 \left[\left(\frac{\phi}{\phi_0} \right)^{2p} - 1 \right]^2 , \tag{B.8}$$

with two parameters, a power index p and a vacuum expectation value ϕ_0. It has been studied under the prior choices listed in the table below.

Name	c_1-prior	c_2-prior
$\mathrm{GDWI_{2s}}$	$p = 2$	$\log(\phi_0/M_{\rm Pl}) \in [-3, 0]$
$\mathrm{GDWI_{2l}}$	$p = 2$	$\log(\phi_0/M_{\rm Pl}) \in [0, 3]$
$\mathrm{GDWI_{3s}}$	$p = 3$	$\log(\phi_0/M_{\rm Pl}) \in [-3, 0]$
$\mathrm{GDWI_{3l}}$	$p = 3$	$\log(\phi_0/M_{\rm Pl}) \in [0, 3]$
$\mathrm{GDWI_{4s}}$	$p = 4$	$\log(\phi_0/M_{\rm Pl}) \in [-3, 0]$
$\mathrm{GDWI_{4l}}$	$p = 4$	$\log(\phi_0/M_{\rm Pl}) \in [0, 3]$
$\mathrm{GDWI_s}$	$p \in [1/10, 10]$	$\log(\phi_0/M_{\rm Pl}) \in [-3, 0]$
$\mathrm{GDWI_l}$	$p \in [1/10, 10]$	$\log(\phi_0/M_{\rm Pl}) \in [0, 3]$

B.9 Hyperbolic Inflation (HBI)

The potential is parameterized by two parameters, a power index n and a vacuum expectation value μ, as

$$V(\phi) = M^4 \sinh^n \left(\frac{\phi}{\mu} \right) . \tag{B.9}$$

The model describes a scalar field embedded within a perfect fluid. As such, we have introduced two models, one, $\mathrm{HBI_o}$, describing this very theoretical setup in which one has $n = 2n_\phi/(n_\phi - n_{\rm f})$ and $\mu/M_{\rm Pl} = 2\sqrt{n_\phi}/(n_\phi - n_{\rm f})$. In that case, the underlying model parameter are n_ϕ and $n_{\rm f}$. In another model, named $\mathrm{HBI_p}$, we consider Eq. (B.9) as a phenomenological potential and set the prior directly on n and $\log(\mu/M_{\rm Pl})$. For both cases, we have also added a hard prior ignoring inflating regions in which $\varepsilon_1 > 0.2$.

Name	c_1-prior	c_2-prior
$\mathrm{HBI_o}$	$n_{\rm f} \in [0, 1]$	$n_\phi - n_{\rm f} \in [0.1, 10]$
$\mathrm{HBI_p}$	$n \in [0, 5]$	$\log(\mu/M_{\rm Pl}) \in [0, 3]$

B.10 Higgs Inflation (HI)

Higgs inflation is a non-minimal model of gravity built upon the Standard Model Higgs field. In the Einstein frame, its potential is parametrically given by

$$\begin{aligned} V(\phi) &= \frac{M_{\rm Pl}^4 \lambda}{4\xi^2}\left(\frac{\bar{h}^2-\bar{v}^2}{1+\bar{h}^2}\right)^2, \\ \frac{\phi}{M_{\rm Pl}} &= \sqrt{\frac{1+6\xi}{\xi}}\ln\left[\sqrt{1+(1+6\xi)\bar{h}^2}+\sqrt{(1+6\xi)\bar{h}^2}\right] \\ &\quad + \sqrt{6}\ln\left[\frac{\sqrt{1+\bar{h}^2}}{\sqrt{1+(1+6\xi)\bar{h}^2}+\sqrt{6\xi\bar{h}^2}}\right], \end{aligned} \tag{B.10}$$

with $\lambda = 0.13$ and $\bar{v} = \sqrt{\xi}v/M_{\rm Pl}$ ($v = 246$GeV). As such, Higgs inflation is also a zero-parameter model because ξ is fixed by the amplitude of the CMB anisotropies. As explained in *Encyclopædia Inflationaris*, at leading order SI and HI are the same model, but we have dropped this approximation here and consider them exactly, and independent, as future data may possibly disambiguate between the two scenarios.

B.11 Hybrid Natural Inflation (HNI)

This is an extension of Natural Inflation that incorporates a tachyonic instability to stop inflation at a field value $\phi_{\rm end}$. The potential is given by

$$V(\phi) = M^4\left[1+\alpha\cos\left(\frac{\phi}{f}\right)\right], \tag{B.11}$$

where the coupling $\alpha \in]0,1[$ and f, the vacuum expectation value, should be super-Planckian to allow for slow roll. With $\phi_{\rm end}$, this is a three-parameter model. However, there are some regimes in which inflation gracefully ends before the tachyonic instability actually takes place, and, for these, $\phi_{\rm end}$ is not relevant. We have accordingly split the model in three scenarios.

Name	c_1-prior	c_2-prior	c_3-prior
$\text{HNI1}_{\rm f}$	$\alpha \in]0,1[$	$\log(f/M_{\rm Pl}) \in [0,3]$	-
$\text{HNI2}_{\rm f}$	$\alpha \in]0,1[$	$\log(f/M_{\rm Pl}) \in [0,3]$	$\phi_{\rm end}/f \in]0,\pi[$
$\text{HNI2}_{\rm l}$	$\log(\alpha) \in [-3,0[$	$\log(f/M_{\rm Pl}) \in [0,3]$	$\phi_{\rm end}/f \in]0,\pi[$

B.12 Mutated Hilltop Inflation (MHI)

The potential of this model reads

$$V(\phi) = M^4\left[1-\operatorname{sech}\left(\frac{\phi}{\mu}\right)\right], \tag{B.12}$$

and was included in the analysis of Ref. [54]. In the present work, we have added one new realization having a deep sub-Planckian vacuum expectation value μ as $\text{MHI}_{\rm xs}$.

Name	c_1-prior
$\mathrm{MHI}_{\mathrm{xs}}$	$\mu = 10^{-2}$

B.13 Non-renormalizable Corrected Loop Inflation (NCLI)

This is an effective-field-theory model that can be seen as including corrections from non-renormalizable operators onto the so-called Loop Inflation model. The potential has three parameters and reads

$$V(\phi) = M^4 \left[1 + \alpha \ln\left(\frac{\phi}{M_{\mathrm{Pl}}}\right) + \left(\frac{\phi}{\phi_0}\right)^{4+2n} \right]. \tag{B.13}$$

We have considered five priors, motivated by the fact that n is a power index, ϕ_0 a sub-Planckian vacuum expectation value of unknown order of magnitude and α a small coupling constant to keep corrections under control. Moreover, we have added hard priors excluding inflating regions with $\varepsilon_1 > 0.2$ or the ones having a total number of e-folds less than 120.

Name	c_1-prior	c_2-prior	c_3-prior
NCLI_1	$\log(\alpha) \in [-6,-1]$	$\log(\phi_0/M_{\mathrm{Pl}}) \in [-3,0]$	$n = 1$
NCLI_2	$\log(\alpha) \in [-6,-1]$	$\log(\phi_0/M_{\mathrm{Pl}}) \in [-3,0]$	$n = 2$
NCLI_3	$\log(\alpha) \in [-6,-1]$	$\log(\phi_0/M_{\mathrm{Pl}}) \in [-3,0]$	$n = 3$
NCLI_4	$\log(\alpha) \in [-6,-1]$	$\log(\phi_0/M_{\mathrm{Pl}}) \in [-3,0]$	$n = 4$
NCLI	$\log(\alpha) \in [-6,-1]$	$\log(\phi_0/M_{\mathrm{Pl}}) \in [-3,0]$	$n \in [1,10]$

B.14 N-Formalism Inflation (NFI)

This is a class of phenomenological models built to generate a power-law behavior of the Hubble-flow functions at leading order in slow roll. The potential is given by

$$V(\phi) = M^4 e^{-a x^b}, \tag{B.14}$$

with $x = \phi/M_{\mathrm{Pl}}$, the two parameters a and b being arbitrary. Depending on their values, various inflationary regimes appear, some of them requiring a third parameter to end inflation, a field value $x_{\mathrm{end}} = \phi_{\mathrm{end}}/M_{\mathrm{Pl}}$ assumed to be associated with a tachyonic instability. As detailed in *Encyclopædia Inflationaris*, the consistency of the scenario requires x_{end} to be bounded by the two known functions $x_{\mathrm{end}}^{\mathrm{min}}(a,b)$ and $x_{\mathrm{end}}^{\mathrm{max}}(a,b)$, and these ones have been required to trigger, at least, 120 e-folds of inflation. This leads to several cases, to which specific priors can be associated, as listed below.

Name	c_1-prior	c_2-prior	c_3-prior
NFI1	$a \in [0,10]$	$b \in]1,10]$	-
$\mathrm{NFI3}_{a<0}$	$a \in [-10,0[$	$b \in [0,1[$	-
$\mathrm{NFI3}_{a>0}$	$a \in]0,10]$	$b \in [-10,0[$	-

NFI2	$a \in [-10, 0]$	$b \in]1, 10]$	$x_{\rm end} \in [x_{\rm end}^{\rm min}, x_{\rm end}^{\rm max}]$
NFI4$_{a>0}$	$a \in [1, 10]$	$b \in]0, 1[$	$x_{\rm end} \in [x_{\rm end}^{\rm min}, x_{\rm end}^{\rm max}]$
NFI4$_{a<0}$	$a \in [-10, 0[$	$b \in [-10, 0]$	$x_{\rm end} \in [x_{\rm end}^{\rm min}, x_{\rm end}^{\rm max}]$

In all these cases, a hard prior requiring inflation to verify $\varepsilon_1 < 0.2$ has been added.

B.15 Non-Minimal Large Field Inflation (NMLFI)

These models correspond to Large Field Inflation where a non-minimal coupling to the Ricci scalar, of strength ξ, is added. In the Einstein Frame, the potential is a parametric function given by

$$\begin{aligned} V(\bar{h}) &= M^4 \frac{\bar{h}^p}{1+\bar{h}^2}\,, \\ \frac{\phi}{M_{\rm Pl}} &= \sqrt{6+1/\xi}\ln\left[\sqrt{1+(1+6\xi)\bar{h}^2}+\sqrt{(1+6\xi)\bar{h}^2}\right] \\ &\quad + \sqrt{6}\ln\left[\frac{\sqrt{1+\bar{h}^2}}{\sqrt{1+(1+6\xi)\bar{h}^2}+\sqrt{6\xi\bar{h}^2}}\right]. \end{aligned} \tag{B.15}$$

There are two parameters, a power index p, and the non-minimal coupling constant ξ. Only for $p = 4$ this potential has a plateau. For all the other cases, it exhibits a hilltop and various inflationary regimes can take place, some of them (NMLFI3) requiring a new mechanism to end inflation [56]. For them, we require inflation to last, at least, 120 e-folds and we demand, by a hard prior, that it occurs with $\varepsilon_1 < 0.2$. The scenarios are summarized in the table below.

Name	c_1-prior	c_2-prior	c_3-prior
NMLFI1$_{\rm s}$	$\log(\xi) \in [-4, 2]$	$p \in [1/10, 4]$	-
NMLFI1$_{\rm l}$	$\log(\xi) \in [-4, 2]$	$p \in [4, 8]$	-
NMLFI1$_1$	$\log(\xi) \in [-4, 2]$	$p = 1$	-
NMLFI1$_2$	$\log(\xi) \in [-4, 2]$	$p = 2$	-
NMLFI1$_3$	$\log(\xi) \in [-4, 2]$	$p = 3$	-
NMLFI1$_4$	$\log(\xi) \in [-4, 2]$	$p = 4$	-
NMLFI1$_5$	$\log(\xi) \in [-4, 2]$	$p = 5$	-
NMLFI1$_6$	$\log(\xi) \in [-4, 2]$	$p = 6$	-
NMLFI3$_{\rm s}$	$\log(\xi) \in [-4, 2]$	$p \in [0.1, 0.5]$	$\log(\bar{h}_{\rm end}) \in [-1, 2]$
NMLFI3$_{\rm l}$	$\log(\xi) \in [-4, 2]$	$p \in [0.6, 3.5]$	$\log(\bar{h}_{\rm end}) \in [-1, 2]$
NMLFI3$_1$	$\log(\xi) \in [-4, 2]$	$p = 1$	$\log(\bar{h}_{\rm end}) \in [-1, 2]$
NMLFI3$_2$	$\log(\xi) \in [-4, 2]$	$p = 2$	$\log(\bar{h}_{\rm end}) \in [-1, 2]$
NMLFI3$_3$	$\log(\xi) \in [-4, 2]$	$p = 3$	$\log(\bar{h}_{\rm end}) \in [-1, 2]$

B.16 Pure Arctan Inflation (PAI)

A pure phenomenological model with a potential given by

$$V(\phi) = M^4 \arctan\left(\frac{\phi}{\mu}\right), \tag{B.16}$$

with a vacuum expectation value μ or unknown order of magnitude. Three priors have been devised.

Name	c_1-prior
PAI	$\log(\mu/M_{\rm Pl}) \in [-3, 3]$
PAI_s	$\log(\mu/M_{\rm Pl}) \in [-3, 0]$
PAI_l	$\log(\mu/M_{\rm Pl}) \in [0, 3]$

B.17 Radiatively Corrected Inflection Point Inflation (RCIPI)

This scenario is motivated by effective-field-theory considerations in which loop corrections, tuned to generate an inflection point, are corrected by higher-order operators preventing the inflection point to appear. The potential has three parameters and reads

$$V(\phi) = M^4 \left(\frac{\phi}{M_{\rm Pl}}\right)^p \left[1 + \alpha \ln\left(\frac{\phi}{M_{\rm Pl}}\right) + \beta \ln^2\left(\frac{\phi}{M_{\rm Pl}}\right)\right], \tag{B.17}$$

where p is a power index, α and β are coupling constants associated with loops and higher-order operators. In this theoretical framework α and β are not arbitrary and should take values close to the ones leading to an exact inflection point. At given β and p, as discussed in Ref. [56], the inflection point appears for $\alpha = \pm\alpha_0$ where $\alpha_0 = 2\sqrt{\beta}\sqrt{1-\beta/p^2}$. A theoretical prior is that $\alpha - \alpha_0$ should be a small quantity and these models will be referred to as "tuned". Various inflationary regimes appear, as the inflection point can become either a hilltop or lead to a monotonous potential. We have also considered RCIPI as a phenomenological potential in which one is allowed to be far from the inflection point. In that case, we have set priors in which α can be quite different from α_0. The resulting models are listed below.

Name	c_1-prior	c_2-prior	c_3-prior
$\text{RCIPI1}^{p=2+}_{\text{tune}}$	$p = 2$	$\log(\alpha - \alpha_0) \in [-5, -2]$	$\log(\beta) \in [-2, \log(4)]$
$\text{RCIPI1}^{p=4+}_{\text{tune}}$	$p = 4$	$\log(\alpha - \alpha_0) \in [-5, -2]$	$\log(\beta) \in [-2, \log(16)]$
$\text{RCIPI1}^{p=2-}_{\text{tune}}$	$p = 2$	$\log(-\alpha - \alpha_0) \in [-5, -2]$	$\log(\beta) \in [-2, \log(4)]$
$\text{RCIPI1}^{p=4-}_{\text{tune}}$	$p = 4$	$\log(-\alpha - \alpha_0) \in [-5, -2]$	$\log(\beta) \in [-2, \log(16)]$
RCIPI1^{-}	$p \in [2, 4]$	$(2\sqrt{\beta} + \alpha)/(2\sqrt{\beta} - \alpha_0) \in [0, 1]$	$\log(\beta) \in [-2, \log(4)]$
RCIPI2_2	$p = 2$	$\alpha/\alpha_0 \in [-1, 1]$	$\log(\beta) \in [-2, \log(4)]$
RCIPI2_3	$p = 3$	$\alpha/\alpha_0 \in [-1, 1]$	$\log(\beta) \in [-2, \log(9)]$
RCIPI2_4	$p = 4$	$\alpha/\alpha_0 \in [-1, 1]$	$\log(\beta) \in [-2, \log(16)]$
RCIPI2_5	$p = 5$	$\alpha/\alpha_0 \in [-1, 1]$	$\log(\beta) \in [-2, \log(25)]$
RCIPI2_6	$p = 5$	$\alpha/\alpha_0 \in [-1, 1]$	$\log(\beta) \in [-2, \log(36)]$
RCIPI2	$p \in [2, 6]$	$\alpha/\alpha_0 \in [-1, 1]$	$\log\left(\beta/\sqrt{p}\right) \in [-2, 0]$

B.18 Radiatively Corrected Large Field Inflation (RCLFI)

The potential is given by

$$V(\phi) = M^4 \left[\left(\frac{\phi}{\mu}\right)^p + \alpha \left(\frac{\phi}{\mu}\right)^4 \ln\left(\frac{\phi}{\mu}\right) \right], \tag{B.18}$$

and models loop corrections to the Large Field Inflation potential (monomial term). There are three parameters, the power index p, the coupling constant α and a renormalization mass scale μ. In this theoretical framework, one may expect the loop corrections to be small, and this perturbative regime is referred to as RCLFI4. As detailed in *Encyclopædia Inflationaris*, when loop corrections become sizable, various novel inflationary regimes appear, named RCLFI1, RCLFI2, RCLFI2, as the potential may develop a local maximum for some parameter values. The separatrix of these different regimes involve some functions, derived and explained in Ref. [56], which are $\alpha_0(p) = -e(p-4)$ and $\alpha_1(p) = -p(p-4)e^{2-p/4}/4$. In some cases, inflation can occur only at the hilltop and there is a minimal value of $\mu = \mu_{\rm min}$ for which the total number of e-folds realized without an extreme tuning can exceed an acceptable value which has been set to 120 here. The precise value of $\mu_{\rm min}$ does not really matter as these situations are actually strongly disfavored. However notice that, tuning these cases even more, by allowing for smaller $\mu_{\rm min}$, would lower their evidences. There are also some fine-tuned cases in which the power index p is forced to remain smaller than a numerically computed value $p_{\rm max}$.

Name	c_1-prior	c_2-prior	c_3-prior
RCLFI1$_{+-}$	$p \in [4.1, 6]$	$\alpha/\alpha_1 \in]1, 10[$	$\log(\mu/\mu_{\rm min}) \in [0, 3]$
RCLFI1$_{--}$	$p \in [0.1, 3.9]$	$\alpha \in [-4, -0.1[$	$\log(\mu/\mu_{\rm min}) \in [0, 3]$
RCLFI1$_{-+}$	$p/p_{\rm max} \in [0.1, 3.9]$	$\alpha/\alpha_1 \in]1, 10]$	$\log(\mu/\mu_{\rm min}) \in [0, 3]$
RCLFI2$_{+-}$	$p \in [4.1, 8]$	$\alpha/\alpha_0 \in]1, 10]$	$\log(\mu/\mu_{\rm min}) \in [0, 3]$
RCLFI2$_{--}$	$p \in [0.1, 3.9]$	$\alpha \in [-2, -0.2]$	$\log(\mu/\mu_{\rm min}) \in [0, 3]$
RCLFI2$_{-+}$	$p/p_{\rm max} \in [0.1, 0.9]$	$\alpha/\alpha_0 \in]1, 10]$	$\log(\mu/\mu_{\rm min}) \in [0, 3]$
RCLFI3$_{++}$	$p \in [4.1, 8]$	$\log(\alpha) \in [-2, 2]$	$\log(\mu/M_{\rm Pl}) \in [-3, 3]$
RCLFI3$_{+-}$	$p \in [4.1, 8]$	$\alpha/\alpha_0 \in]1, 10]$	$\log(\mu) \in [-3, 3]$
RCLFI3$_{-+}$	$p \in [0.1, 3.9]$	$\alpha/\alpha_0 \in]1, 10]$	$\log(\mu/M_{\rm Pl}) \in [-3, 3]$
RCLFI4$_{+}$	$p \in [4.1, 8]$	$\log(\alpha/\alpha_1) \in [-3, 0]$	$\log(\mu/M_{\rm Pl}) \in [-2, 4]$
RCLFI4$_{-}$	$p \in [0.1, 3.9]$	$\log(\alpha/\alpha_1) \in [-3, 0]$	$\log(\mu/M_{\rm Pl}) \in [-2, 4]$

B.19 String Axion Inflation I (SAII)

This is a String Theory motivated model emerging from geometric compactifications with a two-parameter potential given by

$$V(\phi) = M^4 \left[1 - \cos\left(\frac{\phi}{\mu}\right) + \alpha \frac{\phi}{\mu} \sin\left(\frac{\phi}{\mu}\right) \right]. \tag{B.19}$$

The coupling α does not need to be small while the vacuum expectation value μ needs to be super-Planckian for slow-roll inflation to take place. The potential having a hilltop, there are two possible inflationary regimes, SAII1 and SAAI2. A hard prior requires inflation to last, at least, 120 e-folds. We have therefore considered the priors listed below.

Name	c_1-prior	c_2-prior
$\mathrm{SAII1_n}$	$\log(-\alpha) \in [-3,3]$	$\log(\mu/M_{\rm Pl}) \in [0,3]$
$\mathrm{SAII1_p}$	$\log(\alpha) \in [-3,3]$	$\log(\mu/M_{\rm Pl}) \in [0,3]$
$\mathrm{SAII1_f}$	$\alpha \in [-10,10]$	$\log(\mu/M_{\rm Pl}) \in [0,3]$
$\mathrm{SAII2_n}$	$\log(-\alpha) \in [-3,3]$	$\log(\mu/M_{\rm Pl}) \in [0,3]$
$\mathrm{SAII2_p}$	$\log(\alpha) \in [-3,3]$	$\log(\mu/M_{\rm Pl}) \in [0,3]$
$\mathrm{SAII2_f}$	$\alpha \in [-10,10]$	$\log(\mu/M_{\rm Pl}) \in [0,3]$

B.20 String Axion Inflation II (SAIII)

This model shares the same String Theory motivations as SAII in Appendix B.19 but includes additional higher-order corrections. Its potential reads

$$V(\phi) = M^4 \left\{ 1 - \cos\left(\frac{\phi}{\mu}\right) + \alpha \left[\frac{\phi}{\mu} \sin\left(\frac{\phi}{\mu}\right) + \frac{1}{2}\beta \left(\frac{\phi}{\mu}\right)^2 \right] \right\}, \tag{B.20}$$

where the amplitude of the added terms are set by the new parameter β, which verifies $\alpha\beta > 0$. This is a three-parameter model that gives rise to three distinct inflationary regimes labeled as SAIII1, SAIII2 and SAIII3. The parameter separatrices between these regimes are given by some irrational numbers labeled as β_0, β_2 and β_3 derived in Ref. [56]. A hard prior has been added to enforce that inflation lasts, at least, 120 e-folds. We have analyzed all corresponding scenarios with the priors listed in the following table.

Name	c_1-prior	c_2-prior	c_3-prior
$\mathrm{SAIII1_+}$	$\alpha \in]0,3]$	$\beta \in]0,3]$	$\log(\mu/M_{\rm Pl}) \in [-1,2]$
$\mathrm{SAIII1_-}$	$\alpha \in [-3,0[$	$\beta \in [-3,0[$	$\log(\mu/M_{\rm Pl}) \in [-1,2]$
$\mathrm{SAIII2_+}$	$\alpha \in]0,3]$	$\beta \in]0,\beta_2]$	$\log(\mu/M_{\rm Pl}) \in [-1,2]$
$\mathrm{SAIII2_-}$	$\alpha \in [-3,0[$	$\beta \in [\beta_3,0[$	$\log(\mu/M_{\rm Pl}) \in [-1,2]$
$\mathrm{SAIII3_+}$	$\alpha \in]0,3]$	$\beta \in [\beta_0,3]$	$\log(\mu/M_{\rm Pl}) \in [-1,2]$
$\mathrm{SAIII3_-}$	$\alpha \in [-3,0[$	$\beta \in [-3,-1]$	$\log(\mu/M_{\rm Pl}) \in [-1,2]$

B.21 Superconformal α-Attractor B Inflation (SABI)

These scenarios are based on Supergravity in which the conformal symmetry associated with a highly symmetrical theory is broken. Their potential reads

$$V(\phi) = M^4 \left(1 - e^{-\sqrt{\frac{2}{3\alpha}}x}\right)^{2n}, \tag{B.21}$$

with $x = \phi/M_{\rm g}$ and $M_{\rm g} \simeq M_{\rm Pl}$. There are two parameters, a power index n and a coupling constant α (associated with a Kähler potential). We have considered various scenarios as listed below. Let us notice that the case $n = 1$ is a model referred to as Superconformal α-Attractor A Inflation in Ref. [56].

Name	c_1-prior	c_2-prior
SAAI	$\log(\alpha) \in [-3, 3]$	$n = 1$
$\text{SABI}_{1/3}$	$\log(\alpha) \in [-3, 3]$	$n = 1/3$
$\text{SABI}_{1/2}$	$\log(\alpha) \in [-3, 3]$	$n = 1/2$
$\text{SABI}_{3/2}$	$\log(\alpha) \in [-3, 3]$	$n = 3/2$
$\text{SABI}_{5/2}$	$\log(\alpha) \in [-3, 3]$	$n = 5/2$
SABI_3	$\log(\alpha) \in [-3, 3]$	$n = 3$

B.22 Superconformal α-Attractor T Inflation (SATI)

These models are another realization of conformal symmetry breaking (see Appendix B.21) in a highly symmetrical Supergravity theory and are described by the potential

$$V(\phi) = M^4 \tanh^{2n}\left(\frac{\phi}{M_{\rm Pl}\sqrt{6\alpha}}\right). \tag{B.22}$$

There are two parameters, a power index n and the Kähler coupling α. The case $\alpha = 1$ is also known as T-model inflation. The priors chosen for the SATI class are enumerated in the following table.

Name	c_1-prior	c_2-prior
TMI	$\alpha = 1$	$n \in [1, 10]$
$\text{SATI}_{1/3}$	$\log(\alpha) \in [-3, 3]$	$n = 1/3$
$\text{SATI}_{1/2}$	$\log(\alpha) \in [-3, 3]$	$n = 1/2$
SATI_1	$\log(\alpha) \in [-3, 3]$	$n = 1$
$\text{SATI}_{3/2}$	$\log(\alpha) \in [-3, 3]$	$n = 3/2$
SATI_2	$\log(\alpha) \in [-3, 3]$	$n = 2$
$\text{SATI}_{5/2}$	$\log(\alpha) \in [-3, 3]$	$n = 5/2$
$\text{SATI}_{5/2}$	$\log(\alpha) \in [-3, 3]$	$n = 3$

B.23 Symmetry Breaking Kähler Inflation (SBKI)

This scenario is based on embedding quadratic Large Field Inflation (LFI_2) in a Supergravity context where the shift symmetry gets broken by a new term in the Kähler potential. The field potential is given by

$$V(\phi) = M^4 \left(\frac{\phi}{M_{\rm Pl}}\right)^2 \exp\left[\alpha\left(\frac{\phi}{M_{\rm Pl}}\right)^2 + \frac{\alpha^2}{6}\left(\frac{\phi}{M_{\rm Pl}}\right)^4\right], \tag{B.23}$$

and involves one new parameter $|\alpha| \ll 1$ representing a vacuum expectation value in Planck units. We have analyzed the two models listed below.

Name	c_1-prior
$\mathrm{SBKI_n}$	$\log(-\alpha) \in [-4,-1]$
$\mathrm{SBKI_p}$	$\log(\alpha) \in [-4,-1]$

B.24 S-Dual Inflation (SDI)

This model is phenomenological and motivated by S-duality in String Theory where the inflaton field is a dilaton. The potential is parameterized by a vacuum expectation value μ and reads

$$V(\phi) = \frac{M^4}{\cosh\left(\dfrac{\phi}{\mu}\right)}\,. \tag{B.24}$$

As shown in Ref. [56], slow-roll inflation occurs only for super-Planckian values of $\mu > M_{\rm Pl}/\sqrt{2}$ and a hard prior has been added to ensure that it lasts more than 120 e-folds.

Name	c_1-prior
SDI	$\log(\mu/M_{\rm Pl}) \in]1/\sqrt{2}, 3]$

B.25 Smeared Higgs Inflation (SHI)

This scenario arises from an extension of the Colemann-Weinberg model into the context of Grand Unified Theory within a SU(5) symmetry. The potential is parameterized by two parameters, a vacuum expectation value ϕ_0 and a coupling constant α, both of them being unconstrained. It reads

$$V(\phi) = M^4 \left\{ \left[1 - \left(\frac{\phi}{\phi_0} \right)^2 \right]^2 + \alpha \left(\frac{\phi}{\phi_0} \right)^4 \left[\ln\left(\frac{\phi}{\phi_0} \right) - \frac{1}{4} \right] + \frac{\alpha}{4} \right\}, \tag{B.25}$$

and describes a hilltop. We have considered this model in the slow-roll regime only by adding a hard prior enforcing $\varepsilon_2 < 0.2$.

Name	c_1-prior	c_2-prior
SHI	$\log(\alpha) \in [-3,3]$	$\log(\phi_0/M_{\rm Pl}) \in [-2,2]$

B.26 Starobinsky Inflation (SI)

Starobinsky inflation is a non-minimal model of gravity having, in the Einstein frame, a potential given by

$$V(\phi) = M^4 \left(1 - e^{-\sqrt{2/3}\,\phi/M_{\rm Pl}} \right)^2. \tag{B.26}$$

It is a zero-parameter model. However, as discussed in *Encyclopædia Inflationaris*, there are theoretical realizations of this potential that live in the Jordan frame, and, as such, they correspond to a minimally coupled inflaton field. Even though both frameworks have exactly the same potential, the presence of minimal and non-minimal couplings induces slightly different reheating histories that have been taken into account within two different scenarios, SI and $\mathrm{SI_{mc}}$.

B.27 Mukhanov Inflation (VFMI)

This model provides a hydrodynamical description of the background evolution during inflation by fixing the evolution equation for the equation of state parameter $w(N) = \beta/[(3\beta/2)^{1/\alpha} + N_{\rm end} - N)^{\alpha}$, N being the number of e-folds. As discussed in *Encyclopædia Inflationaris*, this is strictly equivalent to the field potential

$$V(\phi) = M^4 \left[1 - \frac{\beta}{2\left(1 + \frac{2-\alpha}{2\sqrt{3\beta}}\frac{\phi}{M_{\rm Pl}}\right)^{\frac{2\alpha}{2-\alpha}}}\right] \exp\left\{\frac{3\beta}{1-\alpha}\left[\left(1 + \frac{2-\alpha}{2\sqrt{3\beta}}\frac{\phi}{M_{\rm Pl}}\right)^{\frac{2(1-\alpha)}{2-\alpha}} - 1\right]\right\}. \tag{B.27}$$

It is parameterized by the two parameters α and β, the order of magnitude of which is unspecified. We have therefore chosen to analyze the model under the following prior choices.

Name	c_1-prior	c_2-prior
VFMI	$\alpha \in [1/10, 10]$	$\beta \in [1/10, 10]$
VFMI$_{\rm s}$	$\alpha \in [1/4, 4]$	$\beta \in [1/4, 4]$

C Posterior distributions for the best models

In this section, we report the marginalized posterior distributions for the primordial parameters associated with the best models, i.e., the ones landing in the favored zone of evidences having $\ln(B_{\rm SR3}/B_{\rm best}) > -1$. In order to avoid redundancies, when several models share the same potential, the same theoretical framework, but only differ by their priors, we have only represented, when it exists, the model having the prior encompassing the others. In all figures, the intrinsic theoretical model parameters are enumerated as c_1, c_2, c_3, ... and we have added various derived primordial parameters as the energy scale of the potential M, the energy density at the end of inflation $\rho_{\rm end}$, the slow-roll parameters ε_i, the spectral index $n_{\rm S}$, the tensor-to-scalar ratio r_ϵ, the scalar running $\alpha_{\rm S}$ (all computed at second order in slow-roll) and the reheating parameter $R_{\rm rad}$.

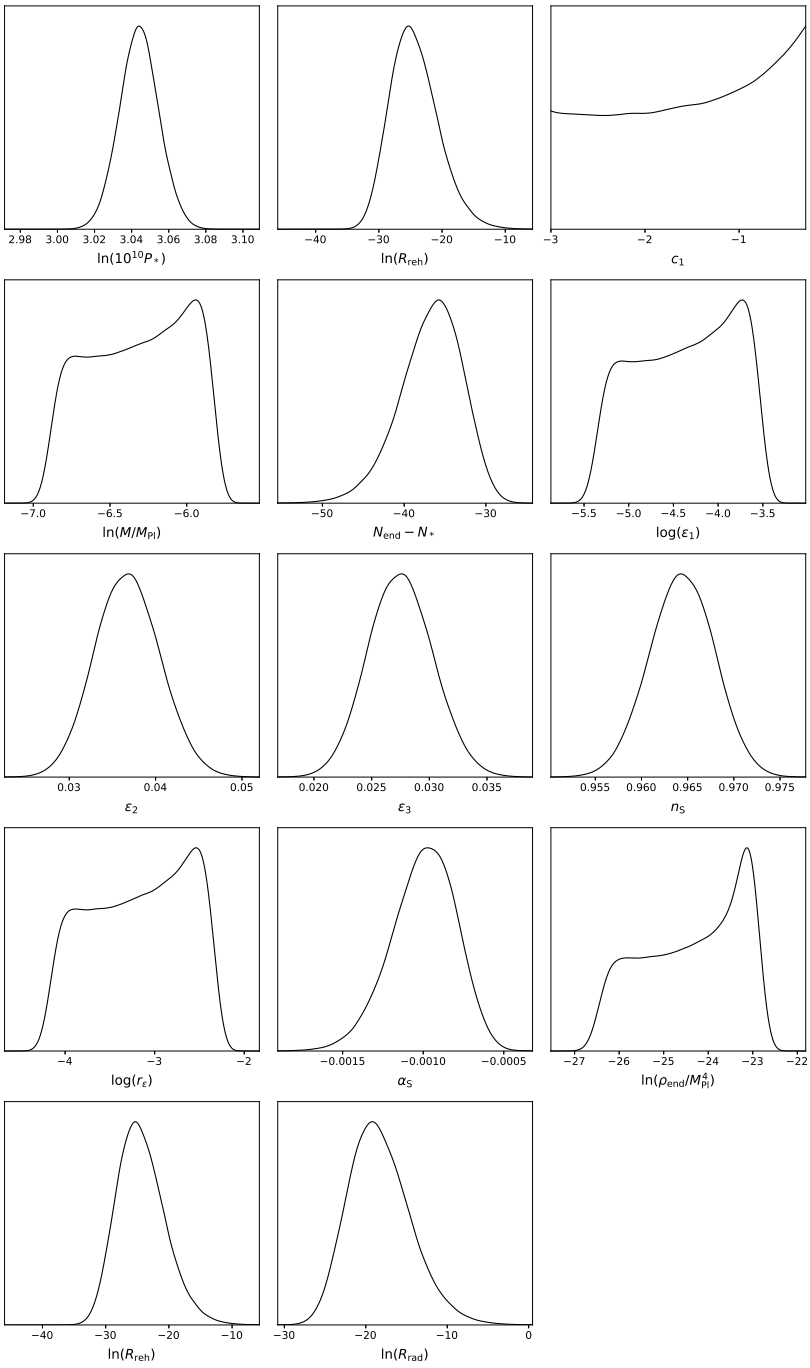

Figure 15. One-dimensional posterior distributions for Arctan Inflation (AI). This is a phenomenological model having only one parameter, a typical vacuum expectation value $c_1 = \log(\mu/M_{\rm Pl})$.

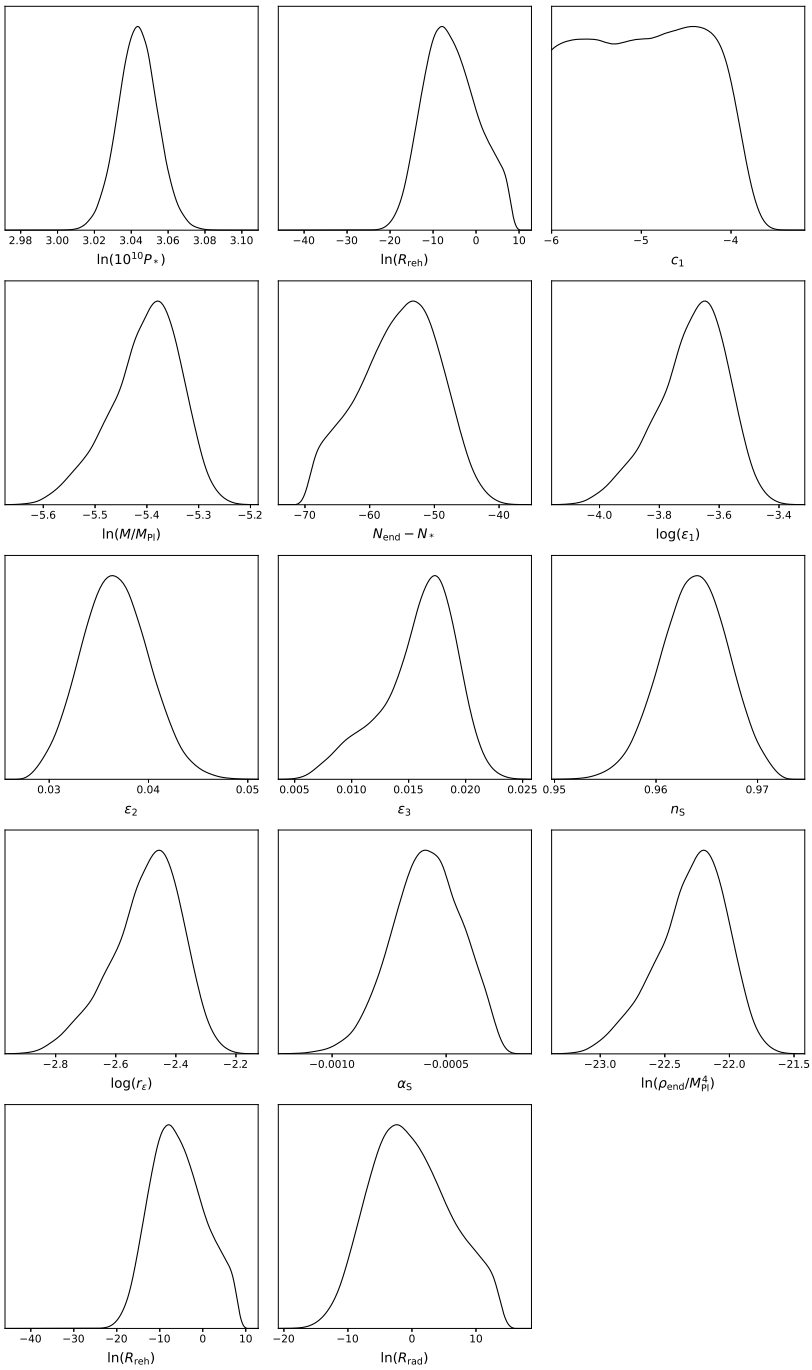

Figure 16. One-dimensional posterior distributions for Cublicly Corrected Starobinsky Inflation 1 (CCSI_1). It has one parameter $c_1 = \log(\alpha)$, where α is a small positive coupling constant.

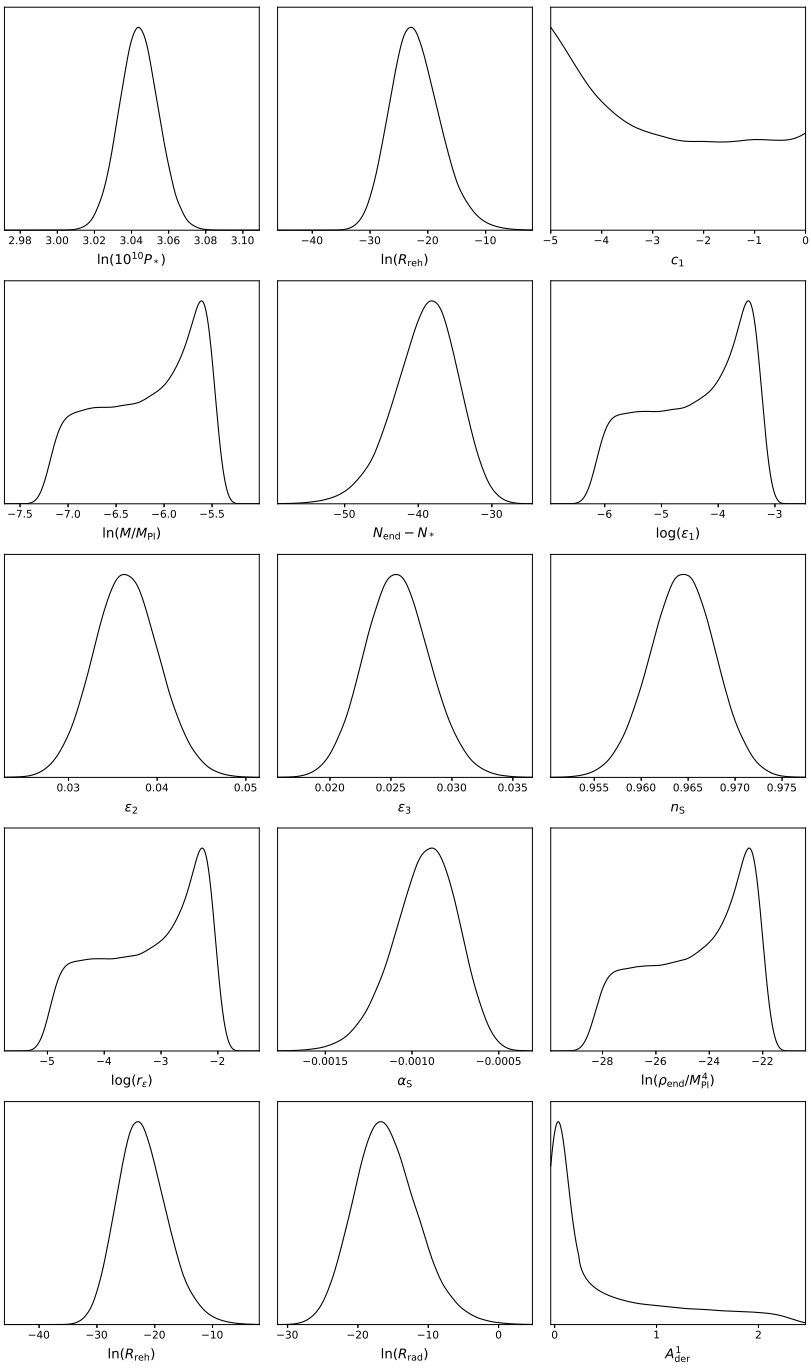

Figure 17. One-dimensional posterior distributions for Dual Inflation (DI). It has one theoretical parameter $c_1 = \log(f)$ where $f < 1$ is a ratio of two vacuum expectation values, which has to be less than unity for the underlying model to be well defined. The derived parameter $A^1_{\rm der} = \Lambda/M_{\rm Pl}$ involves Λ, another typical vacuum expectation value fixing the amplitude of the CMB anisotropies.

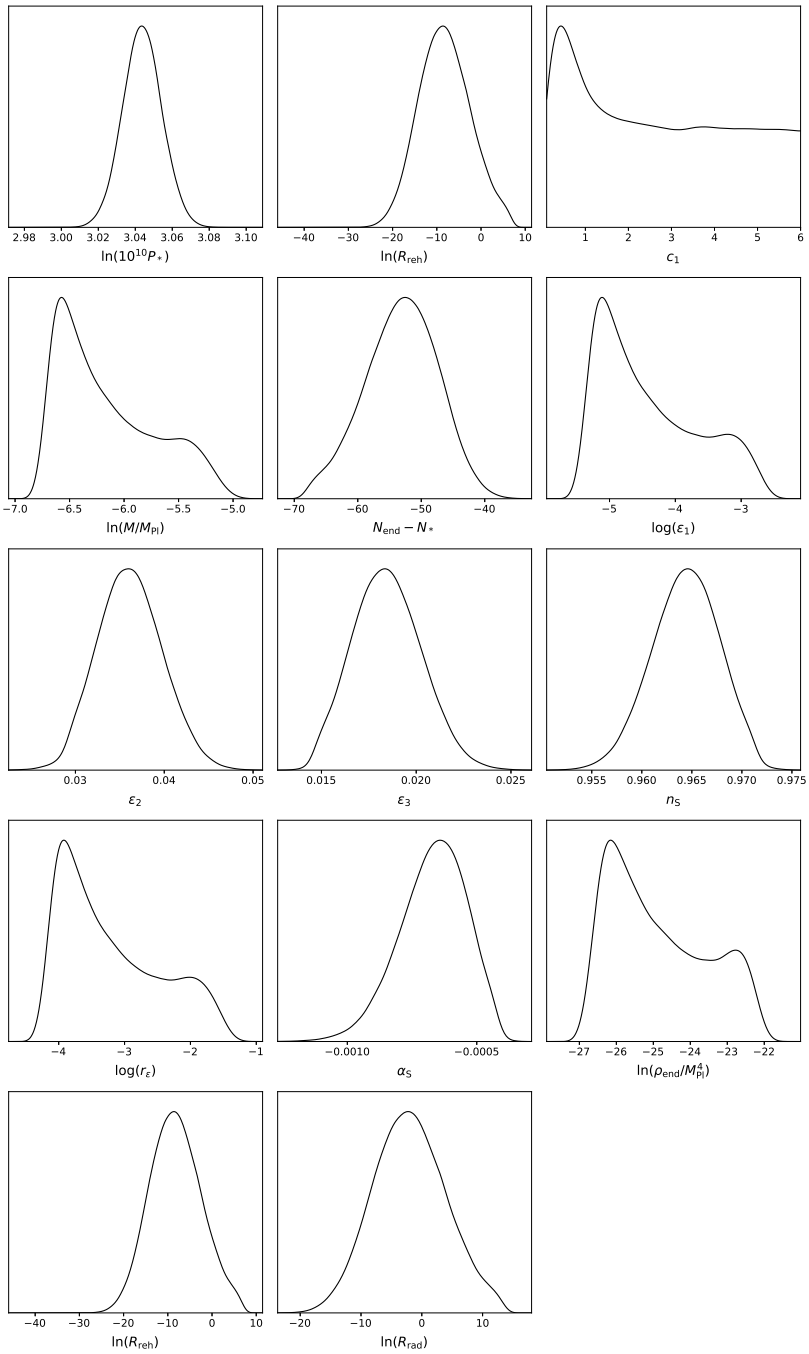

Figure 18. One-dimensional posterior distributions for Exponential SUSY Inflation (ESI). There is one theoretical parameter, a coupling constant of order one $c_1 = q$.

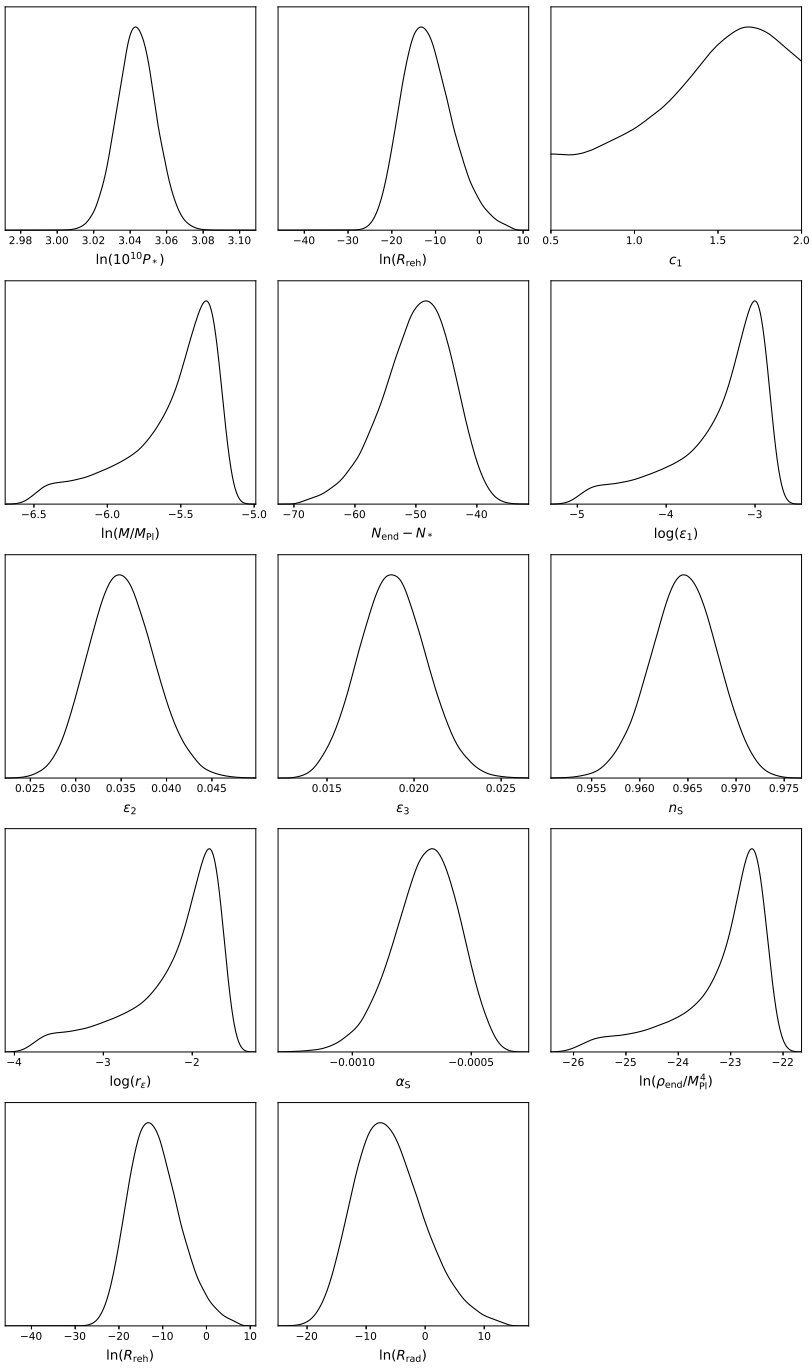

Figure 19. One-dimensional posterior distributions for Exponential SUSY Original Inflation ($\mathrm{ESI_o}$). There is one theoretical parameter $c_1 = \sqrt{2/\beta}$ where β is the normalization of a Kähler potential in the range centered around unity, $\beta \in [1/2, 2]$. It differs from Fig. 18 by the theoretically motivated prior being flat in β as opposed to being flat in c_1. This is the best model of this analysis.

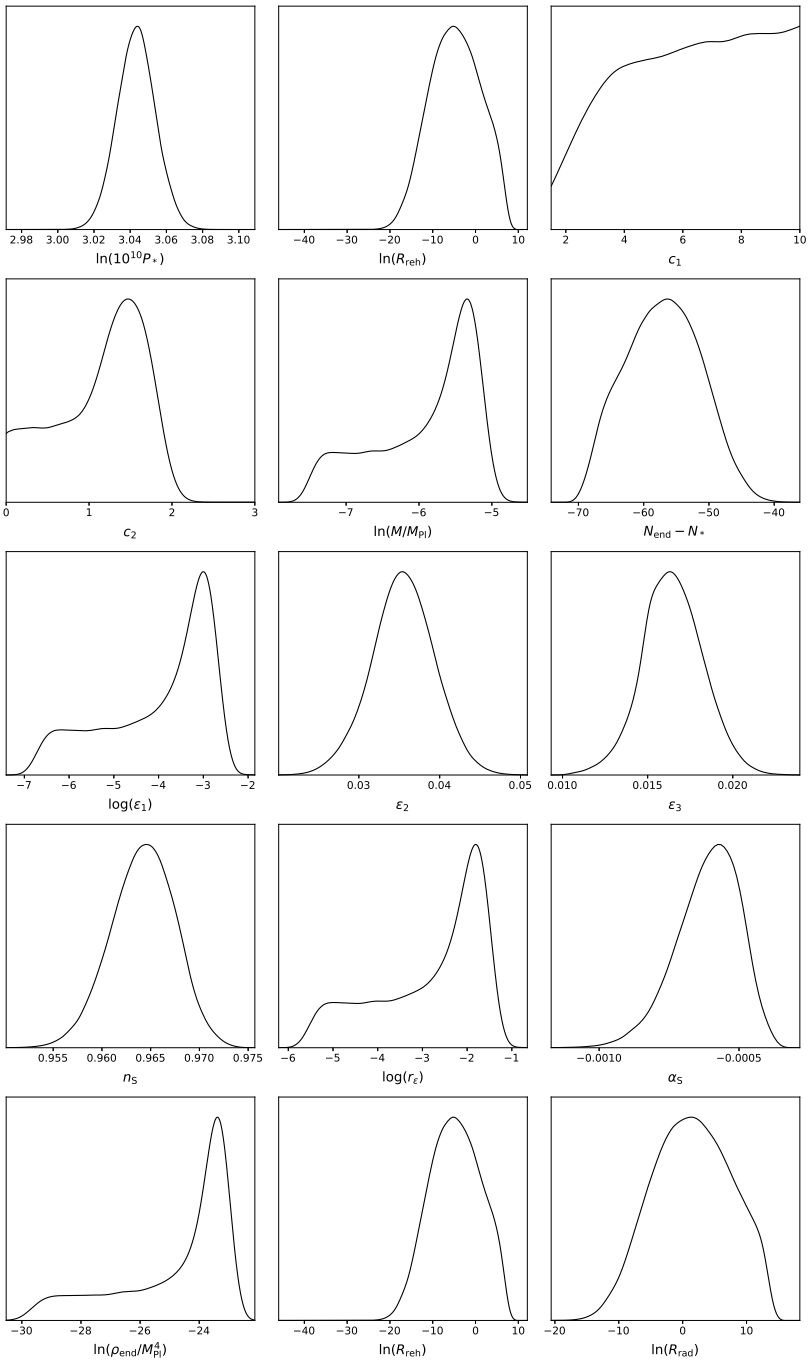

Figure 20. One-dimensional posterior distributions for Generalized Double Well Inflation at large field values ($\mathrm{GDWI_l}$). There are two theoretical parameters, a power index $c_1 = p$ and a super-Planckian vacuum expectation value $c_2 = \log(\mu/M_{\rm Pl})$.

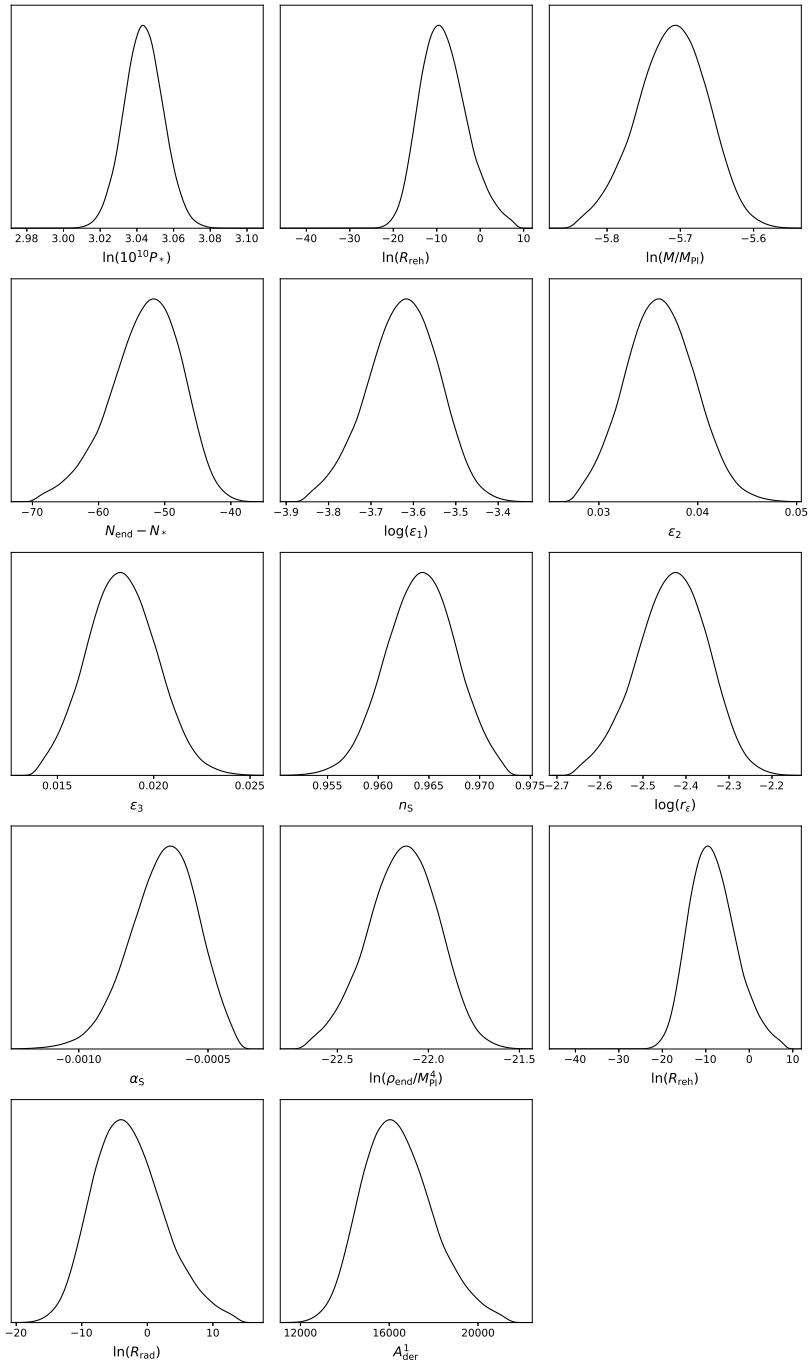

Figure 21. One-dimensional posterior distributions for Higgs Inflation (HI). There is no model parameter, but we have represented the posterior of the derived parameter $A^1_{\rm der} = \xi$, the non-minimal coupling of the Higgs field.

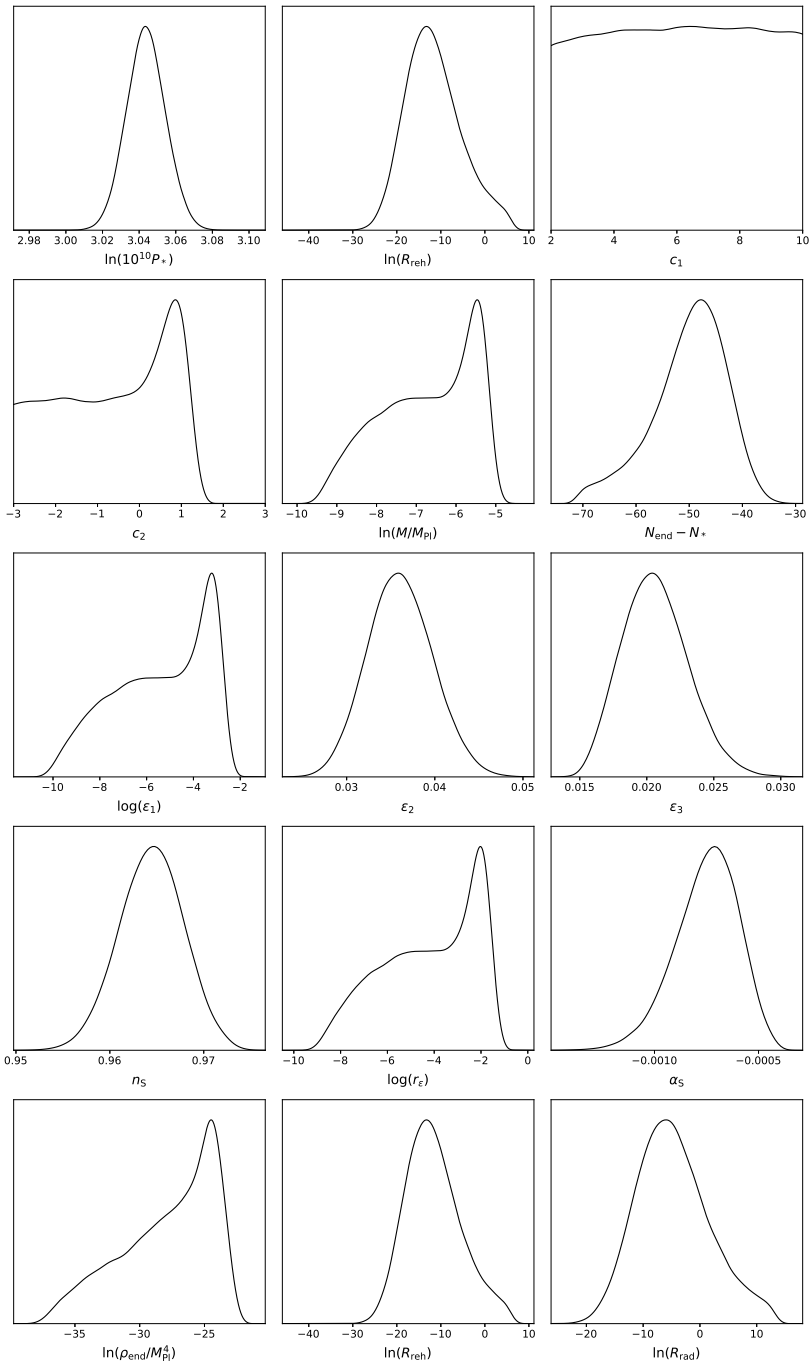

Figure 22. One-dimensional posterior distributions for KKLT Inflation (KKLTI). There are two model parameters $c_1 = p$, a power index, and $c_2 = \log(\mu/M_{\rm Pl})$, a typical vacuum expectation value.

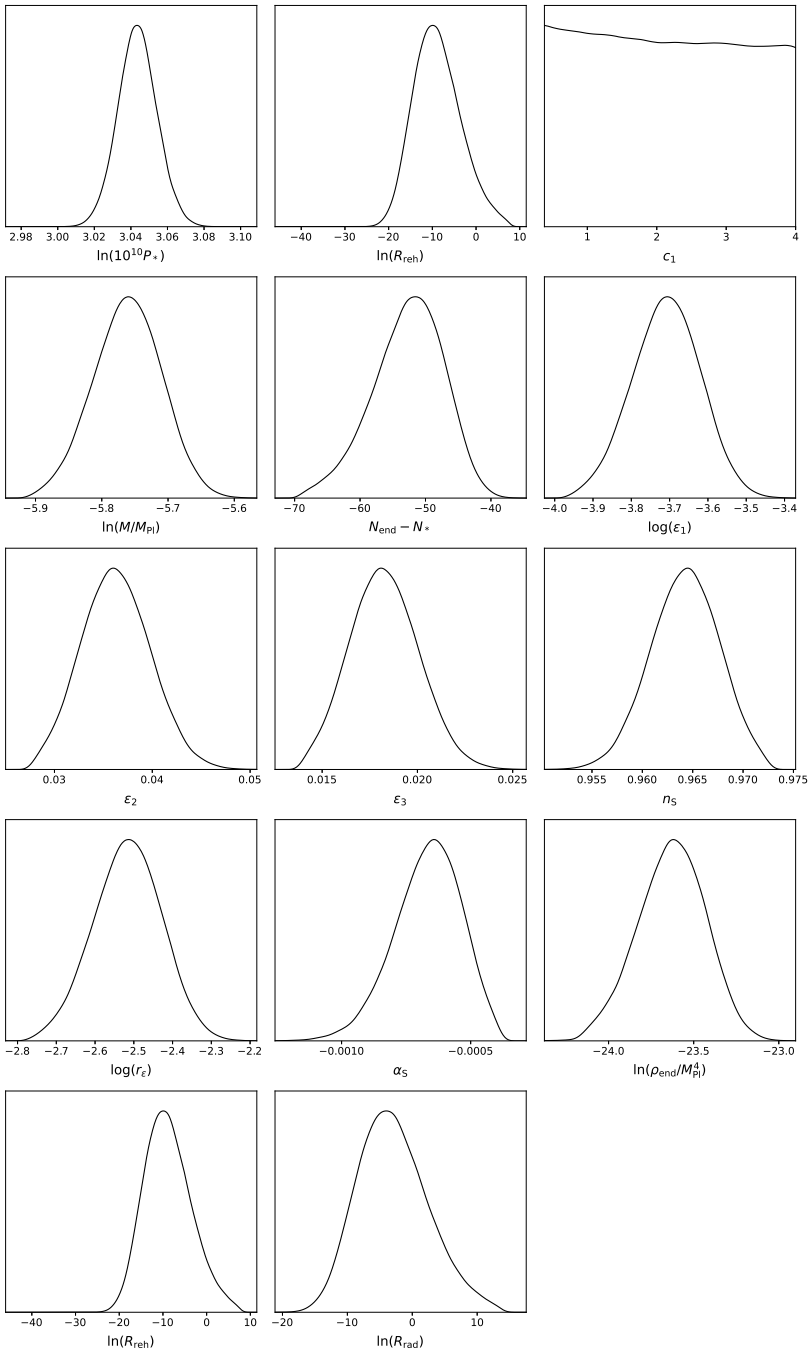

Figure 23. One-dimensional posterior distributions for Kähler Moduli Inflation I (KMII). The unique model parameter is a coupling constant $c_1 = \log(\alpha) \in [0.382, 4]$, this prior range being set by the underlying theory [54].

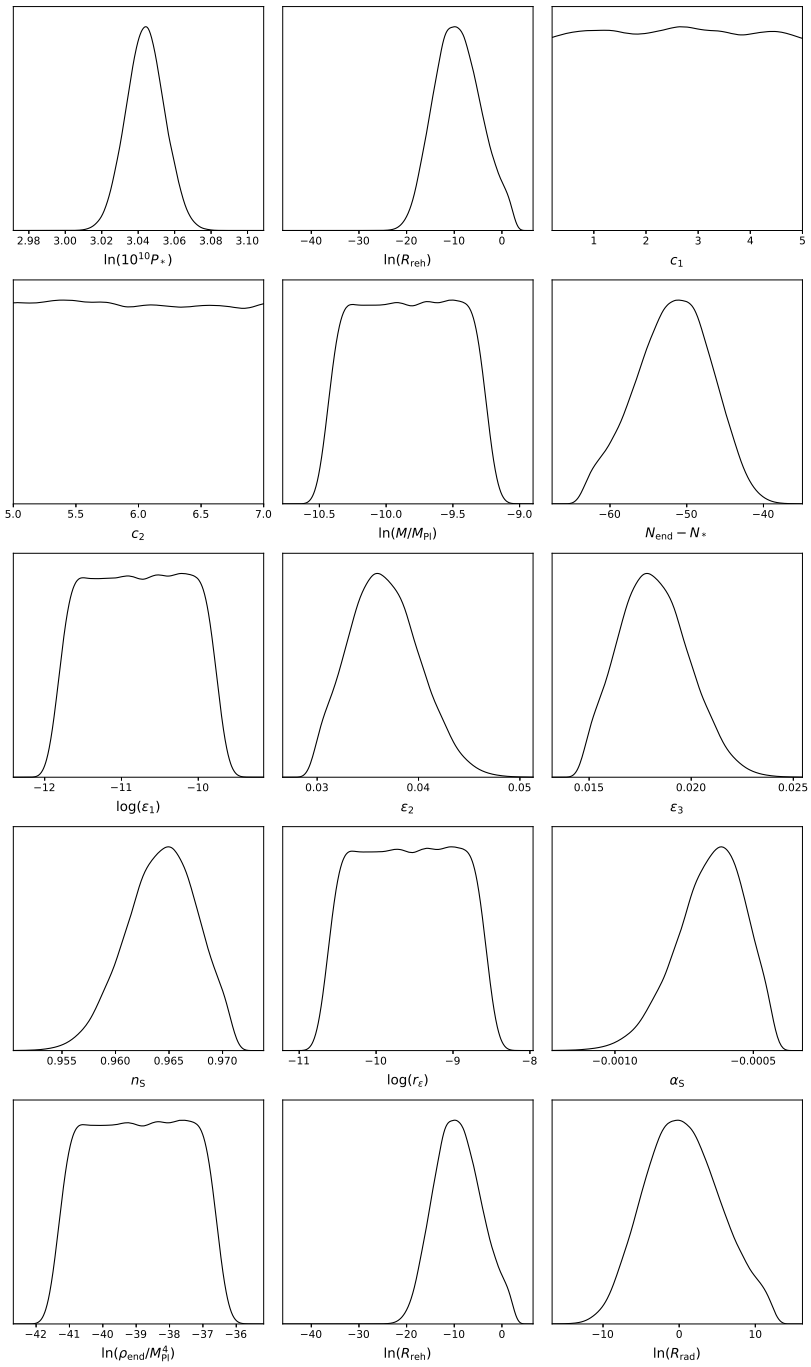

Figure 24. One-dimensional posterior distributions for Kähler Moduli Inflation II (KMIII). It has two model parameters $c_1 = \alpha/(\beta\mathcal{V})$, an order one quantity made of the ratio between coupling constants, and $c_2 = \log(\mathcal{V})$ where $\mathcal{V}$ is a dimensionless compactification volume, whose order of magnitude lies within a decade of 10^6 [54].

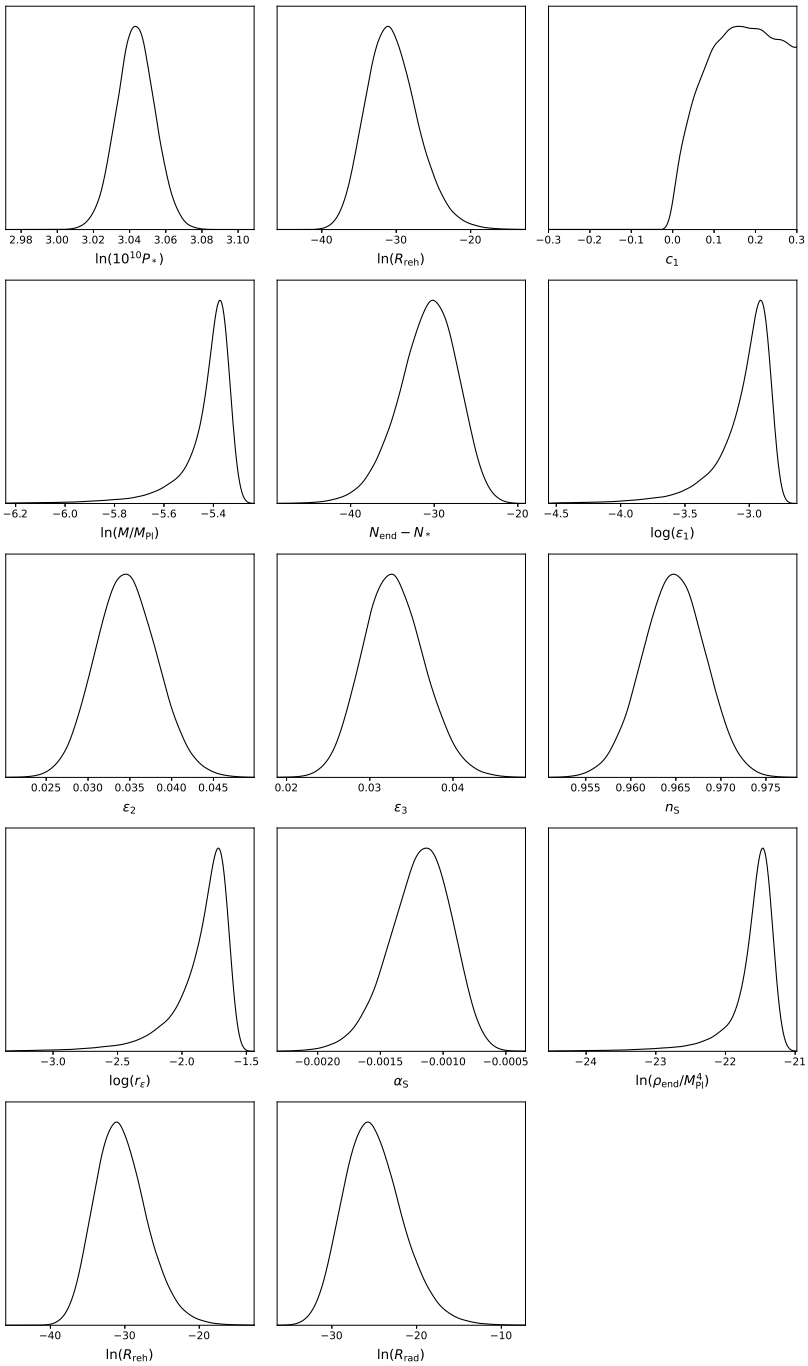

Figure 25. One-dimensional posterior distributions for Loop Inflation (LI). There is a unique model parameter $c_1 = \alpha$, a small coupling constant setting the amplitude of quantum loop corrections and living in a disconnected set $\alpha \in [-0.3, -0.1] \cup [0, 0.3]$ [54].

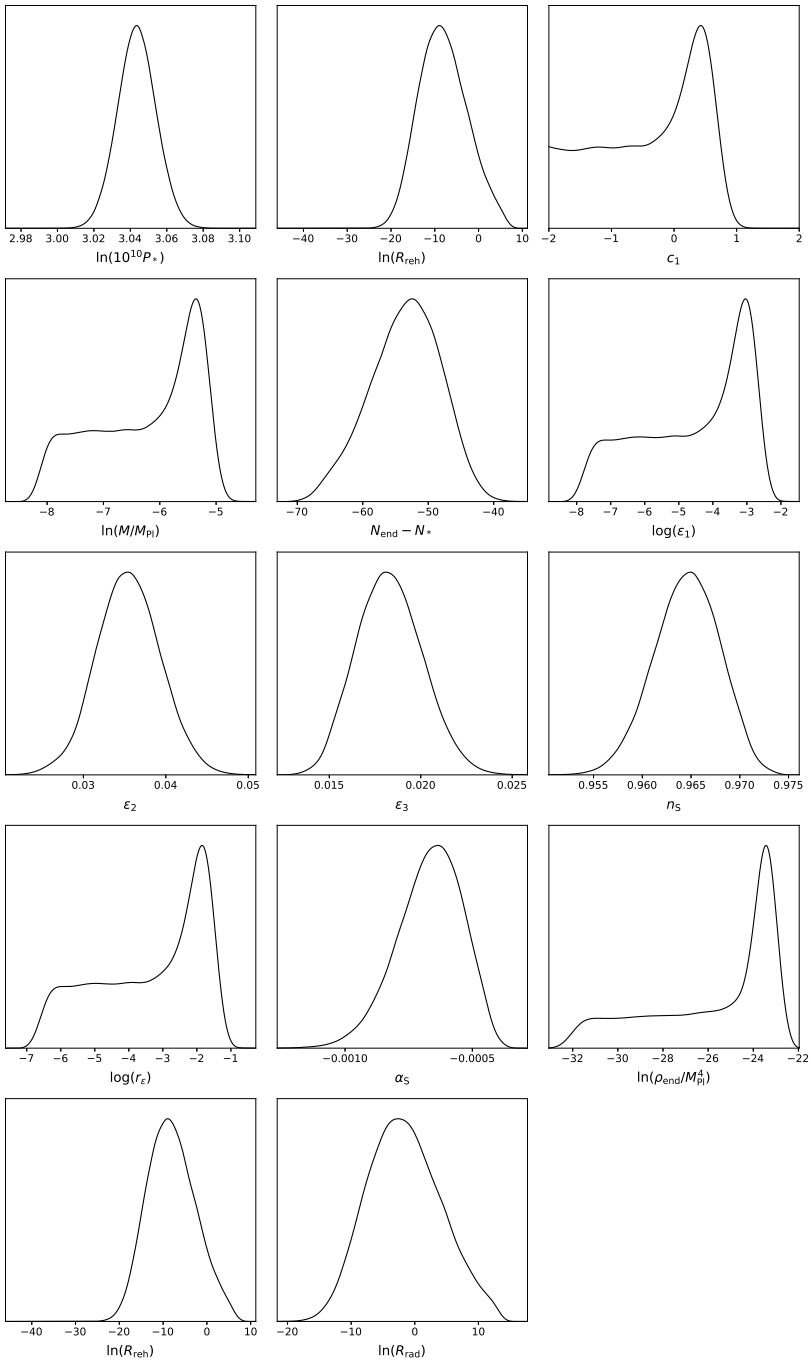

Figure 26. One-dimensional posterior distributions for Mutated Hilltop Inflation (MHI). There is a unique model parameter $c_1 = \log(\mu/M_{\rm Pl})$, where μ is the inflaton typical vacuum expectation value.

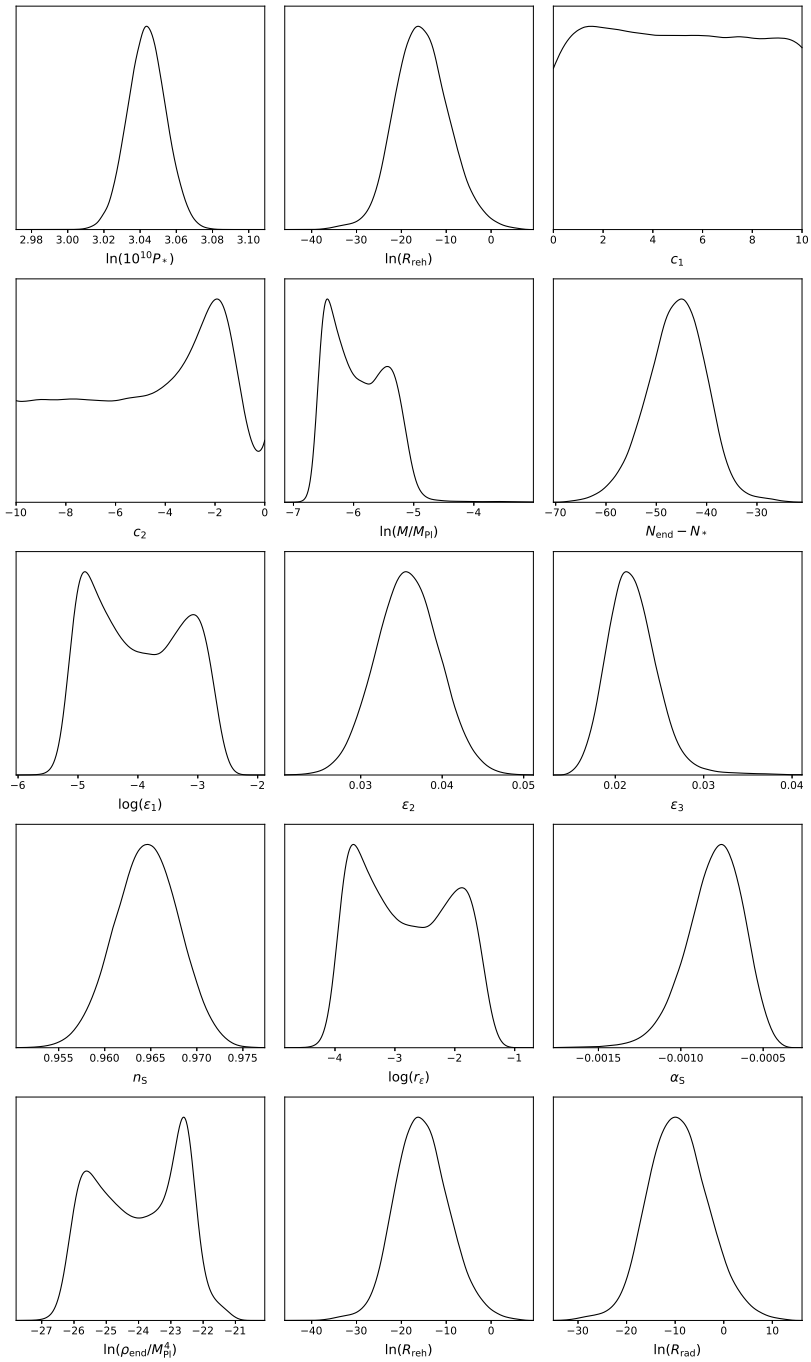

Figure 27. One-dimensional posterior distributions for N-Formalism Inflation in the regime $a > 0$ and $b < 0$ (NFI3$_{a>0}$, see Appendix B.14). The two model parameters are $c_1 = a$ and $c_2 = b$, and are constrained to be smaller than 10 in absolute value (phenomenological model).

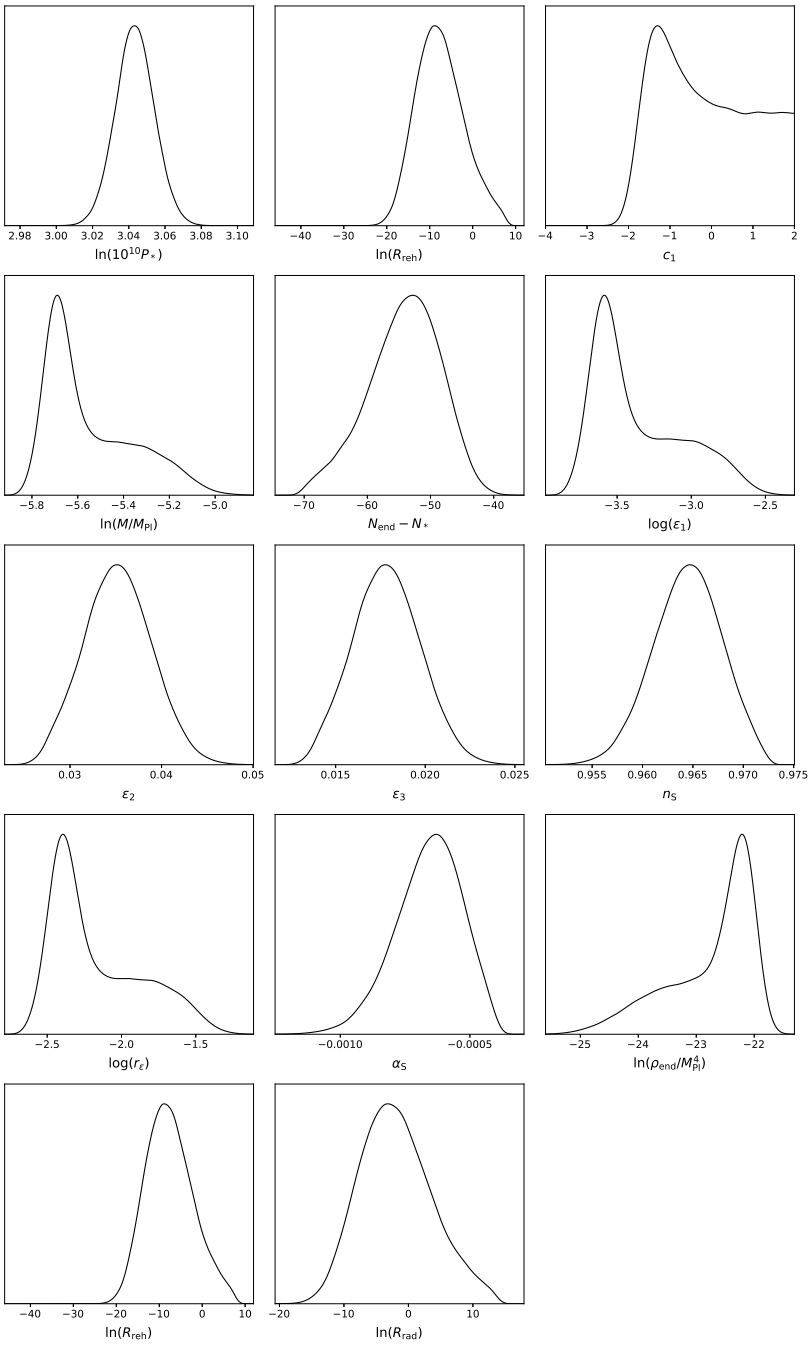

Figure 28. One-dimensional posterior distributions for Non-Minimally Coupled Large Field Inflation, with a quartic power and occurring at decreasing field values (NMLFI1_4). The unique parameter is $c_1 = \log(\xi)$, where ξ is the non-minimal coupling to gravity.

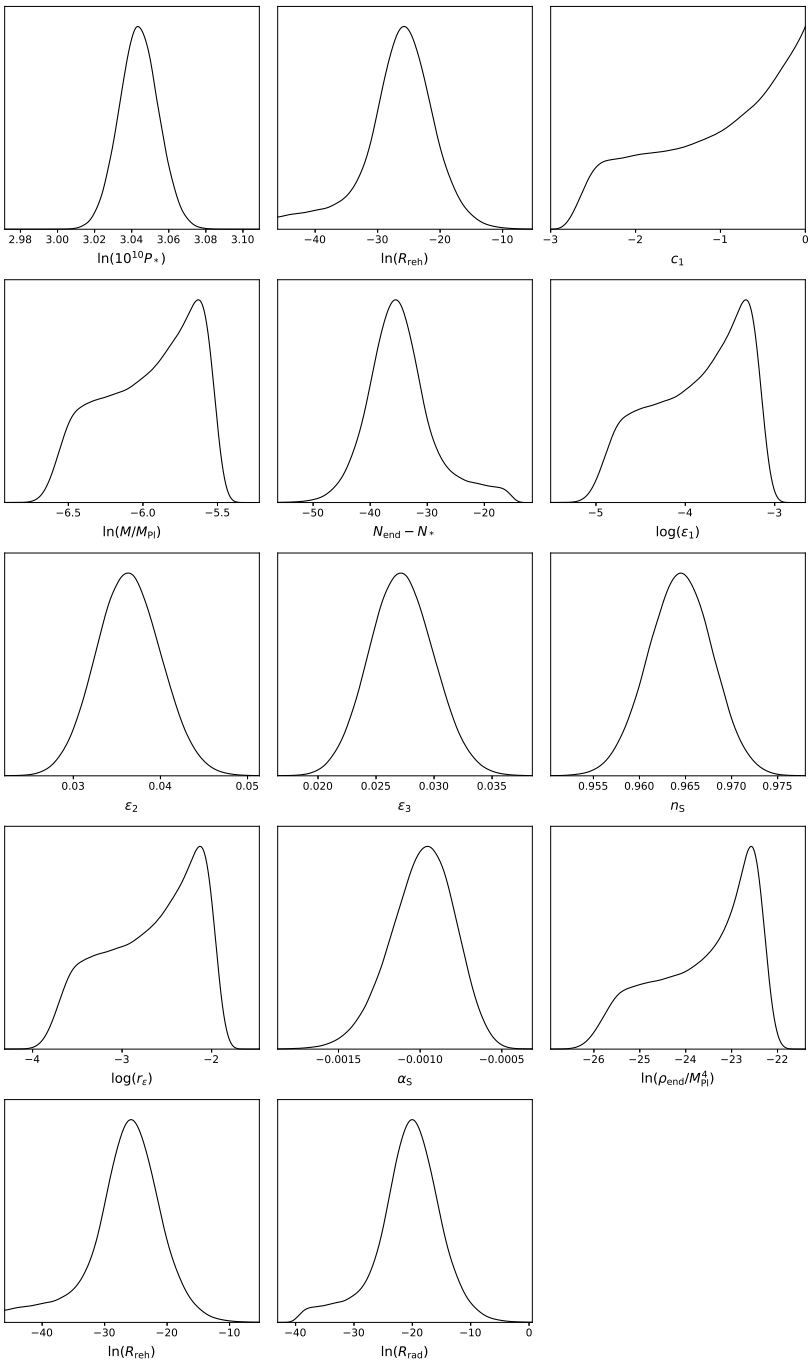

Figure 29. One-dimensional posterior distributions for Pure Arctan Inflation with small vacuum expectation value ($\mathrm{PAI_s}$). This is a phenomenological model having only one parameter $c_1 = \log(\mu/M_{\rm P1})$, μ is a sub-Planckian vacuum expectation value.

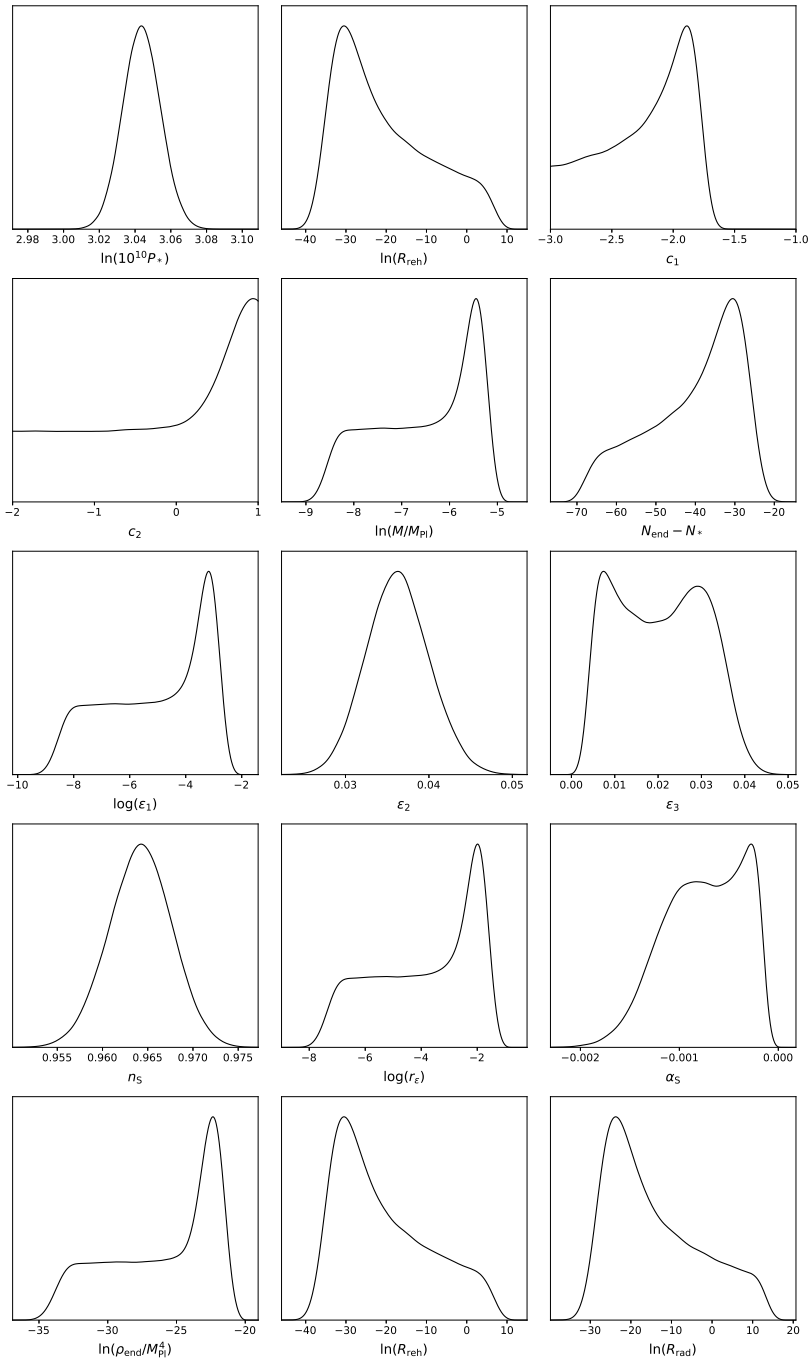

Figure 30. One-dimensional posterior distributions for Pseudo Natural Inflation with a type 2 prior choice ($\mathrm{PSNI_{ft2}}$). This is a semi-phenomenological model having two-parameters $c_1 = \log\left(\alpha M_{\rm Pl}^2/f^2\right)$ and $c_2 = \log(f/M_{\rm Pl})$ [54]. The other versions of this model differ only by different motivated choices for the prior distributions.

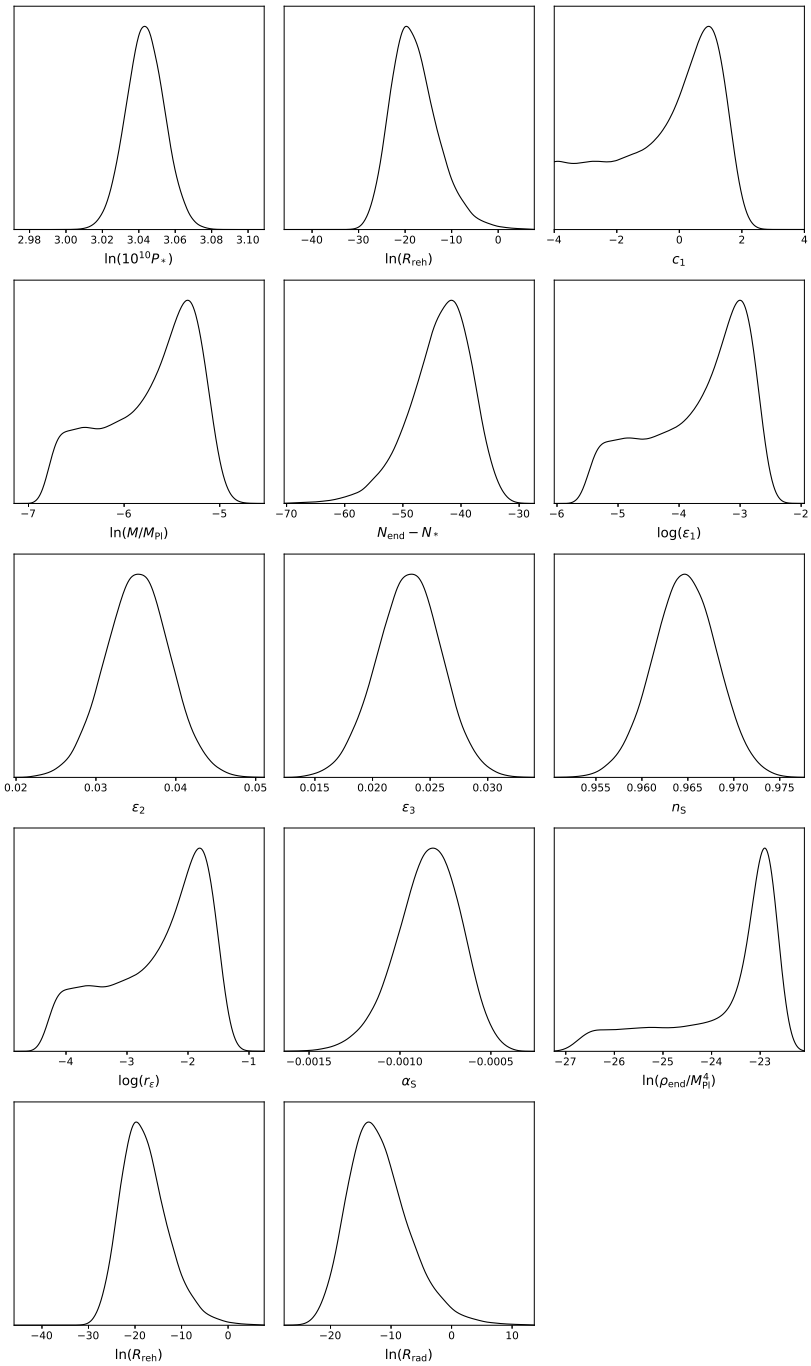

Figure 31. One-dimensional posterior distributions for Radion Gauge Inflation (RGI). There is only one parameter $c_1 = \log(\alpha)$, α being of unknown order of magnitude for the phenomenological version of this scenario [54].

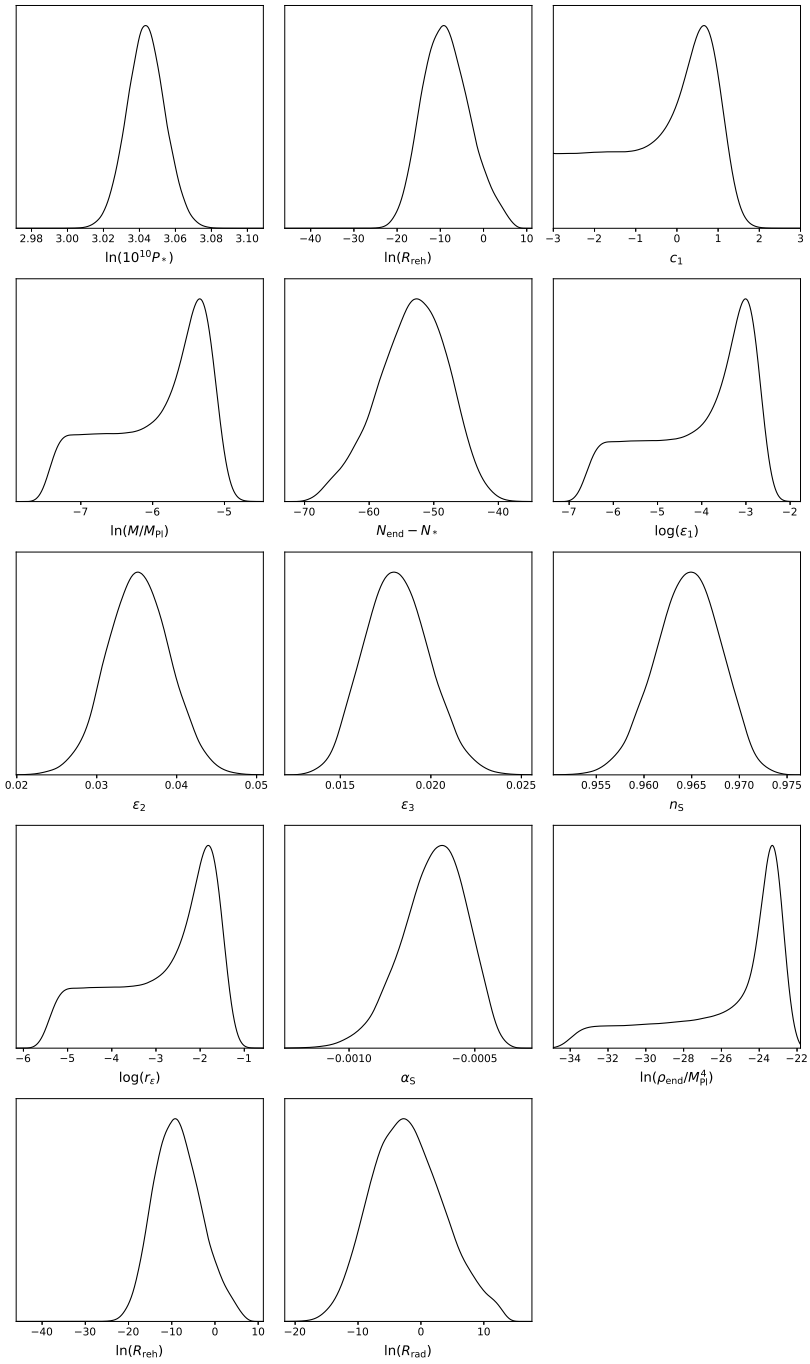

Figure 32. One-dimensional posterior distributions for Superconformal α-Attractor A Inflation (SAAI). There is one parameter $c_1 = \log(\alpha)$, α being of unknown order of magnitude.

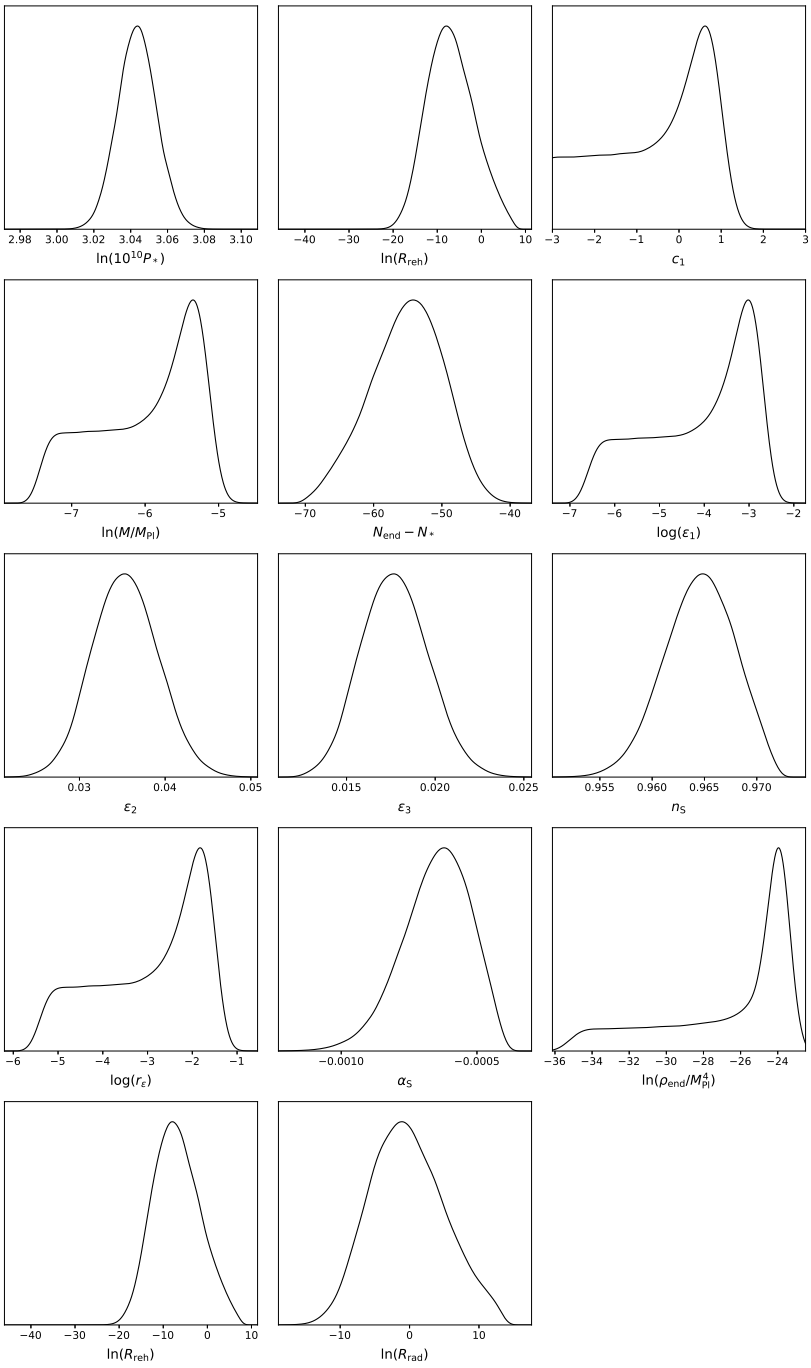

Figure 33. One-dimensional posterior distributions for Superconformal α-Attractor T Inflation with quadratic power (SATI_1). There is one parameter $c_1 = \log(\alpha)$, α being of unknown order of magnitude.

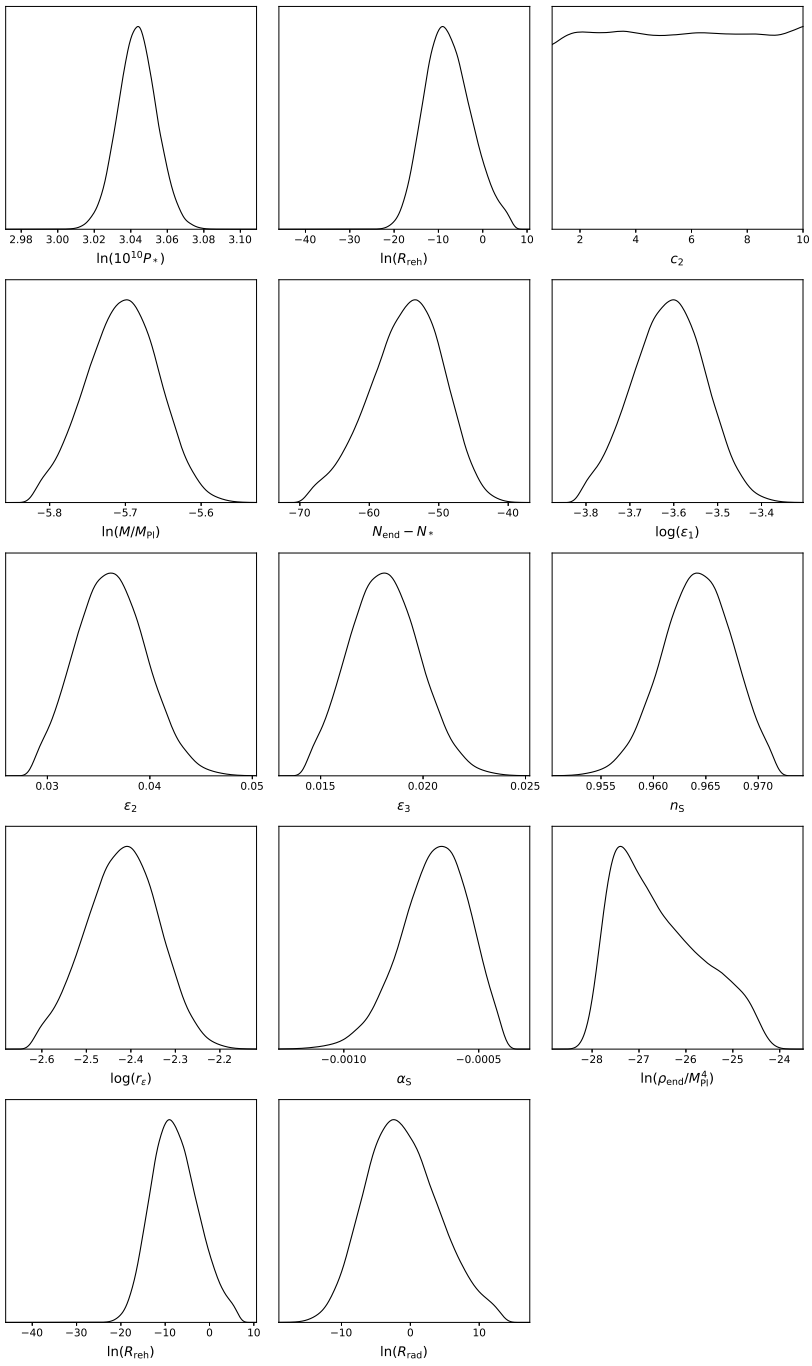

Figure 34. One-dimensional posterior distributions for T-Model Inflation (TMI). There is one parameters $c_2 = n$, a power index.

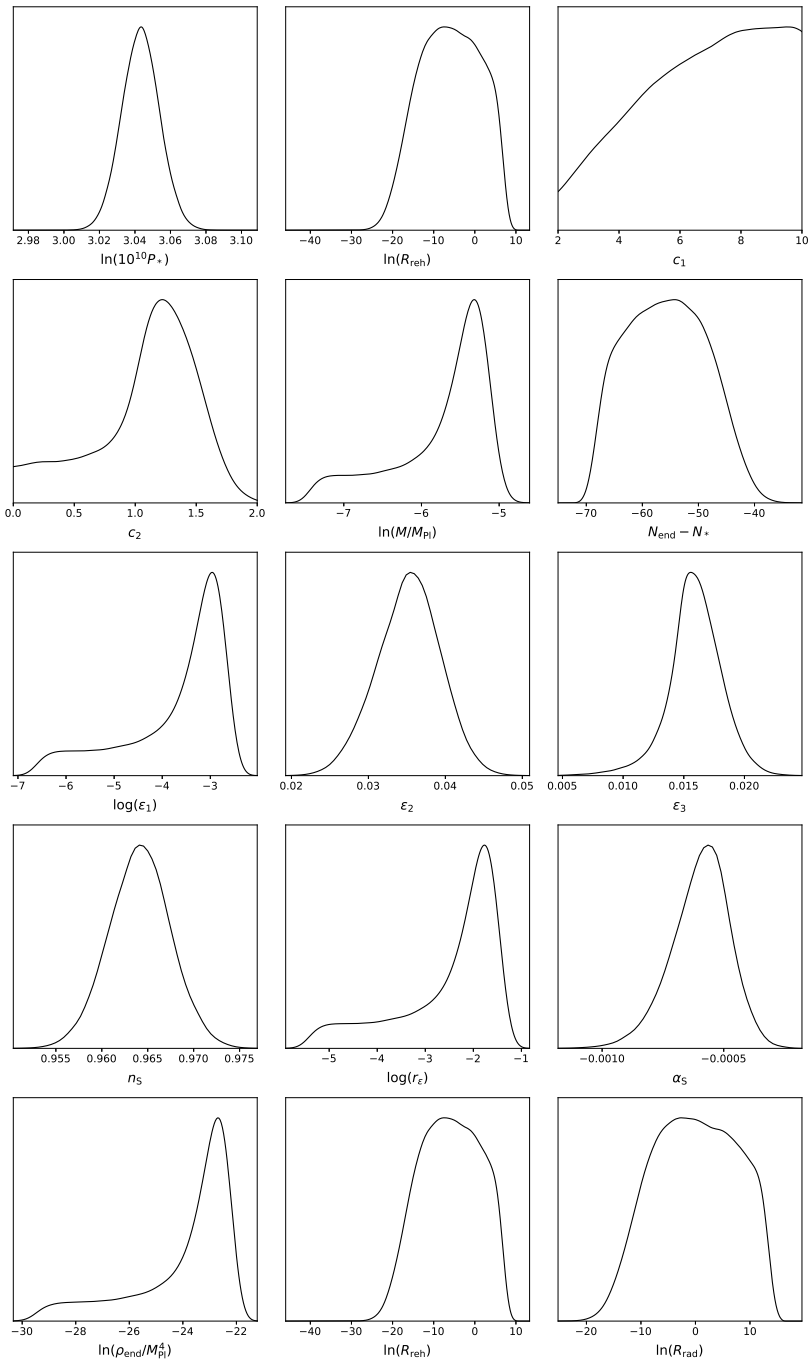

Figure 35. One-dimensional posterior distributions for Small Field Inflation at large vacuum expectation values ($\mathrm{SFI_l}$). There are two parameters: $c_1 = p$, a power index, and $c_2 = \log(\mu/M_{\rm Pl})$, a super-Planckian vacuum expectation value.

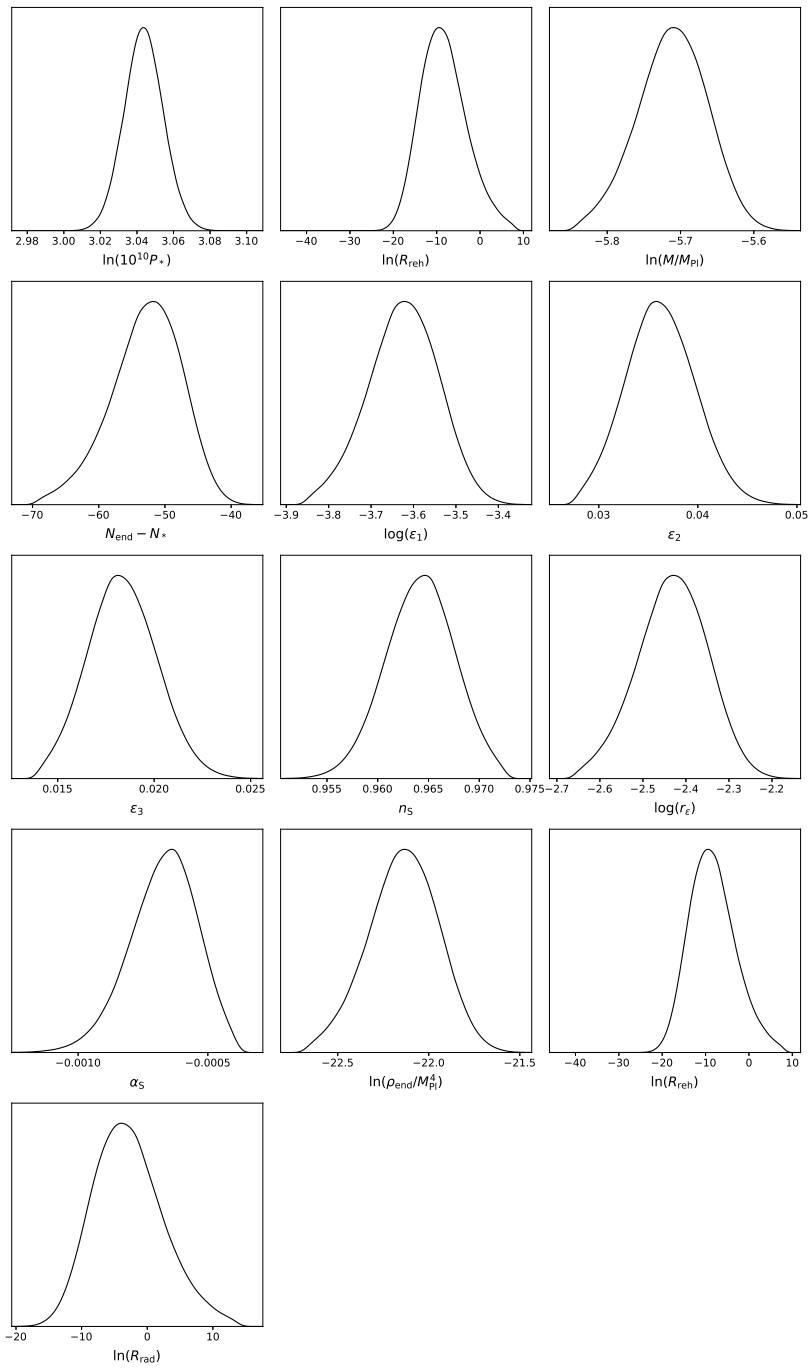

Figure 36. One-dimensional posterior distributions for Starobinsky Inflation (SI). There is no model parameter. As can be checked in Fig. 21, the data do not yet allow disambiguation between SI, $\mathrm{SI}_{\mathrm{mc}}$ and HI.

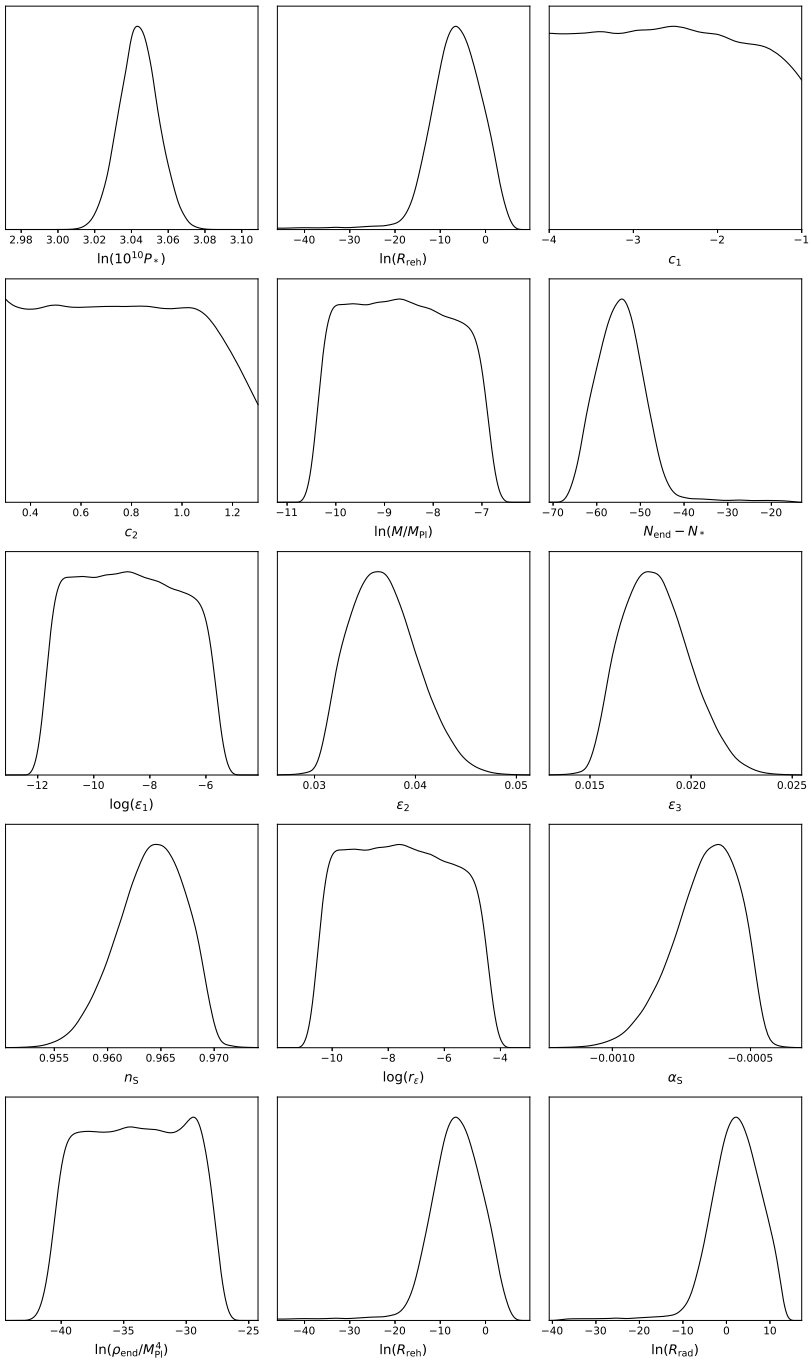

Figure 37. One-dimensional posterior distributions for Twisted Inflation (TWI_{ϕ_0}). This is a two-parameter model with $c_1 = \log(\phi_0/M_{\rm Pl})$, a vacuum expectation value, and $c_2 = \log(\phi_{\rm end}/\phi_0)$, the field value at which inflation ends (in unit of ϕ_0) [54].

References

[1] A.A. Starobinsky, *Relict Gravitation Radiation Spectrum and Initial State of the Universe. (In Russian)*, *JETP Lett.* **30** (1979) 682.

[2] A.A. Starobinsky, *A New Type of Isotropic Cosmological Models Without Singularity*, *Phys. Lett.* **B91** (1980) 99.

[3] A.H. Guth, *The Inflationary Universe: A Possible Solution to the Horizon and Flatness Problems*, *Phys. Rev.* **D23** (1981) 347.

[4] A.D. Linde, *A New Inflationary Universe Scenario: A Possible Solution of the Horizon, Flatness, Homogeneity, Isotropy and Primordial Monopole Problems*, *Phys. Lett.* **B108** (1982) 389.

[5] A. Albrecht and P.J. Steinhardt, *Cosmology for Grand Unified Theories with Radiatively Induced Symmetry Breaking*, *Phys. Rev. Lett.* **48** (1982) 1220.

[6] A.D. Linde, *Chaotic Inflation*, *Phys. Lett.* **B129** (1983) 177.

[7] V.F. Mukhanov and G.V. Chibisov, *Quantum Fluctuation and Nonsingular Universe. (In Russian)*, *JETP Lett.* **33** (1981) 532.

[8] V.F. Mukhanov and G.V. Chibisov, *The Vacuum energy and large scale structure of the universe*, *Sov. Phys. JETP* **56** (1982) 258.

[9] A.A. Starobinsky, *Dynamics of Phase Transition in the New Inflationary Universe Scenario and Generation of Perturbations*, *Phys. Lett.* **B117** (1982) 175.

[10] A.H. Guth and S.Y. Pi, *Fluctuations in the New Inflationary Universe*, *Phys. Rev. Lett.* **49** (1982) 1110.

[11] S.W. Hawking, *The Development of Irregularities in a Single Bubble Inflationary Universe*, *Phys. Lett.* **B115** (1982) 295.

[12] J.M. Bardeen, P.J. Steinhardt and M.S. Turner, *Spontaneous Creation of Almost Scale - Free Density Perturbations in an Inflationary Universe*, *Phys. Rev.* **D28** (1983) 679.

[13] C.L. Bennett, D. Larson, J.L. Weiland, N. Jarosik, G. Hinshaw, N. Odegard et al., *Nine-year Wilkinson Microwave Anisotropy Probe (WMAP) Observations: Final Maps and Results*, ApJS **208** (2013) 20 [1212.5225].

[14] Planck collaboration, *Planck 2013 results. I. Overview of products and scientific results*, *Astron. Astrophys.* **571** (2014) A1 [1303.5062].

[15] Planck collaboration, *Planck 2018 results. X. Constraints on inflation*, *Astron. Astrophys.* **641** (2020) A10 [1807.06211].

[16] D. Chowdhury, J. Martin, C. Ringeval and V. Vennin, *Inflation after Planck: Judgement Day*, *Phys. Rev. D* **100** (2019) 083537 [1902.03951].

[17] S. Ávila, J. Martin and D. Steer, *Superimposed Oscillations in Brane Inflation*, *JCAP* **08** (2014) 032 [1304.3262].

[18] J. Martin and R.H. Brandenberger, *The TransPlanckian problem of inflationary cosmology*, *Phys. Rev. D* **63** (2001) 123501 [hep-th/0005209].

[19] J. Martin and C. Ringeval, *Superimposed oscillations in the WMAP data?*, *Phys. Rev. D* **69** (2004) 083515 [astro-ph/0310382].

[20] J. Martin and C. Ringeval, *Addendum to 'Superimposed oscillations in the WMAP data?'*, *Phys. Rev. D* **69** (2004) 127303 [astro-ph/0402609].

[21] J. Martin and C. Ringeval, *Exploring the superimposed oscillations parameter space*, *JCAP* **01** (2005) 007 [hep-ph/0405249].

[22] H. Kurki-Suonio, P. Laguna and R.A. Matzner, *Inhomogeneous inflation: Numerical evolution*, *Phys. Rev. D* **48** (1993) 3611 [astro-ph/9306009].

[23] W.E. East, M. Kleban, A. Linde and L. Senatore, *Beginning inflation in an inhomogeneous universe*, *JCAP* **09** (2016) 010 [1511.05143].

[24] K. Clough, R. Flauger and E.A. Lim, *Robustness of Inflation to Large Tensor Perturbations*, *JCAP* **05** (2018) 065 [1712.07352].

[25] J.C. Aurrekoetxea, K. Clough, R. Flauger and E.A. Lim, *The Effects of Potential Shape on Inhomogeneous Inflation*, *JCAP* **05** (2020) 030 [1910.12547].

[26] C. Joana and S. Clesse, *Inhomogeneous preinflation across Hubble scales in full general relativity*, *Phys. Rev. D* **103** (2021) 083501 [2011.12190].

[27] C. Joana, *Gravitational dynamics in Higgs inflation: Preinflation and preheating with an auxiliary field*, *Phys. Rev. D* **106** (2022) 023504 [2202.07604].

[28] D. Garfinkle, A. Ijjas and P.J. Steinhardt, *Initial conditions problem in cosmological inflation revisited*, *Phys. Lett. B* **843** (2023) 138028 [2304.12150].

[29] COBE collaboration, *Structure in the COBE differential microwave radiometer first year maps*, *Astrophys. J. Lett.* **396** (1992) L1.

[30] WMAP collaboration, *First year Wilkinson Microwave Anisotropy Probe (WMAP) observations: Determination of cosmological parameters*, *Astrophys. J. Suppl.* **148** (2003) 175 [astro-ph/0302209].

[31] A. de Oliveira-Costa, M.J. Devlin, T. Herbig, A.D. Miller, C.B. Netterfield, L. Page et al., *Mapping the CMB. 3. Combined analysis of QMAP flights*, *Astrophys. J. Lett.* **509** (1998) L77 [astro-ph/9808045].

[32] Boomerang collaboration, *A Flat universe from high resolution maps of the cosmic microwave background radiation*, *Nature* **404** (2000) 955 [astro-ph/0004404].

[33] S. Hanany et al., *MAXIMA-1: A Measurement of the cosmic microwave background anisotropy on angular scales of 10 arcminutes to 5 degrees*, *Astrophys. J. Lett.* **545** (2000) L5 [astro-ph/0005123].

[34] Archeops collaboration, *Archeops results on the cosmic microwave background*, in *38th Rencontres de Moriond on Electroweak Interactions and Unified Theories*, 6, 2003 [astro-ph/0306032].

[35] B. Reichborn-Kjennerud, A.M. Aboobaker, P. Ade, F. Aubin, C. Baccigalupi, C. Bao et al., *Ebex: a balloon-borne cmb polarization experiment*, in *Millimeter, Submillimeter, and Far-Infrared Detectors and Instrumentation for Astronomy V*, W.S. Holland and J. Zmuidzinas, eds., SPIE, July, 2010, DOI.

[36] SPIDER collaboration, *SPIDER: CMB Polarimetry from the Edge of Space*, *J. Low Temp. Phys.* **193** (2018) 1112 [1711.10596].

[37] J.E. Ruhl, M. Dragovan, S.R. Platt, J. Kovac and G. Novak, *Anisotropy of the Microwave Sky at 90 GHz: Results from Python-II*, *Astrophys. J. Lett.* **453** (1995) L1 [astro-ph/9508065].

[38] C.B. Netterfield, M.J. Devlin, N. Jarosik, L. Page and E.J. Wollack, *A Measurement of the angular power spectrum of the anisotropy in the cosmic microwave background*, *Astrophys. J.* **474** (1997) 47 [astro-ph/9601197].

[39] C.L. Reichardt et al., *High resolution CMB power spectrum from the complete ACBAR data set*, *Astrophys. J.* **694** (2009) 1200 [0801.1491].

[40] J.A. Rubino-Martin et al., *The QUIJOTE CMB Experiment*, *Astrophys. Space Sci. Proc.* (2010) 127 [0810.3141].

[41] C.L. Reichardt, O. Zahn, P.A.R. Ade, K. Basu, A.N. Bender, F. Bertoldi et al., *Constraints on the high-l power spectrum of millimeter-wave anisotropies from apex-sz*, *The Astrophysical Journal* **701** (2009) 1958–1964.

[42] J.W. Fowler, V. Acquaviva, P.A.R. Ade, P. Aguirre, M. Amiri, J.W. Appel et al., *The atacama cosmology telescope: A measurement of the* $600 < \ell < 8000$ *cosmic microwave background power spectrum at 148 ghz*, *The Astrophysical Journal* **722** (2010) 1148–1161.

[43] H.C. Chiang, P.A.R. Ade, D. Barkats, J.O. Battle, E.M. Bierman, J.J. Bock et al., *Measurement of cosmic microwave background polarization power spectra from two years of bicep data*, *The Astrophysical Journal* **711** (2010) 1123–1140.

[44] POLARBEAR collaboration, *Measurement of the Cosmic Microwave Background Polarization Lensing Power Spectrum with the POLARBEAR experiment*, *Phys. Rev. Lett.* **113** (2014) 021301 [1312.6646].

[45] J. Kovac, E.M. Leitch, C. Pryke, J.E. Carlstrom, N.W. Halverson and W.L. Holzapfel, *Detection of polarization in the cosmic microwave background using DASI*, *Nature* **420** (2002) 772 [astro-ph/0209478].

[46] CMB-S4 collaboration, *Snowmass 2021 CMB-S4 White Paper*, 2203.08024.

[47] H. Sugai, P.A.R. Ade, Y. Akiba, D. Alonso, K. Arnold, J. Aumont et al., *Updated design of the cmb polarization experiment satellite litebird*, *Journal of Low Temperature Physics* **199** (2020) 1107–1117.

[48] R. Laureijs, J. Amiaux, S. Arduini, J.L. Augueres, J. Brinchmann, R. Cole et al., *Euclid definition study report*, 2011.

[49] A. Weltman et al., *Fundamental physics with the Square Kilometre Array*, *Publ. Astron. Soc. Austral.* **37** (2020) e002 [1810.02680].

[50] https://github.com/cosmicinflation.

[51] K. Tokeshi and V. Vennin, *Why does inflation look single field to us?*, 2310.16649.

[52] J. Martin, C. Ringeval and V. Vennin, *Information Gain on Reheating: the One Bit Milestone*, *Phys. Rev.* **D93** (2016) 103532 [1603.02606].

[53] D.J. Schwarz and C.A. Terrero-Escalante, *Primordial fluctuations and cosmological inflation after WMAP 1.0*, *JCAP* **0408** (2004) 003 [hep-ph/0403129].

[54] J. Martin, C. Ringeval, R. Trotta and V. Vennin, *The Best Inflationary Models After Planck*, *JCAP* **1403** (2014) 039 [1312.3529].

[55] J. Martin, C. Ringeval and V. Vennin, *Encyclopædia Inflationaris*, *Phys. Dark Univ.* **5-6** (2014) 75 [1303.3787v3].

[56] J. Martin, C. Ringeval and V. Vennin, *Encyclopædia Inflationaris (opiparous edition)*, 1303.3787.

[57] E.D. Stewart and D.H. Lyth, *A more accurate analytic calculation of the spectrum of cosmological perturbations produced during inflation*, *Phys. Lett.* **B302** (1993) 171 [gr-qc/9302019].

[58] A.R. Liddle, P. Parsons and J.D. Barrow, *Formalizing the slow roll approximation in inflation*, *Phys. Rev.* **D50** (1994) 7222 [astro-ph/9408015].

[59] T.T. Nakamura and E.D. Stewart, *The Spectrum of cosmological perturbations produced by a multicomponent inflaton to second order in the slow roll approximation*, *Phys. Lett.* **B381** (1996) 413 [astro-ph/9604103].

[60] J.-O. Gong and E.D. Stewart, *The density perturbation power spectrum to second-order corrections in the slow-roll expansion*, *Phys. Lett.* **B510** (2001) 1 [astro-ph/0101225].

[61] M.B. Hoffman and M.S. Turner, *Kinematic constraints to the key inflationary observables*, *Phys. Rev.* **D64** (2001) 023506 [astro-ph/0006321].

[62] D.J. Schwarz, C.A. Terrero-Escalante and A.A. Garcia, *Higher order corrections to primordial spectra from cosmological inflation*, *Phys. Lett.* **B517** (2001) 243 [astro-ph/0106020].

[63] S.M. Leach, A.R. Liddle, J. Martin and D.J. Schwarz, *Cosmological parameter estimation and the inflationary cosmology*, *Phys. Rev.* **D66** (2002) 023515 [astro-ph/0202094].

[64] J. Martin, C. Ringeval and V. Vennin, *K-inflationary Power Spectra at Second Order*, *JCAP* **1306** (2013) 021 [1303.2120].

[65] J. Beltran Jimenez, M. Musso and C. Ringeval, *Exact Mapping between Tensor and Most General Scalar Power Spectra*, *Phys. Rev.* **D88** (2013) 043524 [1303.2788].

[66] J. Martin and D.J. Schwarz, *Wkb approximation for inflationary cosmological perturbations*, *Phys. Rev.* **D67** (2003) 083512 [astro-ph/0210090].

[67] S. Habib, K. Heitmann, G. Jungman and C. Molina-Paris, *The inflationary perturbation spectrum*, *Phys. Rev. Lett.* **89** (2002) 281301 [astro-ph/0208443].

[68] S. Habib, A. Heinen, K. Heitmann, G. Jungman and C. Molina-Paris, *Characterizing inflationary perturbations: The uniform approximation*, *Phys. Rev.* **D70** (2004) 083507 [astro-ph/0406134].

[69] J. Choe, J.-O. Gong and E.D. Stewart, *Second order general slow-roll power spectrum*, *JCAP* **07** (2004) 012 [hep-ph/0405155].

[70] R. Casadio, F. Finelli, M. Luzzi and G. Venturi, *Improved wkb analysis of cosmological perturbations*, *Phys. Rev.* **D71** (2005) 043517 [gr-qc/0410092].

[71] R. Casadio, F. Finelli, M. Luzzi and G. Venturi, *Higher order slow-roll predictions for inflation*, *Phys. Lett.* **B625** (2005) 1 [gr-qc/0506043].

[72] R. Casadio, F. Finelli, M. Luzzi and G. Venturi, *Improved wkb analysis of slow-roll inflation*, *Phys. Rev.* **D72** (2005) 103516 [gr-qc/0510103].

[73] P. Auclair and C. Ringeval, *Slow-roll inflation at N3LO*, *Phys. Rev. D* **106** (2022) 063512 [2205.12608].

[74] S.M. Leach and A.R. Liddle, *Microwave background constraints on inflationary parameters*, *Mon. Not. Roy. Astron. Soc.* **341** (2003) 1151 [astro-ph/0207213].

[75] A.R. Liddle, *Inflationary flow equations*, *Phys. Rev.* **D68** (2003) 103504 [astro-ph/0307286].

[76] V. Vennin, *Horizon-Flow off-track for Inflation*, *Phys. Rev.* **D89** (2014) 083526 [1401.2926].

[77] J. Martin, C. Ringeval and V. Vennin, "ASPIC: Accurate Slow-roll Predictions for Inflationary Cosmology." Astrophysics Source Code Library, record ascl:1806.031, https://github.com/cosmicinflation/aspic, June, 2018.

[78] J. Martin and C. Ringeval, *First CMB Constraints on the Inflationary Reheating Temperature*, *Phys.Rev.* **D82** (2010) 023511 [1004.5525].

[79] C. Ringeval, T. Suyama and J. Yokoyama, *Magneto-reheating constraints from curvature perturbations*, *JCAP* **1309** (2013) 020 [1302.6013].

[80] J. Martin, C. Ringeval and V. Vennin, *Observing Inflationary Reheating*, *Phys. Rev. Lett.* **114** (2015) 081303 [1410.7958].

[81] J. Martin, C. Ringeval and V. Vennin, *Shortcomings of New Parametrizations of Inflation*, *Phys. Rev. D* **94** (2016) 123521 [1609.04739].

[82] J. Martin and C. Ringeval, *Inflation after WMAP3: Confronting the Slow-Roll and Exact Power Spectra to CMB Data*, *JCAP* **0608** (2006) 009 [astro-ph/0605367].

[83] C. Ringeval, *The exact numerical treatment of inflationary models*, *Lect. Notes Phys.* **738** (2008) 243 [astro-ph/0703486].

[84] J. Martin, C. Ringeval and R. Trotta, *Hunting Down the Best Model of Inflation with Bayesian Evidence*, *Phys. Rev.* **D83** (2011) 063524 [1009.4157].

[85] P. Mukherjee, D. Parkinson and A.R. Liddle, *A Nested Sampling Algorithm for Cosmological Model Selection*, *Astrophys. J.* **638** (2006) L51 [astro-ph/0508461].

[86] F. Feroz and M.P. Hobson, *Multimodal nested sampling: an efficient and robust alternative to Markov Chain Monte Carlo methods for astronomical data analyses*, *Mon. Not. R. Astron. Soc.* **384** (2008) 449 [0704.3704].

[87] F. Feroz, M.P. Hobson and M. Bridges, *MULTINEST: an efficient and robust Bayesian inference tool for cosmology and particle physics*, *Mon. Not. R. Astron. Soc.* **398** (2009) 1601 [0809.3437].

[88] W.J. Handley, M.P. Hobson and A.N. Lasenby, *PolyChord: nested sampling for cosmology*, *Mon. Not. Roy. Astron. Soc.* **450** (2015) L61 [1502.01856].

[89] W.J. Handley, M.P. Hobson and A.N. Lasenby, *POLYCHORD: next-generation nested sampling*, MNRAS **453** (2015) 4384 [1506.00171].

[90] C. Ringeval, *Fast Bayesian inference for slow-roll inflation*, *Mon. Not. Roy. Astron. Soc.* **439** (2014) 3253 [1312.2347].

[91] A. Lewis and S. Bridle, *Cosmological parameters from CMB and other data: A Monte Carlo approach*, *Phys.Rev.* **D66** (2002) 103511 [astro-ph/0205436].

[92] J. Torrado and A. Lewis, *Cobaya: Code for Bayesian Analysis of hierarchical physical models*, *JCAP* **05** (2021) 057 [2005.05290].

[93] A. Lewis, A. Challinor and A. Lasenby, *Efficient computation of CMB anisotropies in closed FRW models*, *Astrophys.J.* **538** (2000) 473 [astro-ph/9911177].

[94] A. Lewis, *GetDist: a Python package for analysing Monte Carlo samples*, 1910.13970.

[95] J. Martin, C. Ringeval, R. Trotta and V. Vennin, *Compatibility of Planck and BICEP2 in the Light of Inflation*, *Phys.Rev.* **D90** (2014) 063501 [1405.7272].

[96] Planck collaboration, *Planck 2018 results. V. CMB power spectra and likelihoods*, *Astron. Astrophys.* **641** (2020) A5 [1907.12875].

[97] BICEP, Keck collaboration, *Improved Constraints on Primordial Gravitational Waves using Planck, WMAP, and BICEP/Keck Observations through the 2018 Observing Season*, *Phys. Rev. Lett.* **127** (2021) 151301 [2110.00483].

[98] SPT-3G collaboration, *Measurements of the E-mode polarization and temperature-E-mode correlation of the CMB from SPT-3G 2018 data*, *Phys. Rev. D* **104** (2021) 022003 [2101.01684].

[99] K.S. Dawson et al., *The SDSS-IV extended Baryon Oscillation Spectroscopic Survey: Overview and Early Data*, *Astron. J.* **151** (2016) 44 [1508.04473].

[100] SDSS collaboration, *Sloan Digital Sky Survey IV: Mapping the Milky Way, Nearby Galaxies and the Distant Universe*, *Astron. J.* **154** (2017) 28 [1703.00052].

[101] Planck collaboration, *Planck intermediate results. LVII. Joint Planck LFI and HFI data processing*, *Astron. Astrophys.* **643** (2020) A42 [2007.04997].

[102] M. Tristram et al., *Planck constraints on the tensor-to-scalar ratio*, *Astron. Astrophys.* **647** (2021) A128 [2010.01139].

[103] G. Efstathiou and S. Gratton, *A Detailed Description of the CamSpec Likelihood Pipeline and a Reanalysis of the Planck High Frequency Maps*, 1910.00483.

[104] E. Rosenberg, S. Gratton and G. Efstathiou, *CMB power spectra and cosmological parameters from Planck PR4 with CamSpec*, *Mon. Not. Roy. Astron. Soc.* **517** (2022) 4620 [2205.10869].

[105] Planck collaboration, *Planck 2018 results. VIII. Gravitational lensing*, *Astron. Astrophys.* **641** (2020) A8 [1807.06210].

[106] SPT-3G collaboration, *Constraints on ΛCDM extensions from the SPT-3G 2018 EE and TE power spectra*, *Phys. Rev. D* **104** (2021) 083509 [2103.13618].

[107] SDSS collaboration, *The Seventh Data Release of the Sloan Digital Sky Survey*, *Astrophys. J. Suppl.* **182** (2009) 543 [0812.0649].

[108] J.E. Bautista et al., *The Completed SDSS-IV extended Baryon Oscillation Spectroscopic Survey: measurement of the BAO and growth rate of structure of the luminous red galaxy sample from the anisotropic correlation function between redshifts 0.6 and 1*, *Mon. Not. Roy. Astron. Soc.* **500** (2020) 736 [2007.08993].

[109] H. Gil-Marin et al., *The Completed SDSS-IV extended Baryon Oscillation Spectroscopic Survey: measurement of the BAO and growth rate of structure of the luminous red galaxy sample from the anisotropic power spectrum between redshifts 0.6 and 1.0*, *Mon. Not. Roy. Astron. Soc.* **498** (2020) 2492 [2007.08994].

[110] A. de Mattia et al., *The Completed SDSS-IV extended Baryon Oscillation Spectroscopic Survey: measurement of the BAO and growth rate of structure of the emission line galaxy sample from the anisotropic power spectrum between redshift 0.6 and 1.1*, *Mon. Not. Roy. Astron. Soc.* **501** (2021) 5616 [2007.09008].

[111] J. Hou et al., *The Completed SDSS-IV extended Baryon Oscillation Spectroscopic Survey: BAO and RSD measurements from anisotropic clustering analysis of the Quasar Sample in configuration space between redshift 0.8 and 2.2*, *Mon. Not. Roy. Astron. Soc.* **500** (2020) 1201 [2007.08998].

[112] R. Neveux et al., *The completed SDSS-IV extended Baryon Oscillation Spectroscopic Survey: BAO and RSD measurements from the anisotropic power spectrum of the quasar sample between redshift 0.8 and 2.2*, *Mon. Not. Roy. Astron. Soc.* **499** (2020) 210 [2007.08999].

[113] H. du Mas des Bourboux et al., *The Completed SDSS-IV Extended Baryon Oscillation Spectroscopic Survey: Baryon Acoustic Oscillations with Lyα Forests*, *Astrophys. J.* **901** (2020) 153 [2007.08995].

[114] ACT collaboration, *The Atacama Cosmology Telescope: DR4 Maps and Cosmological Parameters*, *JCAP* **12** (2020) 047 [2007.07288].

[115] ACT collaboration, *The Atacama Cosmology Telescope: a measurement of the Cosmic Microwave Background power spectra at 98 and 150 GHz*, *JCAP* **12** (2020) 045 [2007.07289].

[116] W. Handley and P. Lemos, *Quantifying the global parameter tensions between ACT, SPT and Planck*, *Phys. Rev. D* **103** (2021) 063529 [2007.08496].

[117] Planck collaboration, *Planck 2018 results. II. Low Frequency Instrument data processing*, *Astron. Astrophys.* **641** (2020) A2 [1807.06206].

[118] S. Galli, K. Benabed, F. Bouchet, J.-F. Cardoso, F. Elsner, E. Hivon et al., *CMB Polarization can constrain cosmology better than CMB temperature*, *Phys. Rev. D* **90** (2014) 063504 [1403.5271].

[119] LiteBIRD collaboration, *Probing Cosmic Inflation with the LiteBIRD Cosmic Microwave Background Polarization Survey*, 2202.02773.

[120] Planck collaboration, *Planck 2018 results. III. High Frequency Instrument data processing and frequency maps*, *Astron. Astrophys.* **641** (2020) A3 [1807.06207].

[121] D. Shepard, *A two-dimensional interpolation function for irregularly-spaced data*, in *Proceedings of the 1968 23rd ACM national conference*, ACM '68, (New York, NY, USA), pp. 517–524, ACM, 1968, DOI.

[122] W.I. Thacker, J. Zhang, L.T. Watson, M.A. Birch, Jeffrey B. an d Iyer and M.W. Berry, *Algorithm 905: Sheppack: Modified shepard algorithm for interpolation of scattered multivariate data*, *ACM Trans. Math. Softw.* **37** (2010) 34:1.

[123] W. Handley, *anesthetic: nested sampling visualisation*, *J. Open Source Softw.* **4** (2019) 1414 [1905.04768].

[124] W. Handley and P. Lemos, *Quantifying dimensionality: Bayesian cosmological model complexities*, *Phys. Rev. D* **100** (2019) 023512 [1903.06682].

[125] R. Trotta, *Bayes in the sky: Bayesian inference and model selection in cosmology*, *Contemp. Phys.* **49** (2008) 71 [0803.4089].

[126] C. Gordon and R. Trotta, *Bayesian Calibrated Significance Levels Applied to the Spectral Tilt and Hemispherical Asymmetry*, *Mon. Not. Roy. Astron. Soc.* **382** (2007) 1859 [0706.3014].

[127] M. Kunz, R. Trotta and D. Parkinson, *Measuring the effective complexity of cosmological models*, *Phys. Rev.* **D74** (2006) 023503 [astro-ph/0602378].

[128] S. Kullback and R.A. Leibler, *On information and sufficiency*, *Ann. Math. Statist.* **22** (1951) 79.

[129] R. Easther and H.V. Peiris, *Bayesian Analysis of Inflation II: Model Selection and Constraints on Reheating*, *Phys.Rev.* **D85** (2012) 103533 [1112.0326].

[130] L. Dai, M. Kamionkowski and J. Wang, *Reheating constraints to inflationary models*, *Phys.Rev.Lett.* **113** (2014) 041302 [1404.6704].